



저작자표시-비영리-변경금지 2.0 대한민국

이용자는 아래의 조건을 따르는 경우에 한하여 자유롭게

- 이 저작물을 복제, 배포, 전송, 전시, 공연 및 방송할 수 있습니다.

다음과 같은 조건을 따라야 합니다:



저작자표시. 귀하는 원저작자를 표시하여야 합니다.



비영리. 귀하는 이 저작물을 영리 목적으로 이용할 수 없습니다.



변경금지. 귀하는 이 저작물을 개작, 변형 또는 가공할 수 없습니다.

- 귀하는, 이 저작물의 재이용이나 배포의 경우, 이 저작물에 적용된 이용허락조건을 명확하게 나타내어야 합니다.
- 저작권자로부터 별도의 허가를 받으면 이러한 조건들은 적용되지 않습니다.

저작권법에 따른 이용자의 권리는 위의 내용에 의하여 영향을 받지 않습니다.

이것은 [이용허락규약\(Legal Code\)](#)을 이해하기 쉽게 요약한 것입니다.

[Disclaimer](#)

공학박사 학위논문

**Soluble melanin synthesis and enzyme
coating using tyrosinase catalyzed reaction**

티로시나아제 반응을 이용한 수용성 멜라닌 합성 및 효소
코팅

2022년 8월

서울대학교 대학원
공과대학 화학생물공학부

김 현

**Soluble melanin synthesis and enzyme coating
using tyrosinase catalyzed reaction**

지도 교수 김 병 기

이 논문을 공학박사 학위논문으로 제출함
2022년 8월

서울대학교 대학원
공과대학 화학생물공학부
김 현

김 현의 공학박사 학위논문을 인준함
2022년 8월

위 원 장 _____ (인)

부위원장 _____ (인)

위 원 _____ (인)

위 원 _____ (인)

위 원 _____ (인)

Soluble melanin synthesis and enzyme coating using tyrosinase catalyzed reaction

A Thesis

Submitted to the Faculty of Seoul National University

by

Hyun Kim

In Partial Fulfillment of the Requirements

For the Degree of Doctor of Philosophy

Advisor: Professor Byung-Gee Kim, Ph.D.

August, 2022

School of Chemical and Biological Engineering
Seoul National University

Abstract

Soluble melanin synthesis and enzyme coating using tyrosinase catalyzed reaction

Hyun Kim

School of Chemical and Biological Engineering

Seoul National University

The synthesis of bioactive nanomaterials is an area of increasing interest. For nanomaterials synthesis, physical, chemical, and biological synthesis methods are known. Nanomaterials are generally applied in terms of size and physicochemical properties. Compared to the previous two methods, the enzymatic synthesis method is known as a production method of non-homogeneous particles, so it was difficult to conduct an in-depth analysis of the reaction. However, enzyme catalysis is more environmentally friendly

than chemical catalysis and catalyzes reactions in mild conditions. Therefore, enzymatic synthesis method is suitable for producing bioactive materials that are easily damaged in harsh conditions. Enzymatic synthesis of nanoparticles may provide an alternative approach for the synthesis of nanoparticles in an appropriate manner.

We attempted to synthesize a bioactive nanomaterial capable of fine-tuning using tyrosinase with substrate specificity to monophenol. Tyrosinase is an enzyme with substrate specificity for various monophenolic substrates, and the optimum reaction pH changes depending on the domain structure. Using catechol and quinone produced by consecutive hydroxylation of tyrosinase, crosslinked nanomaterials were synthesized by an enzymatic method, and physicochemical properties were analyzed in detail.

In Chapter 1, *Burkholderia cepacia* tyrosinase, which has strong activity in acidic conditions below pH 5, was used to synthesize homogeneous melanin nanoparticles of 20 nm or less. Melanin, synthesized by random oxidation in a neutral adverse reaction environment, formed an aggregate with protein. However, by inducing protonation of catechol under acidic conditions, random crosslinking was controlled, and as a result, homogeneous melanin nanoparticles were synthesized by an enzymatic method.

In Chapter 2, an enzyme-polysaccharide complex was formed by cross-linking polysaccharides introduced with a phenol moiety to the enzyme surface through a tyrosinase reaction to promote enzyme stabilization. *Streptomyces avermitilis* tyrosinase, which is highly reactive to polymer

substrates due to its short distance from the enzyme surface to the active site, generated cross-links between tyrosine residues on the enzyme surface and monophenols on the polysaccharide surface to which phenol residues are attached. The tyrosinase cross-linking reaction was able to synthesize the model enzyme trypsin and alginate-tyramine complex in a mild environment of pH 8 within 30 minutes. As a result, trypsin's thermal stability, organic solvent stability, and storage stability were improved.

Keyword: Tyrosinase, Acidic condition, Soluble melanin nanoparticle, Crosslinking, Enzyme-polysaccharide coating

Student Number: 2016-22788

Contents

Abstract	i
Contents	iv
List of Tables	viii
List of Figures	ix
Chapter 1. Introduction	1
1.1 Tyrosinase	2
1.1.1 Type-3 copper-containing enzyme, tyrosinase	2
1.1.2 Reaction mechanism and characteristics of tyrosinase	8
1.2 Applications of using tyrosinase as crosslinking agent	14
1.1.1 Melanin synthesis	15
1.1.2 Tyrosinase mediated crosslinking of polymer	16
1.3 Intermolecular interaction of catechol and quinone	17
1.4 Scope of thesis	22
Chapter 2. Synthesis of soluble melanin nanoparticles under acidic condition using <i>Burkholderia cepacia</i> tyrosinase and their characterization	24
2.1 Abstract	25
2.2 Introduction	26
2.3 Materials and methods	30
2.3.1 Materials	30
2.3.2 Plasmid construction	30
2.3.3 Expression and purification of <i>Bc</i>Ty	32
2.3.4 Synthesis of eumelanin-like nanoparticles	33
2.3.5 Instrumental analysis	34
2.3.6 Evaluation of the antioxidant activity of the soluble MNP	35
2.3.7 Synthesis of sticky eMNP-gelatin hydrogel and characterization	36
2.4 Result and discussion	38

2.4.1	Production of soluble eMNPs at acidic pH using <i>BcTy</i>	38
2.4.2	Understanding the synthetic mechanism of soluble eMNP-3 through chemical structure and functional group analysis	52
2.4.3	Characterization of surface zeta potential properties of eMNPs	63
2.4.4	Evaluation of antioxidant effect of soluble and ultra-small eMNP	68
2.4.5	Mussel foot protein (Mfp)-inspired sticky hydrogel in acidic condition	71
2.4.6	Synthesis of linear chain eMNPs from tyrosine derivatives	75
2.5	Conclusion.....	79
Chapter 3.	Preparation of enzyme-polysaccharide coating by tyrosinase to improve enzyme stability	82
3.1	Abstract.....	83
3.2	Introduction	85
3.3	Materials and methods	90
3.3.1	Materials.....	90
3.3.2	Expression and purification of <i>Streptomyces avermitilis</i> tyrosinase (<i>SaTy</i>).....	90
3.3.3	Synthesis of phenol-moiety conjugated polysaccharides.....	91
3.3.4	Fabrication of trypsin-polysaccharide coating with tyrosinase reaction using phenol-moiety conjugated polysaccharides.....	93
3.3.5	Fabrication of immobilized trypsin on glass bead and polysaccharide complex with tyrosinase reaction using phenol-moiety conjugated polysaccharides	93
3.3.6	Measurement of trypsin activities and enzyme kinetics	94
3.3.7	Measurement of thermal stability of enzyme and EPC.....	96
3.3.8	Estimation of storage stability of trypsin by accelerated stability test.....	96
3.3.9	Instrumental analysis	98
3.3.10	Prediction of surface potential of trypsin	99
3.4	Result and discussion.....	100

3.4.1	Fabrication of enzyme-polysaccharide coating (EPC) and identification of physical properties.....	100
3.4.2	Alg-TR synthesis reaction optimization	114
3.4.3	Enzyme kinetics of EPC according to the charge of small molecule substrates.....	122
3.4.4	Measurement of EPC stability increase for thermal and water-miscible organic solvents.....	126
3.4.5	Increased storage stability of TR by EPC formation.....	131
3.4.6	Enzyme-protein coating for the application to various enzymes	137
3.5	Conclusion.....	141
Chapter 4.	Overall Conclusion and Further Suggestions.....	143
4.1	Overall conclusion	144
4.2	Further suggestions	146
4.2.1	Immobilization of tyrosinase enzyme to limit excessive hydroxylation product formation reaction.....	146
4.2.2	Melanin dyeing at pH 5 or lower to maintain the stability of animal fibers.	148
4.2.3	Establishment of polymer design strategy for universal application and biomedical use of enzyme-polymer complex with improved stability.....	150
References	151
Appendix	176
A.1	Introduction.....	177
A.2	Orobol mass production protocol	180
A.2.1	Materials	180
A.2.2	Recombinant <i>Bacillus megaterium</i> tyrosinase (<i>BmTy</i>) subculture for 40L scale large-capacity cell culture	180
A.2.3	Recombinant <i>Bacillus megaterium</i> tyrosinase (<i>BmTy</i>) subculture for 40L scale large-capacity cell culture	181

A.2.4 Cell recovery and preparation of orobol bioconversion reaction mixture	183
A.2.5 Production of orobol in 400 L scale reaction	186
A.2.6 Purificaiton of orobol.....	188
A.3 glycoside hydroxylation	190
A.3.1 Materials	190
A.3.2 Expression and purification of <i>BfTy</i>	190
A.3.3 Synthesis and analysis of ortho-hydroxylated polyphenol glycosides using <i>BfTy</i>	191
A.3.4 Synthesis of ortho-hydroxylated derivatives from O- and C-glycosylated polyphenols.....	192
References	197
국문 초록	200

List of Tables

Table 1.1 Enzyme kinetics of tyrosinase derived from various species for L-tyrosine and 3,4-dihydroxy-L-phenylalanine (L-DOPA).....	5
Table 2.1 Primer list.....	31
Table 2.2 Kinetics of tyrosinases (Ty).	39
Table 2.3 XPS peak binding energy assignments to (a) C 1s, (b) N 1s, and (c) O 1s functional groups and peak area ratio for each functional groups	60
Table 2.4 Average hydrodynamic diameters and zeta potential of eMNP-3, 4, 5 and cMNP measured by DLS.	65
Table 2.5 Comparison of radical scavenging activities (EC_{50}) of ascorbic acid and three MNPs on DPPH.....	69
Table 3.1 Hydrodynamic diameter and surface potential of Free-TR and Alg-TR measured by DLS	121
Table 3.2 Comparison of enzyme kinetics of Free-TR and Alg-TR according to the charge of small molecule substrates	125
Table 3.3 Protein melting temperature (T_m , °C) measurement to estimate the thermal resistance of TR.....	129
Table 3.4 Estimated storage stability time of (a) Free-TR and (b) Alg-TR	135
Table A.2.1 40L <i>BmTy</i> auto induction media composition.....	182
Table A.2.2 400L orobol production reaction solution composition.....	184

List of Figures

Figure 1.1 Schematic representation of tyrosinase reaction mechanism	10
Figure 1.2 Reaction determining steps in tyrosinase reaction	11
Figure 1.3 Five classifications according to the domain structure of tyrosinase .	13
Figure 1.4 Non-covalent interactions of catechol	18
Figure 1.5. Spontaneous crosslinking reaction of quinone	21
Figure 2.1 Optimal pH of <i>BcTy</i> activity.....	40
Figure 2.2 Digital pictures of melanin reaction solutions and Tyndall effect of MNP _s . by irradiating 660 nm red laser synthesized from 3 mg/ml of dopamine using various synthesis methods and their scanning electron microscopy images.....	41
Figure 2.3 Digital pictures of melanin reaction solutions and Tyndall effect by irradiating 660 nm red laser synthesized from 1 mg/ml of dopamine using various synthesis methods and their scanning electron microscopy images	43
Figure 2.4 TEM image of (a) eMNP-3 and (b) Nano-onion like stacking structure of eMNP-3.	45
Figure 2.5 Digital picture of melanin reaction solution and Tyndall effect by irradiating 660 nm red raser synthesized from 3 mg/ml of dopamine at acidic conditions. And their scanning electron microscopy image	46
Figure 2.6 Physical properties of eMNP-3 according to synthesis time	48
Figure 2.7 Synthesis of soluble eMNPs from phenolic substrates.....	50
Figure 2.8 UV spectrum profile between eMNP synthesized according to substrate variation.....	51
Figure 2.9 Comparison of MALDI-TOF mass spectra of (a) eMNP-3 and (b) cMNP.	53
Figure 2.10 The predicted chemical structure of dopamine oligomeric derivatives using positive mode of MALDI-TOF	54
Figure 2.11 (a) Comparison of FTIR spectra of eMNP-3 and cMNP. (b) Increasing trends of C=O stretching and N-H bending were observed according to the decrease in the eMNP synthesis pH at 5.0 to 3.0.	57
Figure 2.12 XPS spectra showing the C 1s, N 1s and O 1s peaks of eMNP-3 and cMNP.....	61
Figure 2.13 XPS survey spectrum of (a) eMNP-3 and (b) cMNP	62
Figure 2.14 Changes in zeta potential of eMNP-3 by varying storage pH buffers.	

.....	66
Figure 2.15 Surface modification of soluble eMNP.....	67
Figure 2.16 Comparison of radical scavenging activity (%) between MNPs and ascorbic acid.....	70
Figure 2.17 Preparation of gelatin hydrogel containing eMNP-3 and measurement of mechanical properties.....	73
Figure 2.18 (a) Schematic image of the mechanical strength and adhesion force of melanin hydrogel. (b) Representative stress-strain curve.....	74
Figure 2.19 Synthesis of linear structured melanin from tyrosine methylester ...	77
Figure 2.20 Proposed schematic illustration of synthesis mechanism of soluble eMNP under acidic condition.....	81
Figure 3.1 Schematic diagram of the synthesis of the entire EPC and the surface properties of the target protein trypsin.....	102
Figure 3.2 ¹ H-NMR spectrum of polysaccharide-phenol moiety conjugated synthesized by EDC-NHS coupling chemistry.....	104
Figure 3.3 Intact mass spectrometer (MS) spectrum of trypsin before and after 3-(4-hydroxyphenyl) propionic acid conjugation by <i>Sa</i> Ty.....	105
Figure 3.4 (a) Digital picture of Alg-TR, Chi-TR, Dex-TR reaction mixture....	109
Figure 3.5 Changes in the activity properties of Alg-TR for small molecule (BAPNA) and large molecule (skim milk) compared to Free-TR.....	110
Figure 3.6 Enzyme stabilization measurement by Alg complex formation of TR immobilized on glass beads.....	112
Figure 3.7 UV spectrum change profile of reaction mixture according to Alg-TR synthesis time.....	117
Figure 3.8 Alg-TR optimal reaction condition screening according to Alg and TR concentration gradient.....	118
Figure 3.9 TR stability assay that changes according to the ionic strength of the Alg-TR synthesis buffer.....	120
Figure 3.10 Changes in the optimum pH properties of AIT-TR.....	124
Figure 3.11 BAPNA activity assay for improvement of thermal stability and organic solvent stability of AIT-TR.....	127
Figure 3.12 Decrease in enzymatic activity of TR according to accelerated temperature activity test.....	133
Figure 3.13 Arrhenius plot on the degradation of (a) Free-TR and (b) Alg-TR.	134
Figure 3.14 Surface charge of various proteins at pH 8.0.....	138
Figure 3.15 Comparison of relative activity after 50 °C incubation for ES, ST, CT,	

and GC.....	140
Figure 4.1 Schematic diagram for crosslink product production through tyrosinase immobilization and continuous flow column reactor production	147
Figure 4.2 Production of natural pigments by bioconversion of plant-derived polyphenols into <i>Burkholderia thailandensis</i> tyrosinase (<i>BtTy</i>) and <i>Burkholderia cepaica</i> tyrosinase (<i>BcTy</i>) with high activity under acidic reaction conditions below pH 5	149
Figure A.2.1 Preparation of cell lysis solution after 40L cell culture	185
Figure A.2.2 Color change of orobol production solution over reaction time ...	187
Figure A.2.3 Separation and purification of the final produced orobol	189
Figure A.3.1 Propensity for boric acid chelation of polyphenol aglycone and glycone	194
Figure A.3.2 Confirmation of enzymatic reactivity through melanogenesis reaction for polyphenol aglycone and glycone of <i>BtTy</i>	195
Figure A.3.3 Bioconversion profile of <i>BtTy</i> to polyphenol glycosides with various backbone structures	196

Chapter 1.

Introduction

1.1 Tyrosinase

1.1.1 Type-3 copper-containing enzyme, tyrosinase

Copper is contained in vitamins, hormones, enzymes, and respiratory organs and is one of the essential trace elements involved in metabolic processes and tissue respiration (Tishchenko, Beloglazkina, Mazhuga, & Zyk, 2016). In vivo, copper is an essential cofactor in various biological redox reactions because it exists in the reduced (Cu^{I}) or oxidized (Cu^{II}) state (Aguilera, McDougall, & Degnan, 2013; Solomon, Baldwin, & Lowery, 1992). Copper interacts with proteins by coordinating with the imidazole groups of aspartic and glutamic acids or histidine (Aguilera et al., 2013). Copper binding proteins are divided into three classes according to the geometry of the active site. i) type-1 blue copper protein (e.g., plastocyanin, azurin, halocyanin) involved in electron transport, ii) type-2 non-blue copper protein (e.g., galactose oxidase) belonging to the oxidoreductase family, and iii) type-3 It is a binuclear copper protein and contains polyphenol oxidase (PPO, e.g., tyrosinase, tyrosinase-related protein, catechol oxidase), laccase and hemocyanin. PPO, laccase and hemocyanin are responsible for oxygen-activated hydroxylation and oxygen transport, respectively (Aguilera et al., 2013; Solomon, Sundaram, & Machonkin, 1996; Tishchenko et al., 2016).

Type-3 copper-containing enzyme has structural features in that there are two pairs of copper sites coordinated by three histidine residues,

respectively. The two pairs of copper cations are tightly bound by the nitrogen of the imidazole ring of histidine. Two coppers located at the active site are arranged at about 2.8-4.6 Å, and the oxygen molecule is reversibly bound (Kampatsikas & Rompel, 2021). Therefore, it can activate oxygen and function as monooxygenase or be involved in respiration because it binds oxygen with two copper atoms.

Tyrosinase (EC 1.14.18.1) is an enzyme found widely in bacteria, fungi, plants, and animals. Type-3 copper-containing monooxygenase that *o*-hydroxylates monophenol to catechol (monophenolase or cresolase) by reducing oxygen molecules bound to copper to water catalyzes hydroxylation with *o*-quinone (diphenolase or catecholase) (Zaidi, Ali, Ali, & Naaz, 2014). In vivo, tyrosinase forms melanin, a dark pigment, using tyrosine as a substrate through a series of reactions, and plays an essential role in melanin production in mammals or bacteria and enzymatic browning in fruits. Since melanin plays a vital role in protecting plants and fungi of human skin from UV rays, UV, radiation, and reactive oxygen species, tyrosinase is an essential enzyme for the survival of organisms (Faccio, Kruus, Saloheimo, & Thöny-Meyer, 2012; Fairhead & Thöny-Meyer, 2012).

The most widely used tyrosinase is a commercially available tyrosinase derived from *Agaricus bisporus*. However, due to its low solvent stability and low-temperature tolerance, tyrosinase to be used as a substitute for biocatalytic reactions was needed (Fairhead & Thöny-Meyer, 2012). Therefore, many efforts have been made to discover bacterial tyrosinase

based on nucleotide sequence and biochemical data. Tyrosinases belonging to the bacterial genera of *Aeromonas*, *Bacillus*, *Burkholderia*, *Marinomonas*, *Nitrosopumilus*, *Pseudomonas*, *Ralstonia*, *Rhizobium*, *Shewanella*, *Stenotrophomonas*, *Streptomyces*, and *Laceyella* have been reported (Agunbiade & Roes-Hill, 2022; Fernandes & Kerkar, 2017) (**Table 1.1**).

Table 1.1 Enzyme kinetics of tyrosinase derived from various species for L-tyrosine and 3,4-dihydroxy-L-phenylalanine (L-DOPA).

Tyrosinase origin	Optimum pH	Substrate	K_m (mM)	k_{cat} (s^{-1})	k_{cat}/K_m ($mM \cdot s^{-1}$)
<i>Agaricus bisporus</i> (Fenoll et al., 2001)	6	L-Tyrosine	0.25 ± 0.03	7.9 ± 0.12	31.60
		L-DOPA	0.28 ± 0.01	107.3 ± 1.45	383.21
<i>Bacillus megaterium</i> (Deri et al., 2016)	8	L-Tyrosine	0.082 ± 0.006	2.1	25.60
		L-DOPA	0.24 ± 0.02	17.8	74.20
<i>Streptomyces avermitilis</i> (N. Lee, Lee, Baek, & Kim, 2015)	7	L-Tyrosine	0.589 ± 0.056	0.021	0.04
		L-DOPA	2.79 ± 0.79	0.19	0.07
<i>Burkholderia thailandensis</i> (Son et al., 2018)	5	L-Tyrosine	0.59 ± 0.055	397.5	668.63
		L-DOPA	0.83 ± 0.13	487.17	586.74
<i>Burkholderia cepacia</i> (This study)	4	L-Tyrosine	0.22 ± 0.04	333.9 ± 31.33	1504.94
		L-DOPA	2.16 ± 0.41	1803.06 ± 297.9	835.42
<i>Aeromonas media</i> strain WS (Wan et al., 2009)	9 / 11	L-Tyrosine	-	-	-
		L-DOPA	1.16 ± 0.02	-	-

<i>Bacillus aryabhatai</i> strains TCCC 111983 (F. Wang et al., 2021)	5	L-Tyrosine	0.163	2.545	15.61
		L-DOPA	0.288	3.755	13.04
<i>Marinomonas mediterranea</i> strain MMB-1 (López-serrano, SAnchez-Amat, & Solano, 2002)	5	L-Tyrosine	0.3	-	-
		L-DOPA	0.8	-	-
<i>Candidatus Nitrosopumilus koreensis</i> (H. Kim et al., 2016)	6	L-Tyrosine	9.2 ± 2.4	4.3 ± 1.08	0.47
		L-DOPA	2.6 ± 0.56	2.2 ± 0.47	0.85
<i>Pseudomonas aeruginosa</i> strain PAO1 (Nadal-Jimenez et al., 2014)	9	L-Tyrosine	1.3 ± 0.05	1.38 ± 0.09	1.06
		L-DOPA	0.75 ± 0.28	0.13 ± 0.01	0.17
<i>Ralstonia solanacearum</i> strain GMI1000 (Molloy et al., 2013)	7	L-Tyrosine	2.1 ± 0.4	85 ± 6	40.4
		L-DOPA	-	-	-
<i>Rhizobium etli</i> strain CFN42 (Cabrera-Valladares et al., 2006)	6.5-7.5	L-Tyrosine	0.19 ± 0.0062	-	-
		L-DOPA	2.44 ± 0.48	-	-
<i>Streptomyces</i> sp. ZL-24 (Panis, Krachler, Krachler, & Rompel, 2021)	9	L-Tyrosine	0.60 ± 0.074	4.8 ± 0.23	7.9
		L-DOPA	15 ± 3.7	520 ± 80	34
<i>Streptomyces kathirae</i> SC-1 (Guo et al., 2015)	6.2	L-Tyrosine	0.19	117.8	620
		L-DOPA	0.42	171.08	406.37
<i>Laceyella sacchari</i>	7	L-Tyrosine	0.055	3.1	56.3

(Dolashki et al., 2012)		L-DOPA	4.5	1177	261.5
<i>Armillaria ostoyae</i>	7	L-Tyrosine	1.63 ± 0.63	188 ± 0.35	115
(T. Li, Zhang, Yan, Jiang, & Yin, 2021)		L-DOPA	1.51 ± 0.44	178 ± 0.26	118
<i>Homo sapiens</i>	7	L-Tyrosine	1.32 ± 0.12 (μM)	36.8 ± 1.5	27.9 (μM ⁻¹ s ⁻¹)
(Kong, Lee, Jo, & Kong, 2010)		L-DOPA	0.34 ± 0.08	34.1 ± 2.3	100.3

1.1.2 Reaction mechanism and characteristics of tyrosinase

Each copper ion coordinated to the active site of tyrosinase exists in the form of *deoxy*- (Cu^{I}), *oxy*- (Cu^{II}), and *met*- (Cu^{II}). In the *deoxy*- form, the two coppers are 4.1–4.6 Å apart, in the *oxy*- form 3.2–4.0 Å, and in the *met*- form 2.8–3.2 Å (Kampatsikas & Rompel, 2021). The *deoxy*- form in which the copper ion is in the Cu^{I} state can combine with oxygen molecules in the $\mu\text{-}\eta^2\text{:}\eta^2\text{-peroxo}$ geometry (Kampatsikas & Rompel, 2021; Zaidi et al., 2014). Alternatively, it can bind to hydroxide ions or water molecules in a bridging mode (Kampatsikas & Rompel, 2021). The tyrosinase reaction proceeds as the monophenolase cycle and the diphenolase cycle through the *deoxy*-*met*-*oxy*-form cycle. In the $\text{Cu}^{\text{I}}\text{-Cu}^{\text{I}}$ form of the *deoxy*-, the starting point of the two cycles begins, and the $\text{Cu}^{\text{II}}\text{-Cu}^{\text{II}}$ form of *oxy*- form is formed in combination with molecular oxygen (H. Kim, Kim, & Choi, 2014; Zaidi et al., 2014) (**Figure 1.1**). Moreover, using monophenol as a substrate, *oxy*- form is involved in the reaction to convert to diphenol or convert diphenol to quinone. Next, tyrosinase is converted to the *met*- form of $\text{Cu}^{\text{II}}\text{-Cu}^{\text{II}}$. The *met*-form tyrosinase further converts diphenol to quinone and then returns to the *deoxy*- form of $\text{Cu}^{\text{I}}\text{-Cu}^{\text{I}}$. It is known that 85% of tyrosinase is in *met*- form in which hydroxide or water molecules are linked to Cu^{II} , and 15% is in *oxy*-form (Faccio et al., 2012). Therefore, when monophenol becomes a substrate,

the initial lag phase of the reaction occurs (**Figure 1.2**).

In order to initiate the tyrosinase reaction, binding to copper according to the deprotonation of the monophenol substrate is essential. Histidine residues located in and around the dicopper center enhance the basicity of copper-coordinated histidine (Kampatsikas & Rompel, 2021) (**Figure 1.2**). They also deprotonate monophenolic substrates that enter the active site pocket. The deprotonated phenolic substrate prepared for catalysis interacts with the oxy form. Therefore, the pH favored for deprotonation above neutral pH (ca. pH 6.0) can be considered as the tyrosinase optimum pH.

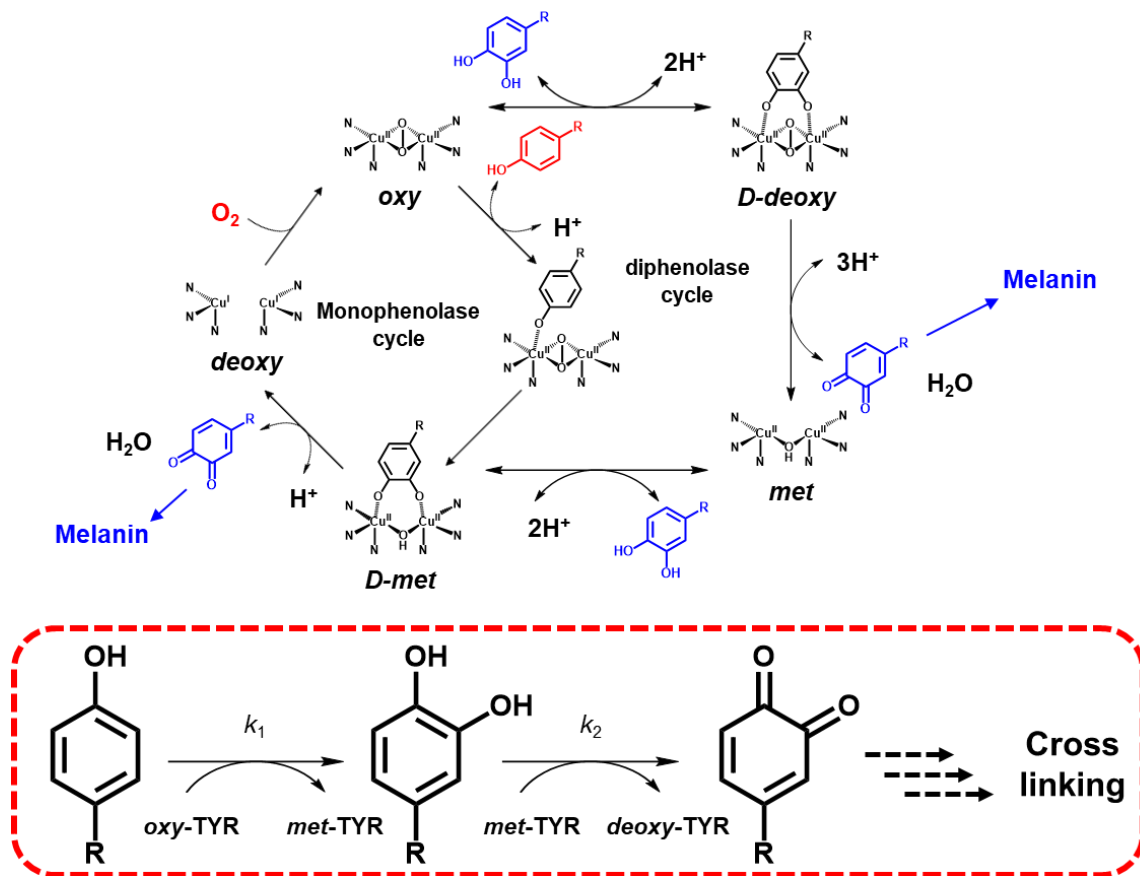


Figure 1.1 Schematic representation of tyrosinase reaction mechanism

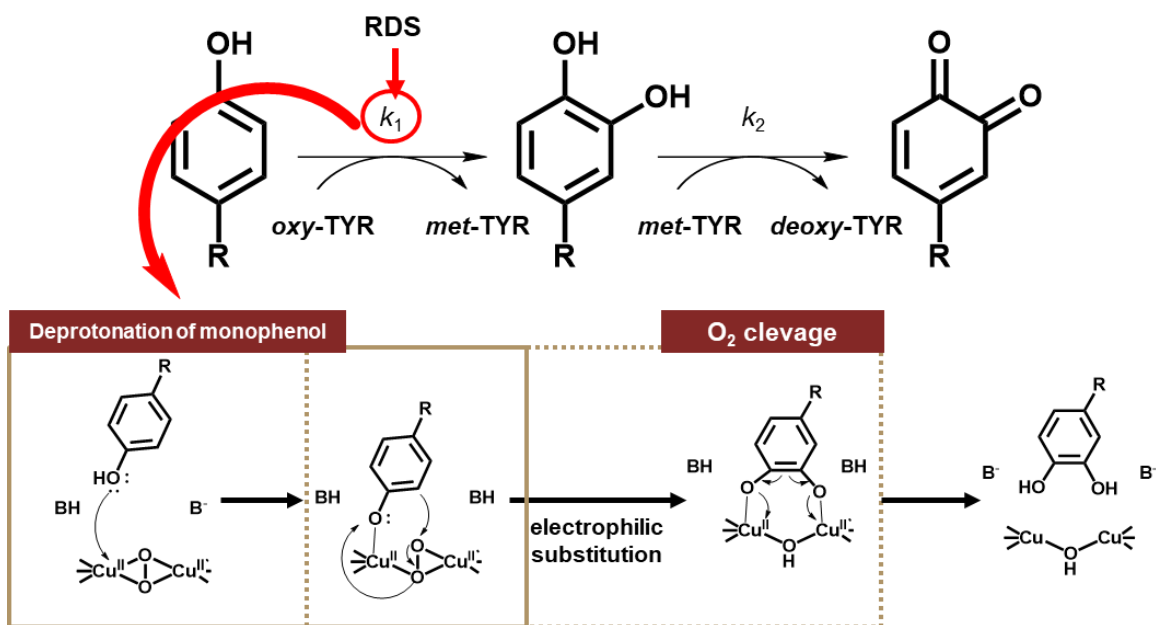


Figure 1.2 Reaction determining steps in tyrosinase reaction

However, tyrosinase has various structures, and the well-conserved typical domain structure of the core active site can be divided into five main types (Fairhead & Thöny-Meyer, 2012; H. Kim et al., 2014) (**Figure 1.3**). Type I tyrosinase is a common type of *Streptomyces* sp. For copper incorporation into tyrosinase, a caddie protein expressed in the same operon is required. Type II tyrosinase is similar in size to *Streptomyces* sp., but does not require a caddie protein and belongs to *Bacillus* sp. tyrosinase. Type III tyrosinase is similar to fungal tyrosinase, with a central copper binding domain followed by a C-terminal cap domain. Although the cap domain must be removed for enzymatic activity, it is known that the cap domain acts together in the tyrosinase of *Burkholderia* species reported by Son et.al. (Son et al., 2018). Type IV tyrosinase is found in *Bacillus thuringensis*, which is smaller and only active in homodimeric form. Type V tyrosinase contains a multifunctional polyphenol oxidase that exhibits both tyrosinase and laccase-like activity. Bacterial tyrosinase comprises various domains centered on the active site, so the isoelectric point (pI) varies significantly from 4.65 to 11.9. This means that the optimal pH for tyrosinase is widely distributed based on neutrality, allowing various acidic or alkaline pH applications (Ba & Vinoth Kumar, 2017).

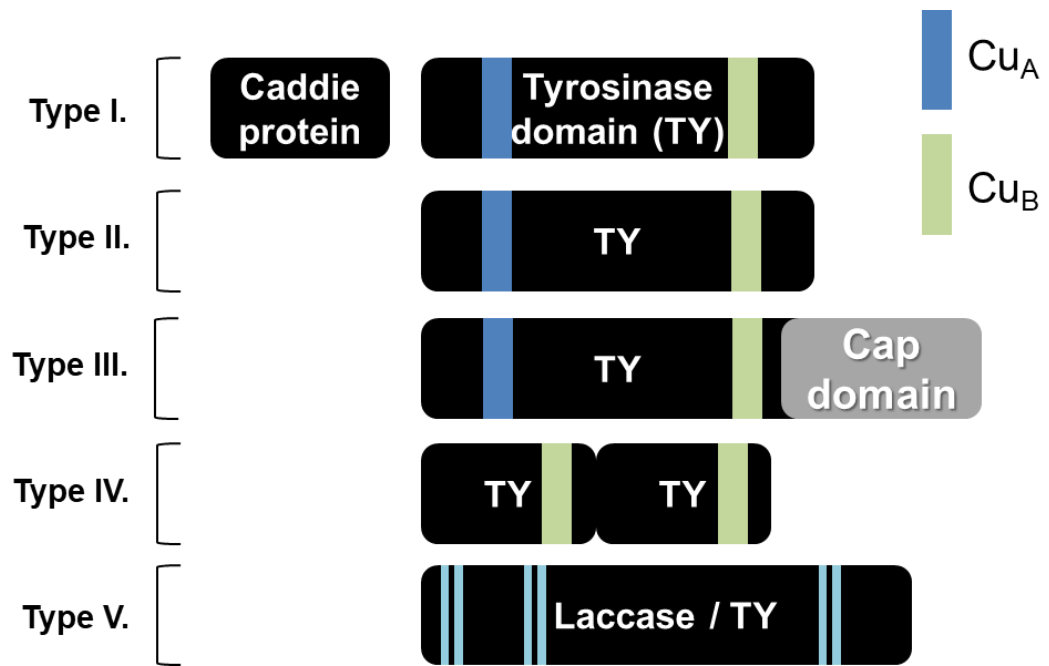


Figure 1.3 Five classifications according to the domain structure of tyrosinase

1.2 Applications of using tyrosinase as crosslinking agent

Tyrosinase induces melanogenesis, an aesthetically undesirable phenomenon in mammals, melanogenesis, and browning of harvested fruits. Therefore, researches to find the tyrosinase inhibitor and inhibit the *in vivo* tyrosinase reaction have been ongoing for a long time (Fernandes & Kerkar, 2017). However, by utilizing the reaction characteristics of tyrosinase, which performs a substrate-specific hydroxylation reaction on phenol, many studies have been conducted to apply it to various fields. First, by utilizing the monophenolase reaction in which catechol is generated from monophenol, the production of L-DOPA used in the pharmaceutical field (Rios et al., 1999), the production of hydroxytyrosol as a food additive (Espín, Soler-Rivas, Cantos, Tomás-Barberán, & Wichers, 2001), and the bioconversion of polyphenols derived from plants as antioxidants into active substances (P. G. Lee, Lee, Hong, Lutz, & Kim, 2019; S. H. Lee, Baek, Lee, & Kim, 2016). And so on, tyrosinase itself was applied as a biocatalyst.

In particular, various recent studies have been conducted to apply a catechol and quinonlic cross-link reaction, which is a product synthesized through a tyrosinase reaction. The crosslinking reaction can be induced physicochemically by chemical crosslinking or enzyme catalysis. The enzymatic hydroxylation of phenolic compound and crosslinking method is

mild compared to the chemical crosslinking method and has the advantage that it can be synthesized under physiological conditions. Enzymes can promote chemical reactions in a buffer solution at a low temperature, acidic to basic, and buffered aqueous solution that is not satisfied by chemical crosslinking. In addition, it is a very selective reaction to the substrate, and it enables a sophisticated reaction by minimizing side reactions (Ehrbar et al., 2007). Tyrosinase converts monophenols to catechol and quinone through a series of hydroxyl reactions. Reactive quinones form covalent bonding with amines, thiols, or other quinone moieties through a non-enzymatic reaction (J. Yang, Stuart, & Kamperman, 2014).

1.1.1 Melanin synthesis

Melanin is one of the most common pigment pigments found in the body. It can be extracted from plant or animal tissue, but the extraction process is expensive and inefficient, and the properties of the extracted melanin are not constant (Martínez, Martinez, & Gosset, 2019). Therefore, methods for mass production by chemical or enzymatic oxidation using a single substrate are of increasing value. Melanin is divided into various types according to the substrate used for melanin synthesis. There is eumelanin, pheomelanin, allomelanin, and pyomelanin (X. Zhou et al., 2019). The tyrosine oxidized by tyrosinase produces eumelanin, and when cysteine is added, it becomes pheomelanin. Substrates such as dihydroxynaphtalene, caffeic acid, and

homogenistic acid are oxidized to form allomelanin and pyomelanin. With various chemical compositions, melanin exhibits very characteristic physicochemical properties. Melanin complex serves to protect against ultraviolet, X-ray, and gamma rays, and can also be used as a photo thermal therapy material by absorbing near infrared. Sometimes it acts as a semiconductor material. Melanin also acts as an antioxidant and is used as an antiviral coating (Liu, Ai, & Lu, 2014).

1.1.2 Tyrosinase mediated crosslinking of polymer

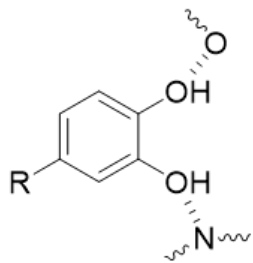
The physicochemical properties of the native extracellular matrix (ECM) can be improved by cross-linking (Choi, Ahn, & Kim, 2022; Heck, Faccio, Richter, & Thöny-Meyer, 2013). There are some limitations in chemically binding ECM materials such as protein and polysaccharide backbone. Chemical crosslinking agents have limited crosslinking ability due to some limited number of out-of-bond or steric access restrictions. In particular, it is known that whey protein can form a crosslink network only when a reducing agent or denaturant is added (Thalman & Lötzbeyer, 2002).

As a crosslinking agent with excellent biocompatibility compared to chemical catalysts, tyrosinase crosslinking studies are attracting attention. It is possible to form a crosslinking network including phenolic residues and amine and thiol residues on the surface of a polymer material or protein in which the phenolic moiety is modified using tyrosinase mediated reaction

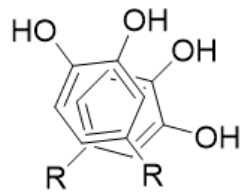
(Pandey et al., 2020). Therefore, tyrosyl residue exposed to the surface of a polymer such as a protein as well as a small molecule substrate acts as a substrate for tyrosinase and is converted into o-quinone to form a spontaneous covalent cross-link (Heck et al., 2013). It is also used for biomaterial manufacturing by cross-linking with a protein or material such as chitosan (H. Kim et al., 2014; S.-H. Kim et al., 2020; S.-H. Kim et al., 2018; Zaidi et al., 2014).

1.3 Intermolecular interaction of catechol and quinone

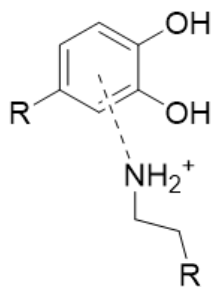
Catechols form non-covalent bonds predominantly. They react with inorganic substances such as metal ions or metal oxide surfaces to create solid but reversible coordination bonds (H. Lee, Scherer, & Messersmith, 2006). The chemical equilibrium of metal-catechol bonds is highly pH-dependent. Coordination bond formation is not favorable at low pH (ca. pH5) due to protonation of the hydroxyl group of catechol, but as the pH increases, ligand affinity improves to form stable bis and tris complexes (Krogsgaard, Nue, & Birkedal, 2016; S. H. Lee et al., 2016). Coordination can protect catechols from oxidation. In addition to the coordination ability of catechols, catechols can participate in hydrogen bonding with polar molecules, π -stacking with aromatic molecules, and cation- π interactions with cations or positively charged groups (Krogsgaard et al., 2016).



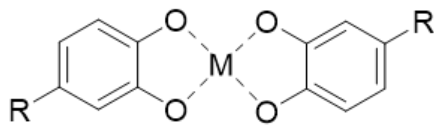
Hydrogen bonding



π - π interaction



π - cation interaction



Metal coordination

Figure 1.4 Non-covalent interactions of catechol

The *o*-quinone group is a highly reactive electrophilic molecule that forms an unstable intermediate, the semi-quinone radical. Thus, quinone produced by tyrosinase can undergo several non-enzymatic secondary reactions to form melanin.(J. Yang et al., 2014) Non-enzymatic secondary reactions include (i) reaction with amine groups; (ii) reaction with thiol groups; (iii) aryloxy radical coupling. *o*-quinones are react with amines via three pathways: (i) Michael-type additions, (ii) Schiff base reaction and (iii) Strecker degradation. The quinone undergoes nucleophilic attack by the amine to form a quinone-amine adduct (Kutyrev & Moskva, 1991; Zaidi et al., 2014). Michael addition between catechol and amine group, covalent crosslinking by Schiff base reaction is affected by pH, type of catechol substituent, and basicity of nucleophilic amine. Since nucleophilic attack must be accompanied by amine deprotonation, the reaction is more friendly at pH above neutral (ca. pH 7) than at low pH (Zaidi et al., 2014).

Similar to the reaction with an amine group, a catechol-thiol adduct can also be formed between the electrophilic *o*-quinone and thiol via Michael addition. The *o*-quinone is spontaneously subjected to a nucleophilic attack by a thiol at position 2 of the benzene ring and can quickly form a catechol derivative. The substituted catechol is re-associated to form an *o*-quinone, which can be subjected to a second nucleophilic attack at position 5 of the benzene ring. Thiol addition to catechol is likewise dependent on the nucleophilic strength. In general, the higher the catechol oxidation rate, the more efficient the conjugation between the two. In addition, the fact that is

crosslinking efficiency changes according to the nucleophilic strength of thiol is also common with amine addition (J. Yang et al., 2014).

o-quinone can react with unoxidized catechol through reverse dismutation to form two highly reactive semi-quinone radicals. Two quinones form a di-catechol crosslinking complex through bonding between the formed radicals (Burzio & Waite, 2000). The ratio between *o*-quinone and catechol determines the rate of quinone-quinone bonding. When all the semi-quinone radicals generated through *o*-quinone dismutation are consumed, crosslinking is terminated (Haemers, Koper, & Frens, 2003). As the reaction pH increases, the catechol oxidation rate increases, so the crosslinking rate naturally increases.

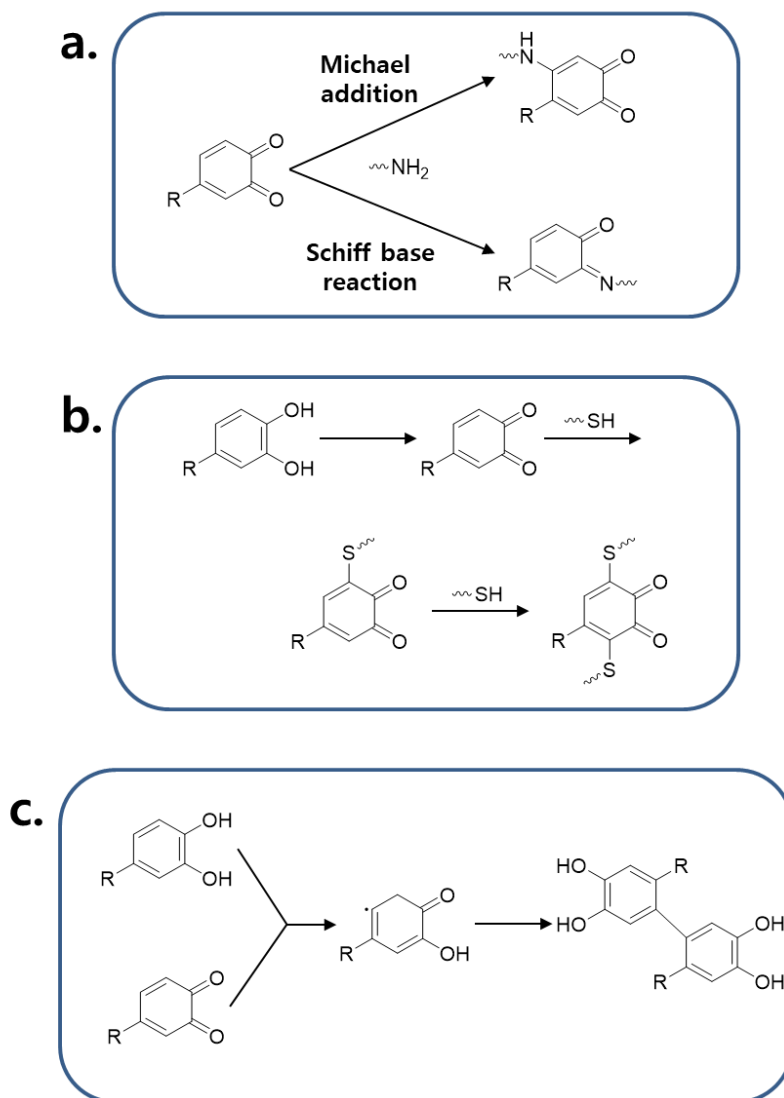


Figure 1.5. Spontaneous crosslinking reaction of quinone

(a) Crosslinking reaction with amine groups, (b) reaction with thiol groups and (c) aryloxy radical coupling

1.4 Scope of thesis

Tyrosinase is a type-3 copper-binding enzyme and consists of domains of various configurations centered on a highly conserved dicopper binding site. Therefore, the substrate specificity and, in particular, the variability of the optimal reaction pH is very widely distributed. Therefore, it has the advantage of designing the reaction by selecting the appropriate tyrosinase by targeting the catecholic or quinolic structure chemicals synthesized through the consecutive hydroxylation reaction from the monophenol substrate. Previously, we identified tyrosinase with unusual activity under acidic conditions, which is considered unfavorable to the tyrosinase reaction mechanism, and tyrosinase with exceptional activity in bulky polymers by analyzing the location of the active site of tyrosinase from the protein surface. We attempted to synthesize a novel biofunctional nanomaterial using tyrosinase with two different properties identified by structure-based analysis.

In Chapter 1, soluble and homogeneous melanin nanoparticle was synthesized by tyrosinase oxidation in acidic conditions where spontaneous oxidation is limited, and physicochemical properties were analyzed. Melanin, which is enzymatically synthesized under neutral to basic pH conditions, is amorphous and heterogeneous due to the complex crosslinking chemistry of catechol and quinone, which limits industrial applications requiring fine-tuning. We focused on the fact that mussel foot protein with surface adhesion functionality is soluble in an acidic environment and cross-linked in a basic

environment. We attempted to synthesize homogeneous and fine-tuning melanin using tyrosinase, which is active in acidic conditions below pH 5.

In Chapter 2, as a method to enhance the stability of the enzyme, we tried to synthesize a robust enzyme-polymer coating through tyrosinase-mediated crosslinking. Through non-covalent interaction with the enzyme, some functional polymers can contribute to improving the stability of the enzyme. Among polymers contributing to enzyme stabilization, the polysaccharide is well known as a biocompatible polymer contributing to enzyme stabilization through hydrophilic and hydrophobic interactions. We tried to provide additional stabilization to the non-covalent bonded complex by introducing a covalent bonding network to the enzyme-polymer coating.

Chapter 2.

Synthesis of soluble melanin nanoparticles under acidic condition using *Burkholderia cepacia* tyrosinase and their characterization

2.1 Abstract

Melanin nanoparticles (MNPs) used for biomedical applications are often synthesized by chemical auto-oxidation of catechol such as dopamine and 3,4-dihydroxyphenylalanine under alkaline conditions. The synthetic method of chemically synthesized MNP (cMNP) was relatively straightforward and more robust to control their homogenous particle size and morphology than corresponding enzymatic methods. In this study, we have demonstrated that a simple enzymatic synthesis of MNP (eMNP) with homogenous and soluble (< 20nm diameter) properties was possible using dopamine and *Burkholderia cepacia* tyrosinase (*BcTy*) under acidic conditions (*i.e.*, pH 3.0). *BcTy* was highly reactive under the pH 5.0 where natural and chemical oxidation of catechol is complex, so melanin was synthesized by hydroxylation of phenolic substrates. Detailed chemical analysis and characterization of physical properties of the eMNPs confirmed higher preservation of catechol and primary amine moieties in the monomer substrate such as dopamine under acidic conditions. The eMNPs showed enhanced antioxidant activity and conferred stickiness to the formed hydrogel compared to the chemical auto-oxidation method owing to a large number of hydroxyl groups remaining as catechol and quinone moiety. Because of these advantages and characteristics, the synthesis of MNPs using *BcTy* under acidic conditions can open another avenue for biomedical applications.

2.2 Introduction

Melanins are natural biopolymers widely distributed in various living organisms. According to their chemical compositions, melanins are classified into three types, eumelanin, pheomelanin, allomelanin (Micillo et al., 2016; Pezzella, Iadonisi, et al., 2009; Sugumaran & Barek, 2016). The most common type of melanin present in the human body is brown-black eumelanin. The eumelanin is usually synthesized by oxidation of tyrosine using copper-containing enzyme tyrosinase, via its cyclized indole compounds such as 5,6-dihydroxyindole-2-carboxylic acid (DHICA) and 5,6-dihydroxyindole (DHI) (Alfieri et al., 2017; Ju, Fischer, & Warren, 2018; Liu et al., 2014; Micillo et al., 2016). Then, eumelanin is synthesized through spontaneous covalent and non-covalent bonding by DHICA and DHI and various precursors derived from thereof (Hong et al., 2012; Hong, Wang, Park, & Lee, 2018; Micillo et al., 2017). The eumelanin from living microorganisms and animals can react and make covalent bonds with other amino acids such as lysine, histidine, and cysteine or proteins during their synthesis, resulting in nano to micro size insoluble particles (25 nm ~ a few μm) with broad size distributions in cells (Ju et al., 2019; Saini, Tripathi, & Melo, 2015). The broad size distribution of melanin particles limits their applications. These insoluble melanin particles with a broad size distribution are limited in their application as they do not have a well-distributed colloidal dispersion.

Thus, MNPs synthesized from the single substrate by chemical method with similar size and morphology (cMNP) are more desirable for industrial and biomedical applications (Bergtold et al., 2018; Huang et al., 2018; Park, Moon, & Hong, 2019; S. J. Yang et al., 2020). Polydopamine nano-particles (here it is called cMNP), synthesized using dopamine monomer by auto-oxidation at alkaline conditions, have a relatively narrow particle size distribution (Ju et al., 2013; Ju, Lee, Lee, Park, & Lee, 2011). However, cMNPs were still somewhat insoluble, and their average diameter of less than 50 nm cannot be easily made. Previous studies have shown that the regulation of the subsequent formation of agglomerates and melanin polymerization rate next to dopamine oxidation reaction affected the process of homogenous melanin nanoparticle formation. To effectively narrow the size distribution of cMNPs during the polymerization, i) varying the concentration of radical initiator/scavenger such as plasma-activated water (T.-P. Chen, Liu, Su, & Liang, 2017), transition metal catalyst (Repenko et al., 2015), potassium manganite (Ju et al., 2018), 2-phenyl-4,4,5,5-tetramethyl imidazoline and edaravone (X. H. Wang et al., 2019), ii) UV irradiation (Lemaster et al., 2019), iii) high temperature and hydrothermal pressure process under acidic condition (Zheng, Fan, Wang, & Jin, 2015) are often employed. However, the enzymatic method could not control MNP synthesis like the simple chemical methods. Therefore, we speculated that if the cross-link of a phenolic substrate inhibited the enzymatic melanin synthesis reaction, it would help produce different forms of eMNPs rather than the large aggregates of cMNPs

and eMNPs.

We noticed that in nature, mussels regulate the degree of crosslinking among DOPA moieties on mussel foot protein (Mfp) by its ambient pH changes to maintain stickiness for surface adhesion. Mussels in seawater secrete Mfp with a high DOPA content (~ 30 mol%) to adhere to the surface of ship bottom or rocks for a living, and the DOPA is known to be generated by post-translational modification of the Mfp via *ortho*-hydroxylation at its tyrosine residues (Danner, Kan, Hammer, Israelachvili, & Waite, 2012; Lin et al., 2007). Mussel uses hydrogen bonding and metal chelation between catechol residues of DOPA and the surface of target materials (Lin et al., 2007; Lu et al., 2013). To maintain the high DOPA content, the mussel should change the pH of Mfp to a more acidic condition (pH 2.0 ~ 5.0) against ambient seawater (pH 8.0). As a result of lowering the pH around Mfp, auto-oxidation of the catechol residue of DOPA is suppressed, and its crosslinkings with the amine or thiol group of highly reactive amino acids are prevented. Based upon such observation, we hypothesized that maintaining such high DOPA content in Mfp is possible by only controlling acidic pH conditions of the Mfp expression. Then, eumelanin-like nanoparticles synthesized under such acidic conditions are expected to be somewhat different from the large aggregates of melanin synthesized by enzymes under neutral to alkaline conditions generally found *in vitro* reaction systems. Therefore, tyrosinase reactions under acidic conditions were examined to support the hypothesis.

Previously, we identified *Burkholderia thailandensis* tyrosinase (*BtTy*,

AWY65947.1) having optimal activity at pH 5.0 (Son et al., 2018), and tried to find new tyrosinases having optimal activity at lower than pH 5.0. Recently, based on the amino acid sequence of *BtTy*, we identified *Burkholderia cepacia* tyrosinase (*BcTy*, SEU13261.1) having activity even at pH 3.0. Here, to prove our hypothesis and better understand melanin biosynthesis, we synthesized a homogenous but also soluble eMNP from dopamine using newly found tyrosinase, *BcTy*. For the comparison, both cMNPs from dopamine by auto-oxidation under acidic to alkaline condition and eMNPs synthesized from dopamine using tyrosinase at alkaline solution were used as controls. Physicochemical properties of the eMNPs and cMNPs were compared using various tools such as UV-vis spectrometer, mass spectrometer, XPS, SEM, TEM, and FTIR. Throughout this study, we could better understand how homogenous and water-soluble eMNP can be synthesized by the enzymatic method under acidic conditions, where auto-oxidation of catechol moiety is suppressed. Then we can apply the synthesis of soluble eMNPs to various other applications using optimized tyrosinase reaction and variations of substrates such as tyramine, tyrosine methyl ester (TME), 3,4-dihydroxyphenyl acetic acid (DOPAC), and synephrine.

2.3 Materials and methods

2.3.1 Materials

NcoI and HindII restriction enzymes were purchased from Thermo Scientific. Luria-Bertani(LB) broth, LB agar were purchased from BD Difco (Sparks, USA). Ni-NTA agarose was purchased from Qiagen (Hilden, Germany). Acetic acid and Amicon 0.5 ml 3K filter was purchased from Merck (Darmstadt, Germany), dopamine hydrochloride, copper sulfate, and all the other chemicals were purchased from Sigma-Aldrich Korea (Seoul, Republic of Korea). *Burkholderia cepacia* (ATCC 25416) were purchased from the Korean Agricultural Culture Collection (KACC, Wanju, Republic of Korea).

2.3.2 Plasmid construction

For the construction of plasmid expressing tyrosinase, pET28a was used in the previous paper (Son et al., 2018), and produced through the circular polymerase extension cloning (CPEC) (Quan & Tian, 2011) method. The primer list is in **Table 2.1**. Genomic DNA for cloning was extracted from *Burkholderia cepacia* (*Bc*) using a G-spin genomic DNA extract kit (Intron, Republic of Korea), and PCR was performed to amplify the *BcTy* gene (gi: 1095297873) with C-terminal His-tag inserted into pET28a vector using NcoI and HindIII restriction enzyme sites.

Table 2.1 Primer list

Primer	Sequence (5' → 3')
<i>BcTy</i> _F	GGAGATATACCATGGCAAATAACGCATCTGGAGTCAG
<i>BcTy</i> _R	CGGCGGCAAGCTTTCGGACCTCGAGCCGGA
<i>BcTy</i> -pET28a-CPEC_F	GTCCGAAAGCTTGCGGCCG
<i>BcTy</i> -pET28a-CPEC_R	AGATGCGTTATTTGCCATGGTATATCTCC

2.3.3 Expression and purification of *BcTy*

For the expression of *Bc* Tyrosinase (*BcTy*), the expression vector was transformed into *E. coli* BL21 (DE3) by heat shock treatment, and the transformed strain was selected on LB agar plate with antibiotic selection marker kanamycin (50 µg/ml). A single colony was inoculated into a test tube with 3 ml of the same LB broth with kanamycin, and the cell was cultured in a shaking incubator at 37 °C, 200 rpm overnight. 500 µl of cultured cells were transformed into 50 ml of fresh LB medium with antibiotic markers, and then cells were grown to approximately 0.6 at OD₆₀₀. Furthermore, the protein expression was induced by adding 0.1 mM of IPTG and 1.0 mM of CuSO₄. After 20 h at 37 °C culture, cells were harvested by centrifugation at 4000 rpm for 20 min. Cell pellets were resuspended in 50 mM Tris buffer, pH 8.0, and disrupted by ultrasonication. After ultracentrifugation at 16,000 rpm for 30 min, the supernatant was collected. The supernatant was applied to the Ni-NTA agarose column for enzyme purification. Cell lysate was subsequently applied onto the Ni-NTA column after pre-equilibrium with 50 mM Tris buffer, pH 8.0 with 5.0 mM imidazole, and 300 mM NaCl buffer. Bounded proteins were washed with 50 mM Tris buffer pH 8.0 with 30 mM imidazole, 300 mM NaCl buffer. The tyrosinase was eluted by 50 mM Tris buffer pH 8.0 with 250 mM imidazole. The concentration of purified enzyme was measured by Bradford assay.

2.3.4 Synthesis of eumelanin-like nanoparticles

The synthesis of chemically synthesized eumelanin-like nanoparticles (cMNP) was followed using the previously reported method. (Ju et al., 2013; Ju et al., 2011) 3 mg/ml of MNP substrates such as tyrosine, dopamine, 3,4-dihydroxyphenylalanine (DOPA), 3,4-dihydroxyphenylacetic acid (DOPAC), synephrine, and tyrosine methylester were dissolved to 2 ml of 50 mM Tris buffer, pH 8.5 in a clear glass bottle. The oxidation reaction was started at 37 °C with 200 rpm agitation for 12 h. For further analysis, MNP aggregates were collected by centrifugation at 4,000 rpm for 10 min and washed three times with distilled water (DW).

For the synthesis of enzymatically synthesized eumelanin-like nanoparticles [eMNP-*i*, (*i* = 3 - 5)], various pH conditions of acetic acid buffer were prepared. First, 100 mM acetic acid was added to DW, and NaOH was added to adjust to the desired pH (pH 3.0, 4.0, 5.0). Next, 200 nM of *BcTy* and 10.0 μM of CuSO₄ tyrosinase Cu²⁺ cofactor were added to 3 ml of acetic acid buffer in a glass bottle. Then 3mg/ml of MNP substrate dissolved in DW were added to the reaction solution. eMNPs were synthesized under 37 °C with 200 rpm agitation for 12 h. eMNP-3PEG was synthesized under the same reaction condition as eMNP-3s. 3 mg/ml of dopamine were added to the reaction mixture to prepare the eMNP-3 for overnight reaction. Next, 1.0 mg/ml of terminal thiol-modified polyethylene glycol (PEG-SH) was added to 100 mM pH 3.0 acetic acid buffer, then eMNP-3PEG was synthesized

under 37 °C with 200 rpm agitation for 12 h. eMNP-3PEG was filtered with Amicon Ultra 0.5 mL 3K filter to remove unreacted PEG-SH.

2.3.5 Instrumental analysis

UV-vis spectrum of cMNP and eMNPs were measured by SPECTROstar Nano UV-vis spectrophotometer (BMG LABTECH, Germany) from 220 nm to 1000 nm. The average hydrodynamic diameter and zeta potential of the MNPs were measured by dynamic light scattering (DLS) using a Zetasizer Nano-ZS system (Malvern Instruments, Inc., UK). The particle size measurement of cMNP and eMNPs were performed using field emission scanning electron microscopy (FE-SEM). cMNP and eMNPs were freeze-dried and platinum-coated in sputter before the FE-SEM analysis. The morphology and size were analyzed by FE-SEM 7800 Prime (JEOL Ltd., Japan) installed at the National Center for Inter-University Research Facilities (NCIRF) at Seoul National University with an accelerating voltage of 5.0 kV. Particle size was analyzed using ImageJ software. The particle size measurement and physical characterization of soluble eMNP-3 were performed using Transmission Electron Microscope (TEM, JEM-2100F, JEOL Ltd., Japan) and Cs-corrected transmission electron microscopy (Cs-TEM, JEM-ARM200F, JEOL, Japan) with an accelerating voltage of 200 kV. The soluble eMNP-3 was placed on a TEM grid (lacey carbon grid, 3 mm, 300 mesh) and dried before TEM analysis. Particle size and the gap between

onion-like stacking structures were analyzed using ImageJ software. Attenuated total reflectance Fourier transform infrared (FTIR/ATR) analysis was performed using TENSOR27 (Bruker, Germany) installed at the NCIRF at Seoul National University. All MNP samples were freeze-dried before the FTIR/ATR analysis. Scans were acquired between 4000 cm^{-1} and 400 cm^{-1} . The peak resolution was 0.4 cm^{-1} , and the number of scans was 32. Baseline correction for each sample was performed using OriginPro 2020b. X-ray photoelectron spectroscopy (XPS) analysis was performed by UHV Multipurpose Surface Analysis System (Sigma Probe, Thermo, UK) operating at base pressure under 10^{-9} mbar. Each Photoelectron spectrum was excited by Al Ka (1486.6 eV) anode operating at a constant power of 105 W (15 kV and 10.0 mA). cMNP and eMNP samples (*i.e.*, 100 μl) were dried on a 1 cm x 1 cm silica wafer under vacuum conditions before the XPS analysis.

2.3.6 Evaluation of the antioxidant activity of the soluble MNP

The antioxidant activity of MNPs was studied using a 2,2-diphenyl-1-picrylhydrazyl (DPPH) color change assay known as the free radical scavenging activity assay. (Mishra, Ojha, & Chaudhury, 2012; Sharma & Bhat, 2009) For the DPPH assay, ascorbic acid, cMNP, eMNP-3, and eMNP-3PEG were compared. For this experiment, 0.2 mM of fresh DPPH solution in methanol was prepared. First, various amounts (0 to 14 μl , final concentration

of 0 to 0.07 mg/ml in 200 μ l) of antioxidants were divided into 100 μ l of pH 7.4 PBS buffer in a 96 well plate. Then, 100 μ l of DPPH solution was added to make the reaction mixture with the final concentration of 0.1 mM of DPPH. The reaction mixture was incubated for 20 min at 37 °C under dark conditions. After the incubation was completed, the absorbance of the solution against the blank was measured at 517 nm. The following equation calculated the radical scavenging activity.

$$I \text{ (Scavenging effect, \%)} = \frac{1 - (A_i - A_j)}{A_c} \times 100$$

Where A_i is the absorbance of test sample, antioxidant and DPPH solution, A_j is the absorbance of antioxidant solution without DPPH as control, and A_c is the absorbance of DPPH solution without antioxidant. The EC_{50} refers to the concentration at which the antioxidant can scavenge radicals corresponding to 50% of DPPH concentration, calculated using the non-linear regression method by GraphPad prism 7.0.

2.3.7 Synthesis of sticky eMNP-gelatin hydrogel and characterization

For the preparation of sticky hydrogel, 10.0 wt% of gelatin was dissolved in 100 mM acetic buffer (pH 3.0) at 40 °C. After gelatin was entirely dissolved and bubbles in the reaction solution were removed by sonication, 3 mg/ml of dopamine and 10.0 μ M of $CuSO_4$ were added into 2 ml of gelatin (10.0 wt%)

solution. Dopamine was not included in the control hydrogel sample. The gelatin mixture was incubated in a water bath at 37 °C for 15 min. Next, the 1.0 μM of *BcTy* was added to the mixture to initiate the crosslinking reaction between gelatin and eMNP. Then, 190 μl of the reaction mixture was crosslinked in the customized polydimethylsiloxane (PDMS) mold of 16 mm diameter and 5 mm thickness overnight, at 37 °C.

The mechanical properties of the hydrogel were measured using a Universal Testing Machine (UTM, 100 N of the load cell, EZ-SX STD, Shimadzu, Japan). After an overnight crosslinking reaction, the hydrogel samples were placed on the sample table. The probe was compressed vertically at a 2 mm distance from the top of the hydrogel to measure the adhesion force. After 10 sec, the probe was lifted to the upward position at a speed of 3 mm/min to measure the adhesion force of the hydrogel attached to the table surface. Each hydrogel was compressed vertically with a 3 mm/min speed to measure the mechanical strength, and Young's modulus was calculated from UTM strain-stress curve data.

2.4 Result and discussion

2.4.1 Production of soluble eMNPs at acidic pH using

BcTy

Based on the hypothesis that soluble eMNPs with high catechol-moiety content at acidic condition, we identified *BtTy* and *BcTy*, a tyrosinase with activity even at pH 5.0 or lower by heterogeneous expression system of *E. coli*. *BcTy* purified through His-tag had the highest enzyme efficiency (k_{cat}/K_M) for l-tyrosine and L-DOPA among bacterial tyrosinases reported so far (**Table 2.2**), and showed optimal activity at pH 4.0 and activity even at pH 3.0 (**Figure 2.1**). Thus, eMNP can be produced from 3 mg/ml of substrates by 200 nM of *BcTy* (0.012 mg/ml) with 10 μ M of CuSO₄ for tyrosinase cofactor in 3 hours. We synthesized eMNPs from dopamine using *BcTy* at pH 3.0 to 5.0 [named eMNP-*i* (*i* = pH value)] and compared their physicochemical properties with those of controls, *i.e.*, eMNP-8 and cMNP synthesized at alkaline condition (**Figure 2.2**).

Table 2.2 Kinetics of tyrosinases (Ty).

	Optimum pH	Substrate	V _{max} ($\mu\text{mol}\cdot\text{min}^{-1}\cdot\text{mg}^{-1}$)	K _m (mM)	k _{cat} (s ⁻¹)	k _{cat} /K _m (mM ⁻¹ ·s ⁻¹)
<i>Agaricus bisporus</i> Ty (Fenoll et al., 2001)	6	L-Tyrosine	10.8	0.25 ± 0.03	7.9 ± 0.12	31.60
		L-DOPA	145.9	0.28 ± 0.01	107.3 ± 1.45	383.21
<i>Bacillus megaterium</i> Ty (Deri et al., 2016)	8	L-Tyrosine	3.62 ± 0.06	0.082 ± 0.006	2.1	25.60
		L- DOPA	30.3 ± 0.6	0.24 ± 0.02	17.8	74.20
<i>Streptomyces avermitilis</i> Ty (N. Lee et al., 2015)	7	L-Tyrosine	1.05 ± 0.037	0.589 ± 0.056	0.021	0.04
		L- DOPA	9.67 ± 1.85	2.79 ± 0.79	0.19	0.07
<i>Burkholderia thailandensis</i> Ty (Son, Lee, Lee et al. 2018)	5	L-Tyrosine	404.24 ± 18.88	0.59 ± 0.055	397.5	668.63
		L- DOPA	495.42 ± 44.66	0.83 ± 0.13	487.17	586.74
<i>Burkholderia cepacia</i> Ty (This study)	4	L-Tyrosine	335.58 ± 31.49	0.22 ± 0.04	333.9 ± 31.33	1504.94
		L- DOPA	1812.12 ± 299.35	2.16 ± 0.41	1803.06 ± 297.9	835.42

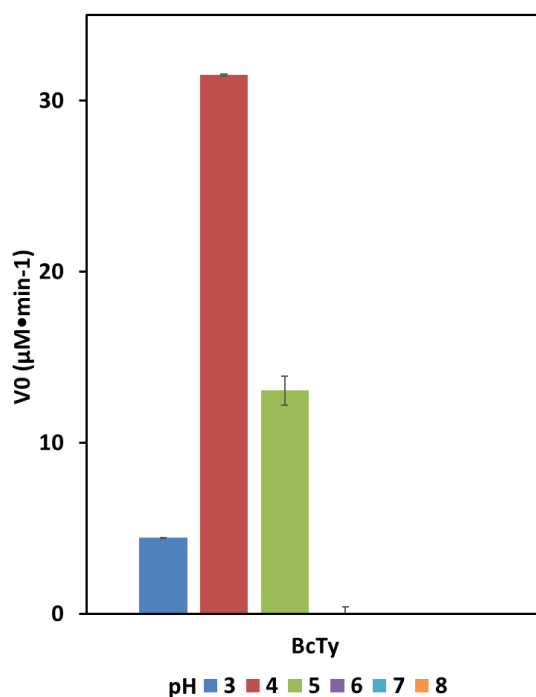


Figure 2.1 Optimal pH of *BcTy* activity.

Assay Assay was performed by measure a conversion of l-tyrosine by *BcTy* under each 50 mM buffer (pH 3.0, 4.0, 5.0: citric buffer, pH 6.0, 7.0: phosphate buffer, pH 8.0: Tris buffer). For the assay, 100 μl of 400nM *BcTy* solution with 10 μM of CuSO_4 was mixed with 100 μl of 2 mM l-tyrosine solution. The total reaction volume was 200 μl at 37°C. For initial velocity measurements, UV absorption at 475 nm ($\epsilon = 3600 \text{ M}^{-1}\text{cm}^{-1}$) was recorded every 1 min by a UV spectrometer for a total of 30 min. The initial velocity of *BcTy* (V_0) was calculated by plotting the initial 5 points of the response, based on the triplet set of the experiment.

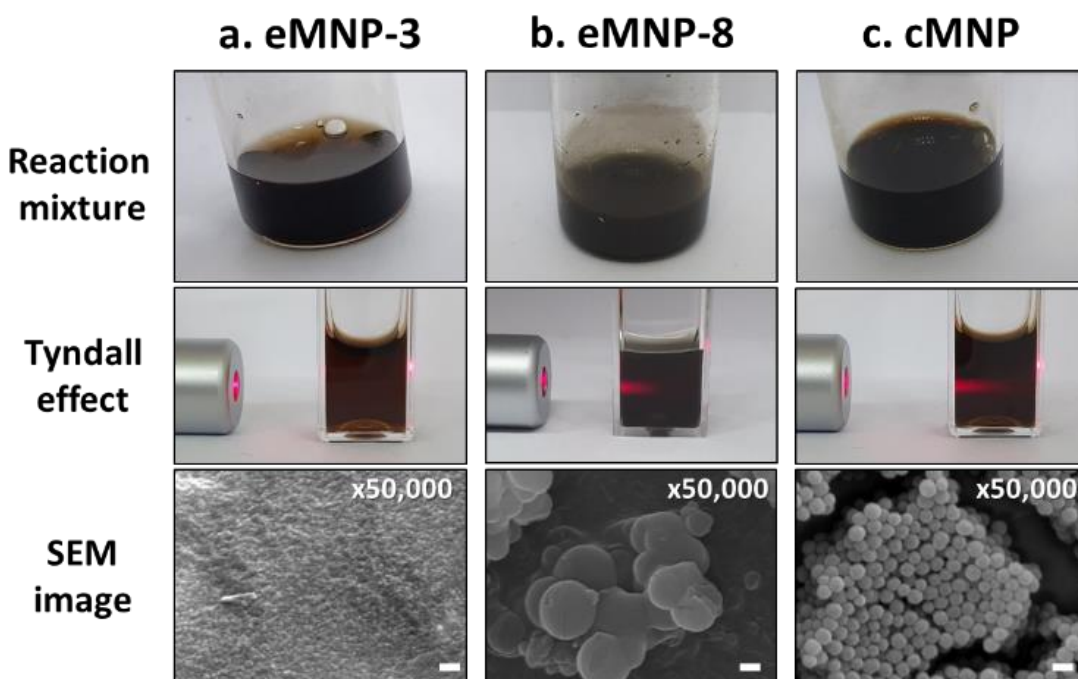


Figure 2.2 Digital pictures of melanin reaction solutions and Tyndall effect of MNPs. by irradiating 660 nm red laser synthesized from 3 mg/ml of dopamine using various synthesis methods and their scanning electron microscopy images

(a) pH 3.0 – BcTy 200 nM, (b) pH 8.0 – BmTy 200 nM, (c) pH 8.5 – chemical auto-oxidation method using Tris base. Scale bar: 200 nm. The samples for Tyndall effect observation were diluted with water from 3 mg/ml to 0.05 mg/ml.

To investigate the characteristics of eMNPs synthesized from dopamine in acidic conditions of pH 3.0 to 5.0, eMNP-8 was synthesized with *Bacillus megaterium* tyrosinase, which has higher activity than *Agaricus bisporus* tyrosinase at neutral to alkaline pH (S. H. Lee et al., 2016) to compare the properties of eMNPs according to the reaction pHs. In addition, as a control, auto-oxidation of dopamine ($pK_a = 8.93$ (Perrin, 1972)) cannot occur under acidic conditions (pH 3.0 to 5.0), so cMNP was obtained by oxidizing dopamine at 1 mg/ml (6.53 mM) using ammonium persulfate (APS), a strong chemical oxidizing agent. However, cMNPs were not synthesized even using the same mass concentration of APS (*i.e.* 1 mg/ml, 4.38 mM) as dopamine, under acidic conditions at pH 3.0 to 5.0 (**Figure 2.3**). The reaction mixture subjected to the oxidation reaction for a longer time, such as 24 hours, displayed red brown colors by forming melanin-like insoluble particles (**Figure 2.3a, b, and c**). However, UV spectra of cMNP-3, 4, and 5 indicated that most dopamine was not completely oxidized to quinone and remained in the reaction mixture (**Figure 2.3d**). In order to compare the properties of cMNPs synthesized through complete oxidation of the substrate, we compared the physicochemical properties of eMNPs synthesized from *BcTy* with those of cMNP synthesized under basic conditions like in many previous studies.

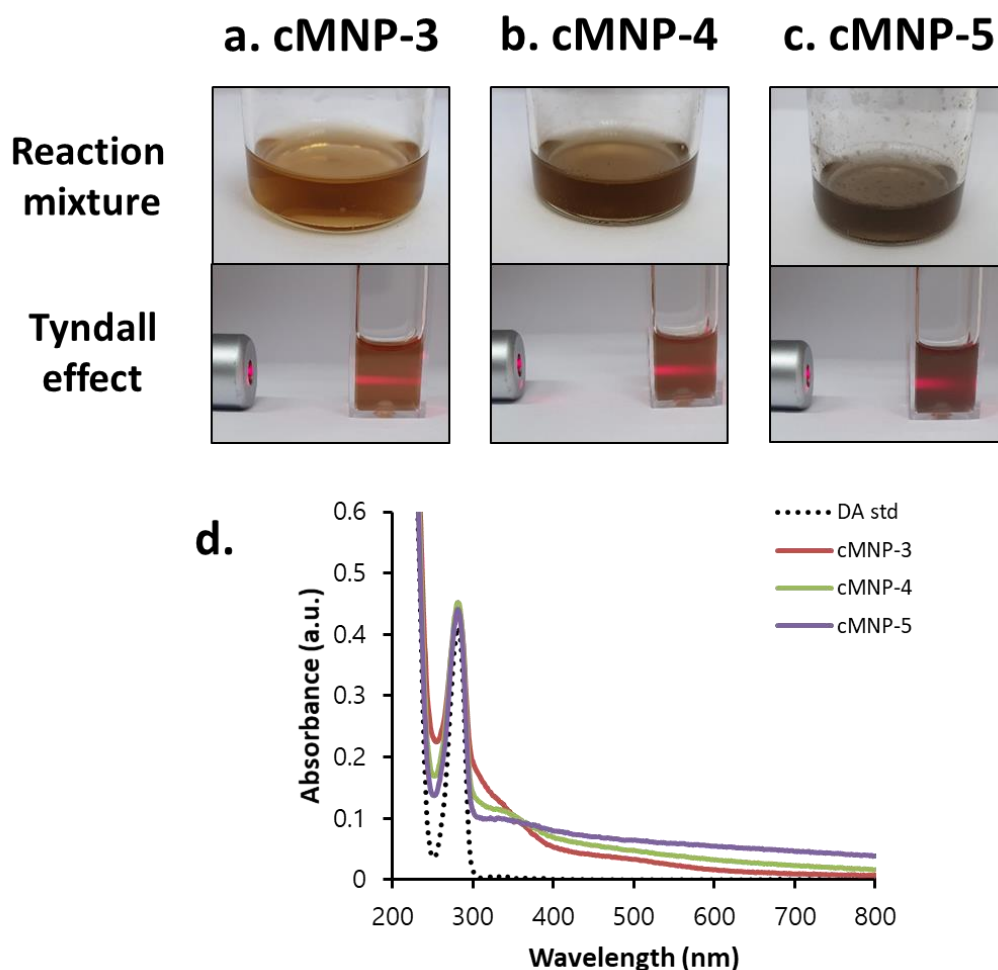


Figure 2.3 Digital pictures of melanin reaction solutions and Tyndall effect by irradiating 660 nm red laser synthesized from 1 mg/ml of dopamine using various synthesis methods and their scanning electron microscopy images

(a) pH 3.0 - APS, (b) pH 4.0 - APS, (c) pH 5.0 – APS. (d) UV spectrum profile of cMNP-3, 4, and 5. The black dot line represents the dopamine 3 mg/ml standard dissolved in DW. The samples for UV spectrum were diluted with water from 3 mg/ml to 0.05 mg/ml.

Both cMNP and eMNP-8 showed insoluble MNPs with the naked eyes, but eMNP-3 synthesized at pH 3.0 was completely soluble (**Figure. 2.2**). When the red laser light (640~660 nm) was irradiated to the reaction mixture, the Tyndall scattering effect was not observed only in eMNP-3, suggesting that the soluble MNP was synthesized under this condition (Ma et al., 2018). SEM image of homogenous eMNP-3s displayed average particle size of *ca.* 7 nm diameter with narrower size distribution than that of cMNPs (**Figure 2.3d, e, and Figure 2.4a**). Moreover, TEM pictures of the eMNP-3 reaction solution contained onion-like pi-pi stacking structures among the phenolic moieties usually found eumelanin-like nanoparticles (**Figure 2.4b**) (Yu, Fan, Liu, Shi, & Jin, 2014). Whereas eMNP-4, -5, and -8 samples tended to produce rather heterogeneous and large micron-sized agglomerates, generating insoluble MNP reaction mixtures (**Figure 2.2b and 2.5**).

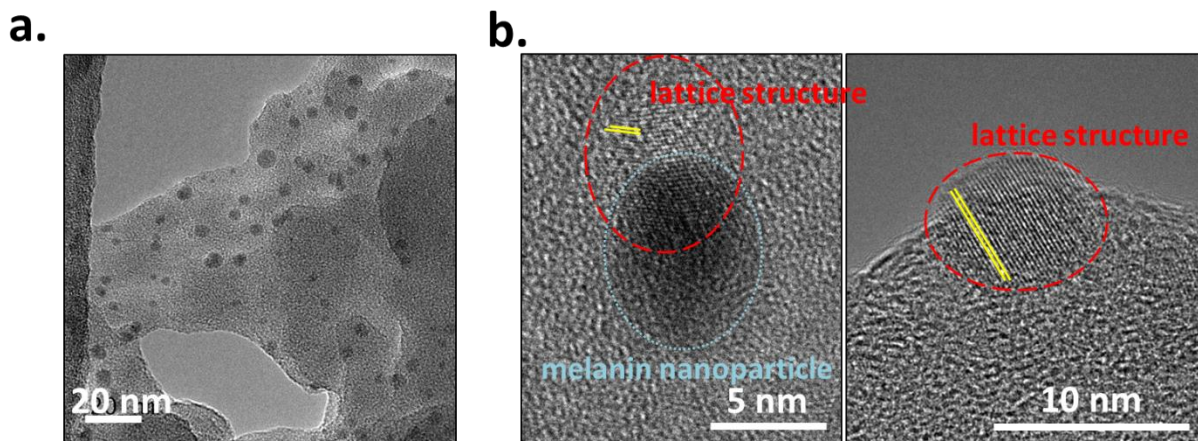


Figure 2.4 TEM image of (a) eMNP-3 and (b) Nano-onion like stacking structure of eMNP-3.

The blue dot line represents melamin nanoparticles, and the red dot line shows the corresponding onion-like stacking structure. The length of each gap between the lattice is approximately 0.3 nm (Yellow line shows the gap between lattice.).

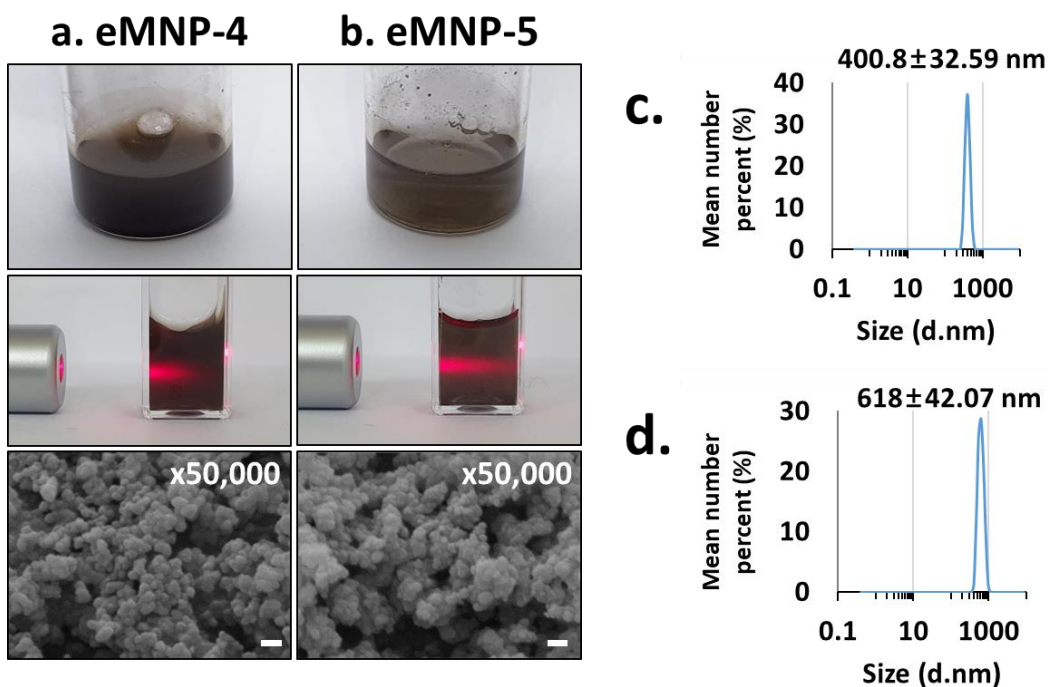


Figure 2.5 Digital picture of melanin reaction solution and Tyndall effect by irradiating 660 nm red laser synthesized from 3 mg/ml of dopamine at acidic conditions. And their scanning electron microscopy image

(a) pH 4 - *BcTy*, (b) pH 5 - *BcTy*. Scale bar: 200 nm. Average hydrodynamic diameters of (a) eMNP-4 and (b) eMNP-5 measured by DLS. The sample for the tyndall effect and DLS was diluted with water from 3 mg/ml to 0.05 mg/ml.

In general, when dopamine is spontaneously oxidized at neutral to alkaline pH, it immediately forms an indole-ring structure by rapid ring cyclization and shows strong absorbance at 475 nm, indicating a dopachrome (C.-T. Chen et al., 2014; Ju et al., 2018; Xie et al., 2019). Since auto-oxidation of dopamine is suppressed under an acidic environment, *i.e.*, pH 3.0 to 5.0, the solution is colorless (data not shown). However, when *BcTy* is added to the pH 3.0 reaction mixture, the dopamine oxidation reaction is initiated, and the solution immediately turns yellow, then red, and gradually changes to brown-black color at the termination of the reaction after 3 h (**Figure 2.6a**). UV spectrum change profile shows that dopamine is oxidized immediately after the reaction starts, and a yellow dopamine quinone ($\lambda = 390$ nm) is formed within 15min (**Figure 2.6b**). Since the decay rate of dopamine quinone is strongly pH-dependent (Thompson, Land, Chedekel, Subbarao, & Truscott, 1985), the production rate of aminochrome by subsequent cyclization of dopamine quinone is diminished. Accordingly, aminochrome ($\lambda = 475$ nm), a cyclization product of dopamine quinone, exhibits the maximum absorbance after 60 min of initiation of the reaction under acidic conditions (C.-T. Chen et al., 2014; Lemaster et al., 2019; Q. Lyu, N. Hsueh, & C. L. Chai, 2019; Micillo et al., 2017; Ponzio et al., 2016; Salomäki, Marttila, Kivelä, Ouvinen, & Lukkari, 2018). As the reaction proceeds, the oligomeric structure of MNP is formed, gradually showing broadband absorption of light spectra, and the product color becomes black. After completion of the reaction, the reaction mixture formed dark brown, and

soluble eMNP-3 was generated in the presence of *BcTy*.

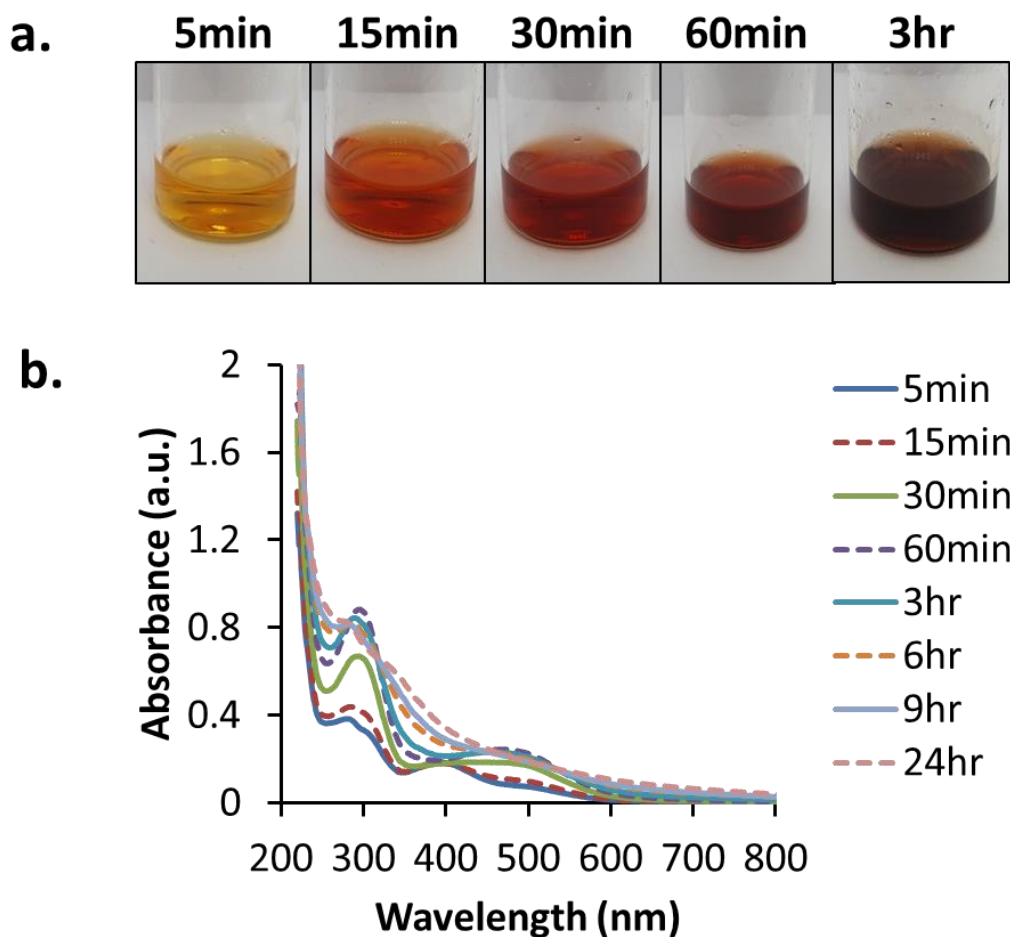


Figure 2.6 Physical properties of eMNP-3 according to synthesis time

(a) Time point image of eMNP-3 reaction solution. (b) UV spectrum profile (220 – 1000 nm) change of the eMNP-3 reaction mixture over time and representative digital picture corresponding to each time points.

To confirm that such soluble eMNP synthesis at acidic pH (*i.e.*, *ca.* pH 3) is a general phenomenon for the synthesizing of soluble eMNPs using other phenolic substrates such as monophenolic, diphenolic, and catecholamine type compounds, further eMNP synthesis using *BcTy* was undertaken at pH 3. All of the phenolic substrates, such as tyramine, tyrosine, DOPA, tyrosine methyl ester (TME), 3,4-dihydroxyphenylacetic acid (DOPAC), and synephrine produced soluble and evenly dispersed eMNPs under this condition (**Figure 2.7 and 2.8**). In addition, the digital image and UV spectra of the reaction solutions of eMNP synthesized from various phenolic substrates, including dopamine, showed that substrates could be oxidized to make eumelanin-like particles, suggesting that the synthesis of the soluble eMNP-3s is a general phenomenon for various substrates at acidic pH.

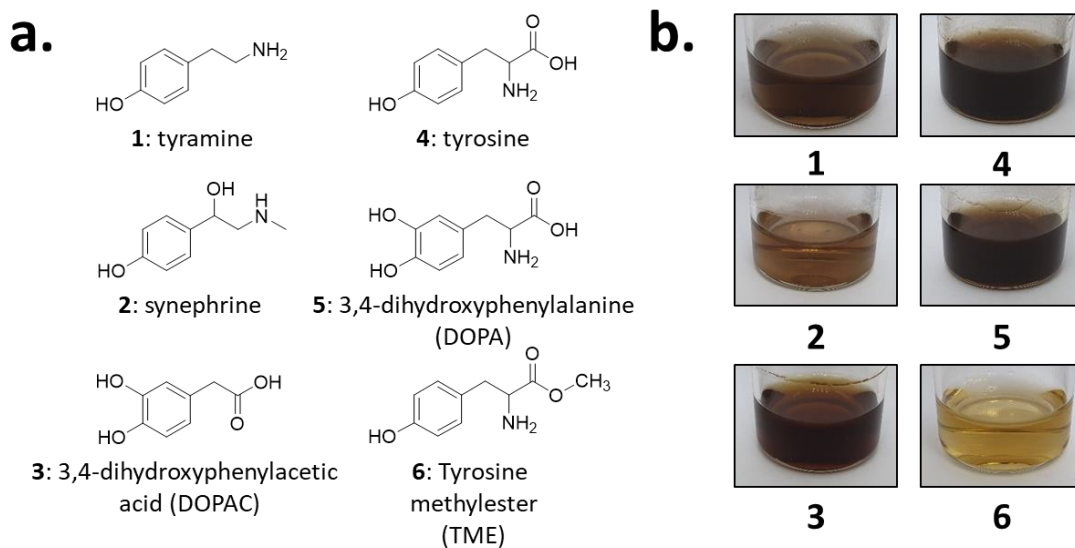


Figure 2.7 Synthesis of soluble eMNPs from phenolic substrates

(a) Chemical structure of eMNP substrates based on the phenolic compound and (b) representative digital image of produced soluble eMNPs.

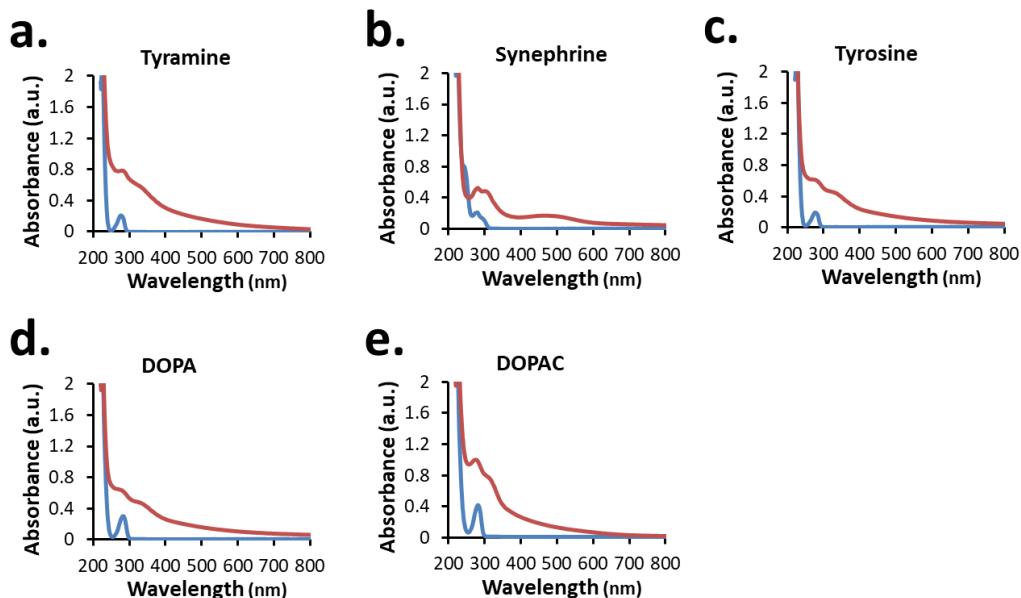


Figure 2.8 UV spectrum profile between eMNP synthesized according to substrate variation

(a) tyramine, (b) synephrine, (c) tyrosine, (d) DOPA, (e) DOPAC - and substrate standard. Blue line indicates substrate standards; red line indicates eMNPs. All sample were diluted with water from 3 mg/ml to 0.05 mg/ml before UV spectroscopy.

2.4.2 Understanding the synthetic mechanism of soluble eMNP-3 through chemical structure and functional group analysis

To better understand how eMNP-3 has a homogeneous particle size distribution like in cMNP but is soluble in water, a detailed analysis was carried out on its chemical structure and surface properties. Although a well-defined chemical structure of MNPs from dopamine cannot be easily identified, the structural details of its oligomeric precursors have been reported using mass spectrometry (Alfieri et al., 2017; Q. Lyu, N. Hsueh, & C. L. L. Chai, 2019; Y. Yang et al., 2015). MALDI-TOF spectra of eMNP-3 and cMNP were compared for the structural analysis (**Figure 2.9**). Here, MNP precursors up to maximum trimers synthesized from dopamine ($[M+H]^+ = 273.20, 305.34, 402.39, 522.75$, **Figure 2.9a, b and 2.10**) and unknown dopamine tri-, tetramer precursors ($m/z = 487.48, 503.60, 521.38$, **Figure 2.9b**) were annotated (Alfieri et al., 2017; Q. Lyu et al., 2019; Y. Yang et al., 2015). There were no significant differences in the oligomeric chemical structure of MNPs. However, in the eMNP mass spectra, unlike that of the cMNPs, the dopamine monomer ($[M+H]^+ = 154.09$, **Figure 2.9a and 2.10** / $[M+Na]^+ = 176.07$, **Figure 2.9b and 2.10**) and dopamine quinone ($[M+H]^+ = 152.07$, **Figure 2.9a and 2.10**) were detected, suggesting the presence of non-cyclized and/or non-cyclized monomers in the eMNPs.

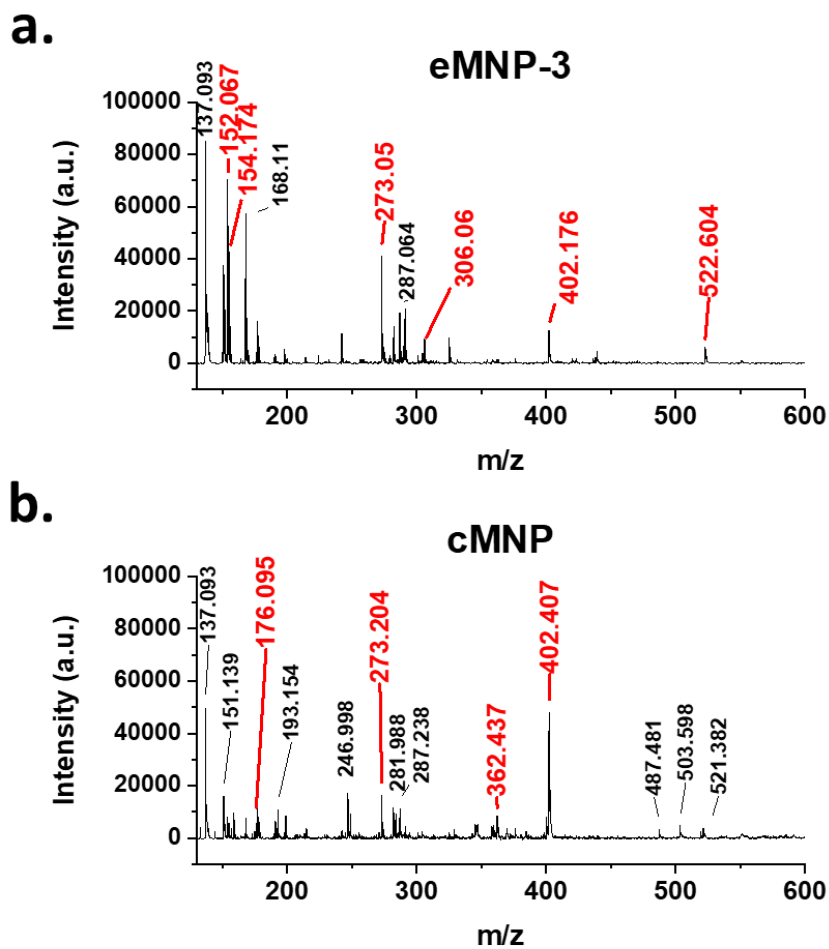


Figure 2.9 Comparison of MALDI-TOF mass spectra of (a) eMNP-3 and (b) cMNP.

The mass values indicated by the red line and red text are values that can predict the chemical structure, and the expected chemical structure is indicated in **Figure 2.10**.

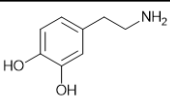
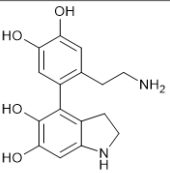
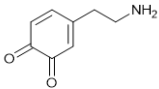
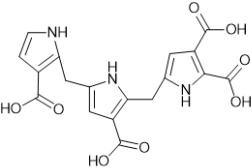
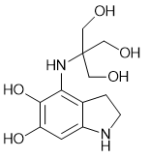
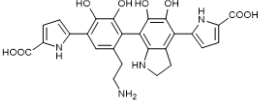
Chemical structure	m/z	Chemical structure	m/z
	154.09		305.34
	152.07		152.07
	273.20		273.20

Figure 2.10 The predicted chemical structure of dopamine oligomeric derivatives using positive mode of MALDI-TOF

Further ATR-FTIR spectroscopy was used to identify functional groups on cMNPs and eMNPs using the dry powder of cMNPs and eMNPs (**Figure 3**). The broad peaks spanning 3600-2800 cm^{-1} in the FTIR spectra of cMNP and eMNP-3 (**Figure 3a**) indicate O-H stretching in both MNPs (X. H. Wang et al., 2019). The peaks that can be annotated as indole structures appeared over 1600-1050 cm^{-1} (Q. Lyu et al., 2019) (**Figure 3a**). In both eMNP-3 and cMNP FTIR spectra, absorption of benzene ring C-C or -NH in the heterocycle ring at 1507 cm^{-1} and hydroxyindole O-H group at 1276 cm^{-1} was observed (Luo et al., 2015; Sun, Zu, Koch, Rappich, & Hinrichs, 2019). In addition to the peak of hydroxyindole in which the dopamine substrate is ring-cyclized, eMNP-3 showed somewhat smaller absorption peaks at 1507 cm^{-1} and 1276 cm^{-1} than that of cMNP, indicating the presence of a non-cyclized hydroxyindole monomer. The absorption of the aliphatic carbon peak at 2980 cm^{-1} , the aromatic C=C or C-O of benzene ring of dopamine at 1604 cm^{-1} and the carbonyl C=O bond peak of hydroxyquinone at 1705 cm^{-1} is observed in eMNP-3 spectrum (Dreyer, Miller, Freeman, Paul, & Bielawski, 2012; Kashima, Tomotake, & Omote, 1987). The peak absorption intensity of 1705 and 1604 cm^{-1} increased according to the decrease in the reaction pH of eMNP synthesis (**Figure 2.11**). Intermolecular covalent bond is formed by Michael addition and Schiff base reaction between quinone-type melanin precursors generated after dopamine oxidation reaction, and if intramolecular cyclization is increased, absorption of indole ring related peak will increase. Therefore, the presence of higher absorbance peaks of aliphatic C-H and C=O stretching

in the FTIR spectrum of eMNP-3 than that in the spectrum of cMNP suggest the presence of a non-cyclized dopamine monomer (Dreyer et al., 2012).

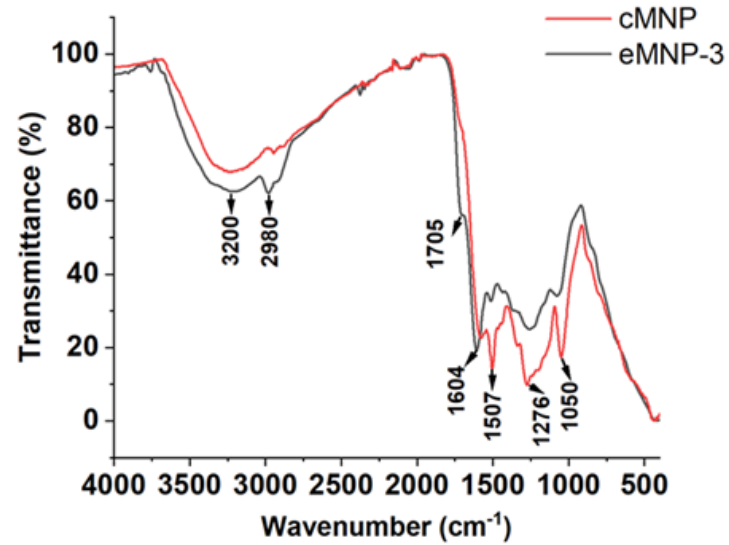
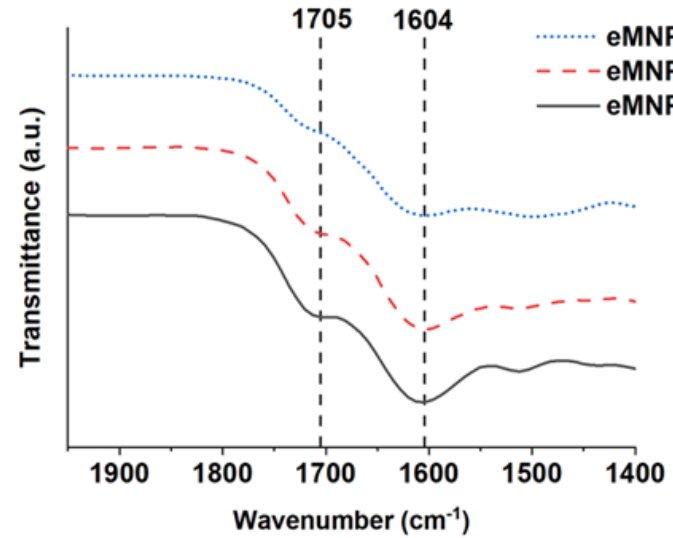
a.**b.**

Figure 2.11 (a) Comparison of FTIR spectra of eMNP-3 and cMNP. (b) Increasing trends of C=O stretching and N-H bending were observed according to the decrease in the eMNP synthesis pH at 5.0 to 3.0.

To specify the functional groups of the non-cyclized monomer, surface element compositions and chemical state of eMNP-3 and cMNP were analyzed and compared through XPS (**Table 2.3, Figure 2.12 and 2.13**) (F. Li et al., 2018; Zheng et al., 2015). In eMNP-3, the C-N and C-O bond peaks decreased, whereas the C-C (sp^1) and C-H bond peaks increased (**Table 2.3, Figure 2.12a, and 2.12d**). In addition, according to the O 1s elemental composition data of eMNP, the peak area ratio of C=O functional groups to C-O/N-O bonds increased slightly to 6.81 (= 87.2/12.8) (**Table 2.3c and Figure 2.12c**), compared to that of cMNP *i.e.*, 4.03 (= 80.1/19.9) (**Table 2.3c and Figure 2.12f**). The C 1s and O 1s deconvolution spectrum showed cMNPs had a more covalently cross-linked structure among MNP precursors with a cyclized indole structure than eMNPs (F. Li et al., 2018; Zheng et al., 2015). C1s, N1s and O1s deconvolution spectra, together with mass analysis and FTIR spectrum, consistently suggested that more acyclic monomers remain in eMNP-3. Primary amines remaining without cyclization in the chemical structure of dopamine monomer could be confirmed by the N 1s deconvolution spectrum (Ponzio et al., 2016; Zheng et al., 2015). The primary amine peak in XPS spectra (R-NH₂, 402.03 eV) was substantially increased in eMNP-3 to 81.0% compared to 32.0% in cMNP (**Table 2.3b, Figure 2.12b and 2.12e**). In addition to the inhibition of self-cyclization of dopamine under acidic reaction conditions below pH 5, deprotonation of the primary amine group of dopamine is also inhibited. Consequently, the particle size with less than 20nm eMNP-3 is attributed to the low pH condition acting

critically. Although dopamine quinone is rapidly formed by the added tyrosinase, as acidic conditions inhibit additional cyclization, the content of residual dihydroxy and quinone forms of dopamine derivatives participating in MNP polymerization is relatively high. Due to the abundance of non-cyclized dopamine derivatives, the presence of a large amount of positively charged primary amines under neutral pH storage solution (e.g., pH 7.4 PBS), eMNP-3 could be expected to have a higher surface charge potential than cMNP.

Table 2.3 XPS peak binding energy assignments to (a) C 1s, (b) N 1s, and (c) O 1s functional groups and peak area ratio for each functional groups

a. C 1s (area, %)		
Chemical bond (binding energy, eV)	eMNP-3	cMNP
C-C and C-H (284.87)	50.0	35.0
C-N and C-O (286.21)	48.4	57.9
C=O (288.37)	1.6	7.1
b. N 1s (area, %)		
Chemical bond (binding energy, eV)	eMNP-3	cMNP
R ₂ -NH (400.17)	19.0	68.0
R-NH ₂ (402.03)	81.0	32.0
c. O 1s (area, %)		
Chemical bond (binding energy, eV)	eMNP-3	cMNP
C-O / N-O (531.62)	12.8	19.9
C=O (533.35)	87.2	80.1

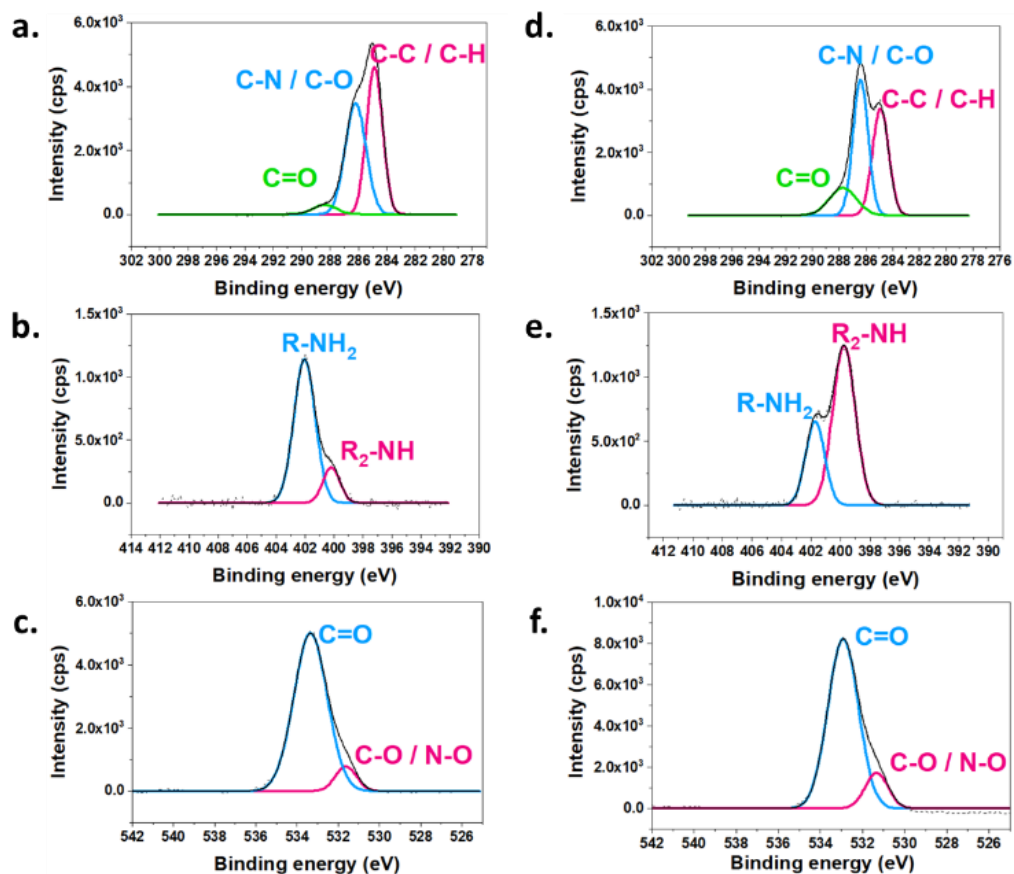
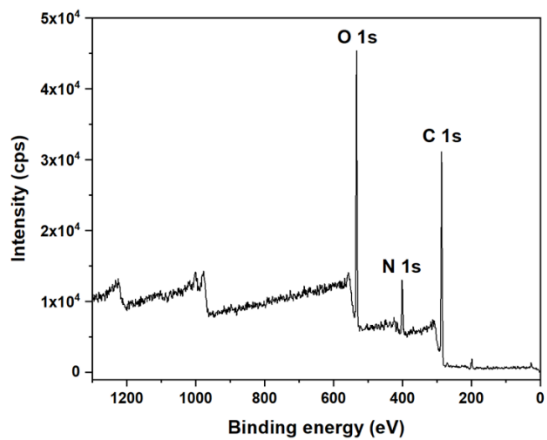


Figure 2.12 XPS spectra showing the C 1s, N 1s and O 1s peaks of eMNP-3 and cMNP.

(a) C 1s of eMNP-3, (b) N 1s of eMNP-3, (c) O 1s of eMNP-3, (d) C 1s of cMNP, (e) N 1s of cMNP, (f) O 1s of cMNP are shown, respectively.

a.



b.

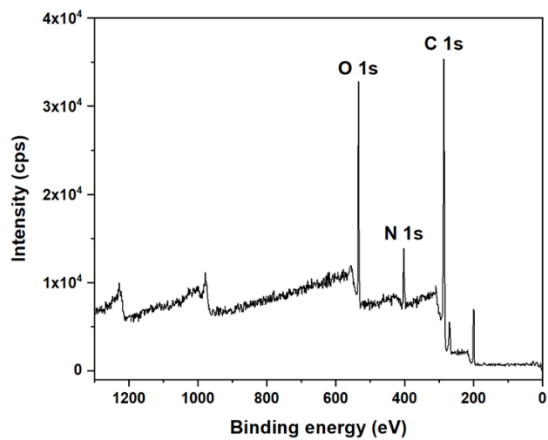


Figure 2.13 XPS survey spectrum of (a) eMNP-3 and (b) cMNP

2.4.3 Characterization of surface zeta potential properties of eMNPs

Melanin nanoparticles generally appear to have rather negatively charged surface properties due to free radicals generated by *o*-quinone moieties on the surface. The zeta potential of eMNP-3s at pH 3.0 was *ca.* +30.13 mV, but the value changed and was eventually determined by the pH of their storage buffer solution. Therefore, the zeta potential of eMNP-3s in DW displayed a negative value (*i.e.*, -6.51 mV) but smaller than that of cMNPs (-34.4 mV). eMNP-3s dissolved in pH 7.4 PBS buffer had a potential of -10 mV (**Table 2.4**), suggesting that the values of surface zeta potential of eMNP-3s are somewhat negatively proportional to the increase in pH of the storage solution (**Figure 2.14**).

It was well known that when the surface charges of the colloidal nanoparticles are within the range of -5 to +5 mV, the electrostatic attraction among the particles tends to induce particle agglomeration. Since the surface zeta potential of eMNP-3s at physiological pH (*i.e.*, pH 7.4) gradually tends to decrease down to *ca.* -10 mV, electrostatic repulsive forces become dominating, and they are readily dispersible and stable enough to be applied under biological conditions without any problems. However, the eMNP-3s in pH 7.4 PBS buffer were slowly aggregated within four weeks of storage and completely precipitated (**Figure 2.15a**). To improve the dispersity of the soluble eMNP-3s under physiological conditions, surface coating with

terminal thiol modified polyethylene glycol(PEG-SH) was carried out following a previous report (**Figure 2.15b**) (Ju et al., 2016; Ju et al., 2013). The resulting surface PEGylated eMNP-3s had a larger hydrodynamic diameter of 32.67 ± 12.72 nm (**Figure 2.15c**), and the soluble eMNP-3PEGs were well dispersed and stably maintained in pH 7.4 PBS buffer for more than three months under ambient conditions (data not shown).

Table 2.4 Average hydrodynamic diameters and zeta potential of eMNP-3, 4, 5 and cMNP measured by DLS.

*All of the samples for zeta potential measurement were diluted to 0.05 mg/ml using PBS (pH 7.4).

	Hydrodynamic diameter (nm)	Zeta potential (mV)*
eMNP-3	7.13 ± 0.97	-6.51
eMNP-4	400.8 ± 32.59	-9.15
eMNP-5	618 ± 42.07	-12.8
cMNP	153.96 ± 19.71	-34.4

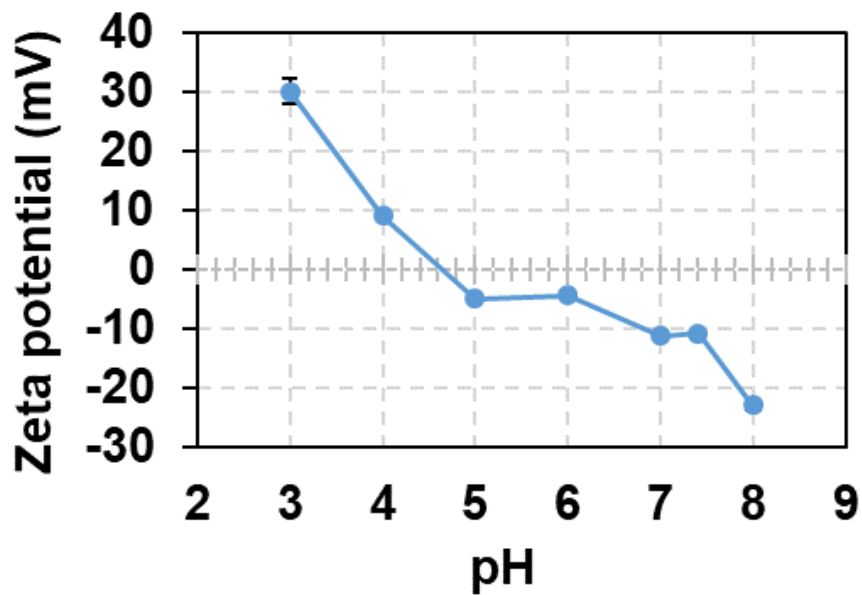


Figure 2.14 Changes in zeta potential of eMNP-3 by varying storage pH buffers.

All of the samples were diluted with storage buffer from 3 mg/ml to 0.05 mg/ml.

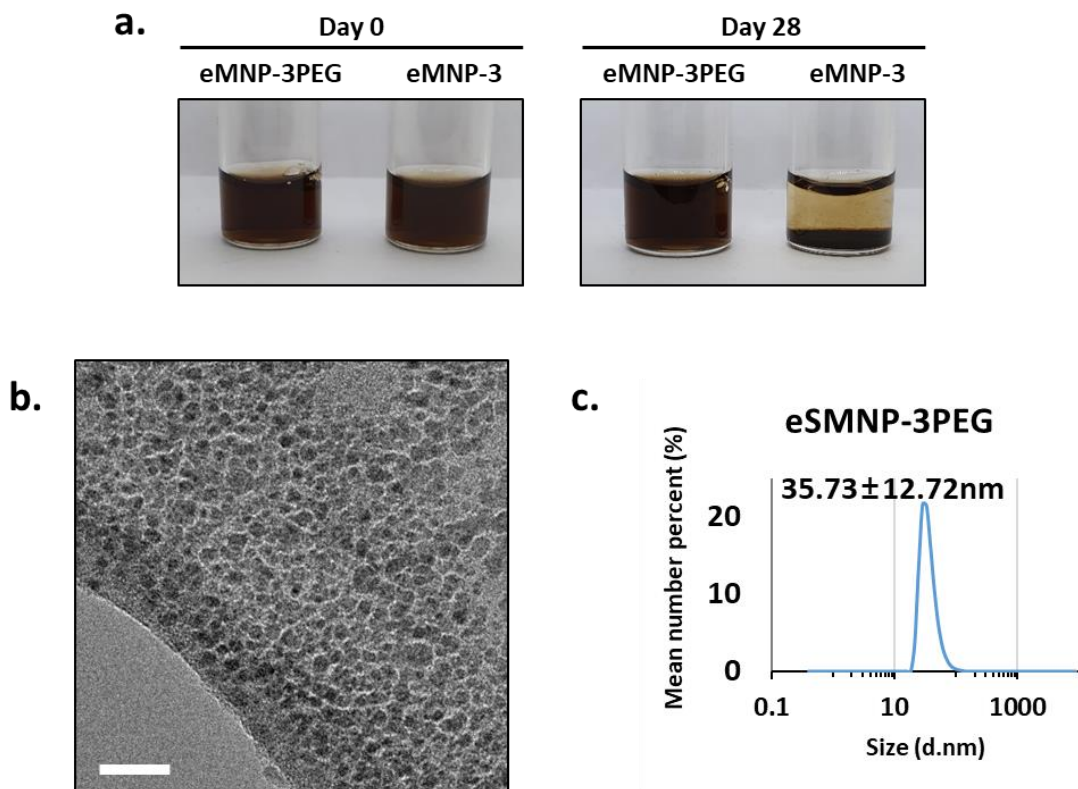


Figure 2.15 Surface modification of soluble eMNP.

(a) PEG-modified eMNP (eMNP-3PEG) stably dispersed in phosphate-buffered saline (PBS) over 4 weeks. (b) TEM image and (c) hydrodynamic diameter of eMNP-3PEG. Scale bar: 20 nm. The sample was diluted with water from dopamine concentration of 3 mg/ml to 0.05 mg/ml.

2.4.4 Evaluation of antioxidant effect of soluble and ultra-small eMNP

The exact cause of the action of melanin as a radical scavenger is difficult to conclude, and various causes are known. However, as one of the important factors, melanin is considered a very good antioxidant biomaterial because the subunits contain a significant amount of a catechol and quinone moiety that can act as both an electron acceptor and a donor (Hu et al., 2020). Therefore, as the contact surface with the radical scavenging functional group located on the MNP surface increases, the surface area of the nanoparticles decreases, and the antioxidant effect also increases (Ju et al., 2011; X. H. Wang et al., 2019; Xiang et al., 2017). Since eMNP-3s are nanoparticles with a diameter of below 10 nm, they can show high free radical scavenging activity owing to a high surface-to-volume ratio. In addition, like in the previous functional group analysis, it can be expected that the radical scavenging activity is further increased by the catechol and quinone form of dopamine, which plays an essential role in the scavenging of radicals present with significant content in eMNPs. According to the analysis of the reduction of DPPH concentration in the reaction mixture, the antioxidant activities (EC_{50}) of cMNPs and eMNP-3s were estimated as 30.86 μM and 8.95 μM , respectively (**Table 2.5 and Figure 2.16**). The EC_{50} of eMNP-3PEGs, which were PEGylated to improve the dispersity of eMNP-3s further, was 2.99 μM , showing antioxidant activity similar to that of ascorbic acid (2.98 μM).

Table 2.5 Comparison of radical scavenging activities (EC_{50}) of ascorbic acid and three MNPs on DPPH.

	EC_{50} ($\mu\text{mol/L}$)
Ascorbic acid	2.98
eMNP-3	8.95
eMNP-3PEG	2.99
cMNP	30.86

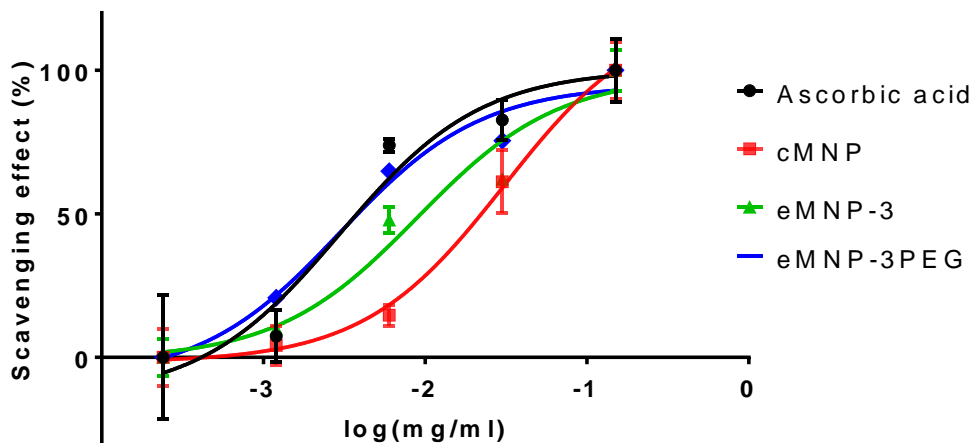


Figure 2.16 Comparison of radical scavenging activity (%) between MNPs and ascorbic acid.

The antioxidant activity of eMNP was measured in PBS buffer (pH 7.4) to mimic the physiological condition with EC_{50} for the antioxidant activity required to reduce the concentration of 0.1 mM DPPH, a free radical generator, by 50%.

2.4.5 Mussel foot protein (Mfp)-inspired sticky hydrogel in acidic condition

Based on the characterization of eMNP-3, it was revealed that the MNPs synthesized with dopamine at low pH have a significant content of catechol and protonated primary amine like Mfp that mediates attachment of mussel to the solid surfaces such as rock and surface of ship bottom (Danner et al., 2012; Lin et al., 2007; Lu et al., 2013). If a hydrogel is made of such eMNP-3s, its adhesive forces of the gel can be enhanced by the high contents of dihydroxy functional groups and primary amine to the gelation materials, respectively. When biocompatible gelatin is used as a gelation base material, tyrosine residues are contained in gelatin (*i.e.*, less than 0.5%)(Kariduraganavar, Kittur, & Kamble, 2014) can partially participate in the oxidation and subsequent crosslinking reactions by *BcTy*. We have prepared the two gelatin hydrogels with or without eMNP-3s synthesized from dopamine using *BcTy*, yielding both hydrogels with a size of 0.8 cm diameter and 0.5 cm height. Mechanical strengths and adhesive forces on the surface of the two gelatin-based hydrogels were measured by changing the experimental probe of the universal testing machine (UTM) (**Figure 2.17a and Figure 2.18**). Since eMNP-3s display a low degree of crosslinking, the eMNP-3-gelatin hydrogel was not expected to have high contents of covalent bonding network such as C-C bond, C-N bond, and C-S bond.(Liebscher, 2019) The mechanical strength of gelatin-eMNP-3s hydrogel was improved

by only about 3.1% compared to that of gelatin alone hydrogel as control (**Figure 2.17b**). Whereas the adhesion force of gelatin-eMNP-3s hydrogel was increased by 3.2 fold after its compression for 10 sec (**Figure 2.17c**), confirming our hypothesis that the hydrogel's stickiness contained eMNP-3s was greatly enhanced by their high contents of catechol-quinone and protonated primary amine group under the acidic condition.

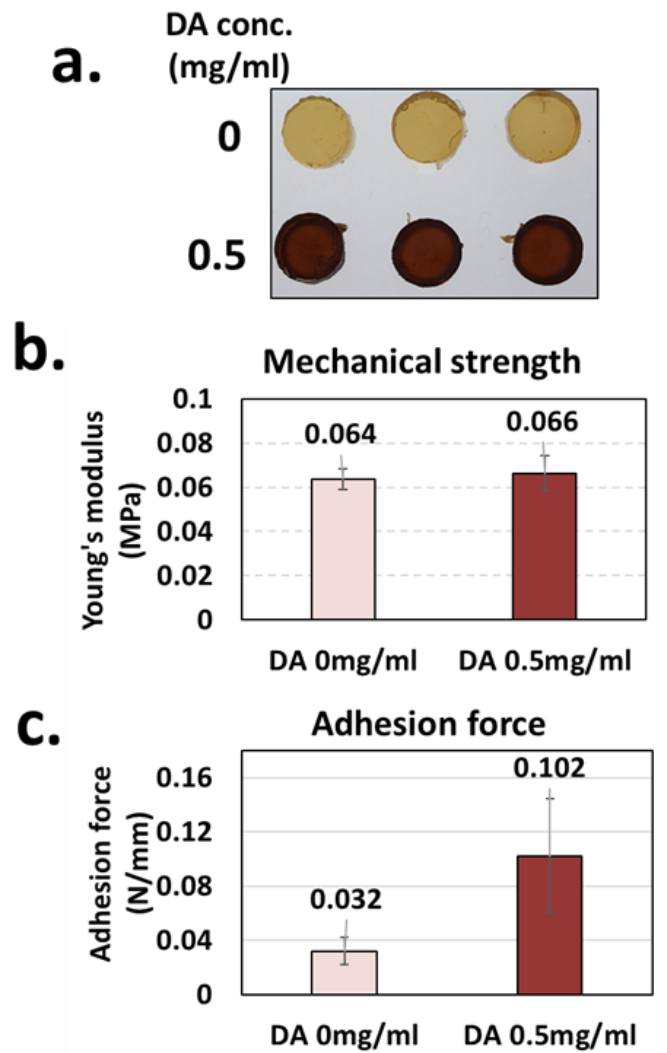
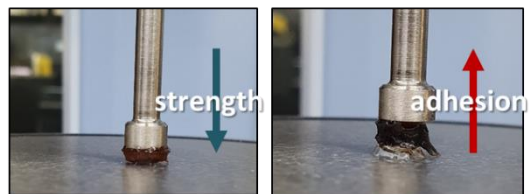


Figure 2.17 Preparation of gelatin hydrogel containing eMNP-3 and measurement of mechanical properties

(a) Representative image of gelatin-eMNP hydrogel according to the added dopamine (DA) concentration. (b) Mechanical properties of control gelatin hydrogel and gelatin-eMNP-3 hydrogel. (c) Adhesion force of gelatin hydrogel and gelatin-eMNP-3 hydrogel.

a.



b.

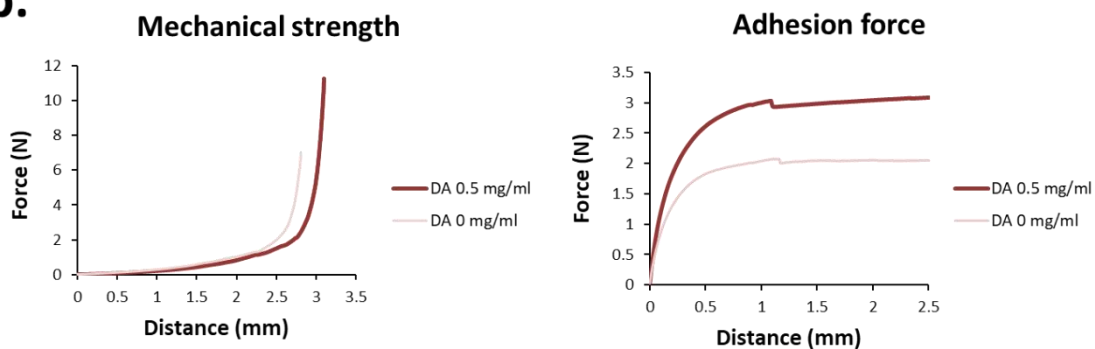


Figure 2.18 (a) Schematic image of the mechanical strength and adhesion force of melanin hydrogel. (b) Representative stress-strain curve.

2.4.6 Synthesis of linear chain eMNPs from tyrosine derivatives

Since the *BcTy* reaction with dopamine at pH 3 was able to control the crosslinking among the melanin precursors, we hypothesized that the chemical structure of the MNP oligomers could be controlled by using designed substrates. Particularly, melanins with linear aromatic structures with conjugated double bonds drew our attention since such materials can be applied as coating materials with electrical conductivity like polyacetylene, polypyrrole, polyindole (K. Lee et al., 2020; Xiao, Chen, Yang, Sun, & Geng, 2020). We attempted to synthesize linear structured eMNPs from tyrosine methylester (TME) (**Figure 2.19a**). When tyrosine is used as a substrate for tyrosinase reaction under neutral to basic pH conditions, DHI is produced from tyrosine by spontaneous decarboxylation from DHICA. The synthesis of melanin from DHI is limited owing to side-chain oligomerization initiated by the reactive C-2 position inside the indole ring of DHI (Q. Lyu et al., 2019; Pezzella, Iadonisi, et al., 2009; Ryu, Messersmith, & Lee, 2018). Whereas, in the case of TME, since methyl group shields the spontaneous decarboxylation of DHICA, it is more likely to synthesize linear melanins without any protection and deprotection of the dihydroxy group of indole ring (Qinghua Lyu et al., 2019; Micillo et al., 2017) (**Figure 2.19a**). This hypothesis was examined by synthesizing melanin using *BcTy* and TME under acidic

conditions below pH 5.0. The synthesized TME melanin was soluble and showed a light brown color compared to the DHI/DHICA based melanin and showed absorption profiles of $\lambda_{\max 1} = 287\text{nm}$ and $\lambda_{\max 2} = 333\text{nm}$ (**Figure 2.19b**). MALDI-TOF analysis of eMNP-TME showed that the synthesized MNPs contain a little bit more linear oligomers, up to octamer (**Figure 2.19c**). Eumelanin has a monotonic absorption profile and brown- black color due to broadband UV absorption caused by random structure and heterogeneous chemical properties (Qinghua Lyu et al., 2019; Q. Lyu et al., 2019; Zou et al., 2020). Unlike eMNP-3 and cMNP having a random chemical structure, TME melanin exhibits a non-monotonic absorption profile from a linearly aligned chemical structure (Repenko et al., 2015). Using this TME melanin, construction of a putative conductive fabric was attempted by coating a synthesized TME melanin on hydroxymethylcellulose paper. (H. Kim et al., 2020) on the top, and wanted to find out whether or not the linear melanin solution containing up to octamers of TME can be used as a conductive material. However, the TME melanin paper did not show any meaningful values indicating apparent electrical properties (Data not shown). Therefore, when we compare it with an electrically conductive polymer such as a linear polymer of polyaniline(H. Kim et al., 2020), at least 15 mers of TME is required to construct any conductive paper sheets. Further study is needed in the use of linear melanin as an electro-conductive biomaterial through additional chemical characterization.

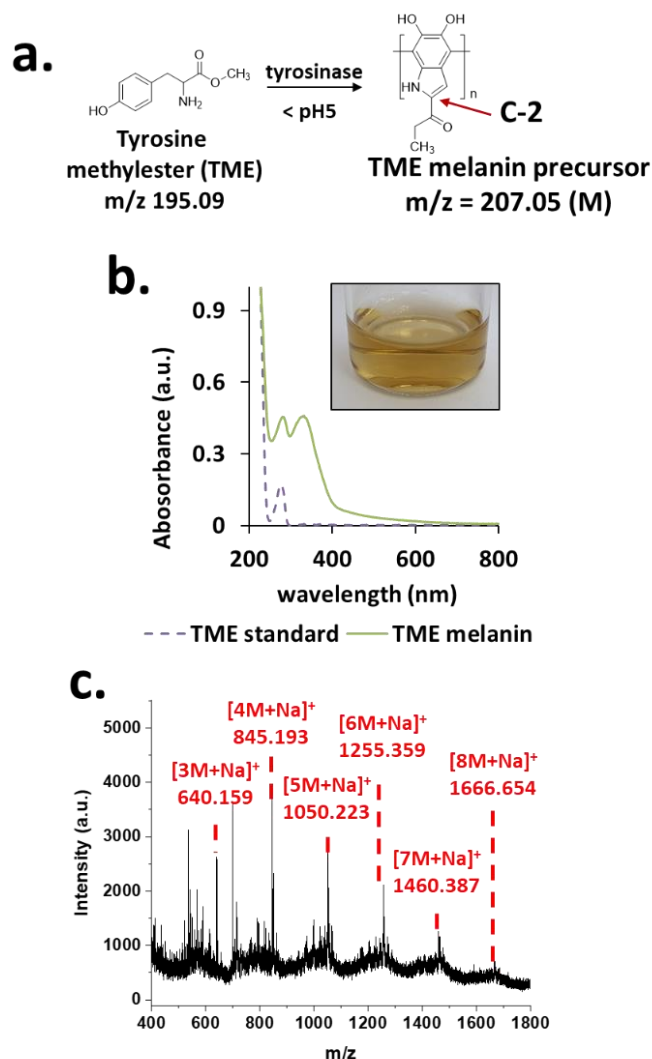


Figure 2.19 Synthesis of linear structured melanin from tyrosine methylester

(a) Schematic reaction pathway of linear melanin synthesis from tyrosine methylester (TME). Synthesis of linear melanin by preventing decarboxylation of c-2 of indole ring and preventing side reaction using acidic condition. The m/z of the TME melanin precursor (207.05) is set to M. (b)

UV spectra and representative digital picture of the reaction mixture of the TME linear melanin. (c) MALDI-TOF mass spectrum of linear melanin.

2.5 Conclusion

The MNP synthesized by the enzymatic method, especially using tyrosinase, can be made from various single monomer substrates such as dopamine and DOPA as well as monophenolic substrates. Usage of enzymes for the MNP synthesis can utilize broad substrate specificity and establish a green process, but it was not easy to control one-step homogenous MNP synthesis only using a free enzyme. Most of the melanins produced by enzyme reactions such as tyrosinase, laccase, peroxidase can easily bind to surrounding cell extract proteins or chelate with metal ions. In result, homogenous MNPs of one size could not be obtained, and their morphology was quite heterogenous, limiting further industrial applications. In consequence, there were no clear advantages of the enzymatic synthesis method over the chemical method in making MNPs, such as simple chemical auto-oxidation of dopamine or DOPA at alkaline condition.

In this study, we showed homogenous eMNP could be synthesized using tyrosinase, especially *BcTy*, which showed optimal reaction conditions at acidic pH ca. pH 3~ 5. The enzymatic method was able to synthesize soluble eMNPs of 5 ~ 20 nm size with various substrates by adjusting the reaction below pH 5.0 but above pH 3.0. Several chemical, structural and instrumental analysis revealed that i) a significant fraction of dihydroxy group moiety is maintained and ii) the amine group in dopamine is protonated due to its low

reaction pH below its pK_a value in eMNP-3s (**Figure 2.20**), which are quite similar to unique properties of Mfp under acidic environment. As the synthetic pH decreased down to 3.0, the particle size of eMNPs also decreased, but in return, its solubility was enhanced. Besides, based on the chemical characteristics of functional groups in the acidic condition and the broad substrate specificity of tyrosinase reaction, we could synthesize soluble MNP from various monophenolic substrates. According to our hypothesis, eMNP-3s preserved a high ratio of catechol to quinone moiety content, which displayed a strong antioxidant property, and caused to increase the stickiness of the eMNP-3-gelatin hydrogel. In addition, we could also demonstrate that i) melanin of linear aromatic ring structure can be easily synthesized using tyrosine ester substrate by avoiding random cross-linking of the substrate, ii) eMNP-3s form mussel-like sticky hydrogels with high contents of catechol/quinone, iii) soluble eMNPs have high free-radical scavenging activity, hence showing good antioxidant activity. As a result, we could demonstrate the synthesis of homogenous eMNPs through a biocompatible one-step synthesis method. We look forward to further wide applications of eMNPs as antioxidants, surface coatings, imaging reagents, and electronic materials.

Chapter 3.

Preparation of enzyme-polysaccharide coating by tyrosinase to improve enzyme stability

3.1 Abstract

Enzymes with high substrate selectivity mediate various reactions in industrial and pharmaceutical fields as highly efficient catalysts. Therefore, to increase enzyme stability, various researchers have made tremendous efforts, from protein engineering to chemical modification. Many studies have enzymatically immobilized and polymeric complexed by chemical modification. In this study, we developed a method for stabilizing an enzyme by an enzymatic method. In a more favorable environment for the enzyme, a selective reaction of *Streptomyces avermitilis* tyrosinase to a phenol-modified polymer formed an enzyme-polysaccharide coating (EPC) to stabilize the enzyme. The main forces for the stabilization we selected as the enzymatic stabilization method are as follows: i) the electrostatic interaction between the charged polymer and the charged protein surface ii) the polysaccharide is known to help stabilization by strengthening the internal and external hydrogen bonds, non-covalent bonds inside and outside the structure of the enzyme, the interaction between proteins iii) a covalently bonded crosslinking network generated by a tyrosinase reaction. The EPC made by the model proteins trypsin and tyramine-modified alginate was able to dramatically improve thermal stability, organic solvent stability, and storage stability compared to native enzyme even after a short synthesis time of 30 min. The stabilization method by the enzyme synthesis method we have constructed

will enable biocompatible modification in mild conditions for various industrial and medical enzymes in the future.

3.2 Introduction

Since most enzymes that exist naturally are not used to harsh environments such as thermal, organic solvent, and dehydration, it was not easy to apply them to industrial applications. Therefore, the enzyme was improved using various strategies to maintain high activity by preventing denaturation of the enzyme in harsh conditions. There is a method to directly discover stable enzymes through molecular biology and protein engineering methods (Silva, Martins, Jing, Fu, & Cavaco-Paulo, 2018; Upadhyay et al., 2019), but methods for stabilizing the structure of the enzyme by using a single chemical or solid material have also been studied. Attempts were made to achieve the stabilization of the enzyme's tertiary structure by adding chemicals to the reaction medium or by binding the enzyme itself to the solid material using covalent / non-covalent bonding (Chapman & Stenzel, 2019; Gibson, Higgins, & Woodward, 1992; Jesionowski, Zdarta, & Krajewska, 2014; Lozano, Combes, & Iborra, 1994; Marshall & Rabinowitz, 1975; Nguyen & Kim, 2017; Silva et al., 2018).

However, in immobilizing an enzyme on a solid surface, the enzyme is trapped on an insoluble solid surface. Therefore, there is a disadvantage in that the problem of enzyme activity decrease due to the decrease in substrate diffusion is easy to occur. As a method to improve stability while maintaining the activity of free enzymes, there is an alternative method through i) mixing polyol and sugar in the reaction mixture and ii) forming an enzyme-polymer

network. Polyol and sugar form hydrogen bonds with proteins to replace hydrogen bonds between water, buffer ion, and proteins, and at the same time, the CH moiety of sugar interacts with CH- π to stabilize the tertiary structure of target proteins (Ajito, Iwase, Takata, & Hirai, 2018; Mensink, Frijlink, van der Voort Maarschalk, & Hinrichs, 2017). In addition, protein-polymer complexes are formed by entrapment proteins in cross-linked networks or bulk polymer such as metal organic frameworks (MOFs), polymersomes, and micelles with easy size control (Falatach et al., 2015; Pelegri-O'Day & Maynard, 2016; Rodriguez-Abetxuko, Sánchez-deAlcázar, Muñumer, & Beloqui, 2020; Stevens, Kaur, & Klok, 2021; Waltmann et al., 2022). Then, enzyme stabilization is achieved without worrying about diffusional issues.

In order to apply the polyol stabilization and enzyme-polymer complex as a whole, a method of forming a single enzyme nanoparticle by *in situ* polymerization on the enzyme surface (Beloqui, Kobitski, Nienhaus, & Delaittre, 2018; Şahutoğlu & Akgül, 2020; Yan, Ge, Liu, & Ouyang, 2006) or coating a synthetic polymer consisting of a charged polymer-polysaccharide-polyacrylamide on the enzyme surface was studied (Y. Wang et al., 2020; Y. Wang, Milewska, Foster, Chapman, & Stenzel, 2021). However, several disadvantages occur in enzyme stabilization through chemical polymerization. Part of the initial activity is lost because the protein surface charge stability is lost due to the pre-modification of the lysine residue to attach the polymer to the enzyme surface. In addition, since it is necessary to produce a synthetic polymer complex that needs to be coated on the surface in a 1:1 ratio for each

single enzyme molecule, it may bring disadvantages to mass production. Therefore, we tried to develop a new stabilization method that can overcome the limitations of the chemical fabrication method. The crosslinking reaction by tyrosinase can replace the existing chemical synthesis method to form an enzyme-polymer complex by immobilizing a biocompatible polysaccharide while maintaining the enzyme stability.

Tyrosinase is a type III copper-containing hydroxylation enzyme, well-known as a melanin synthesis in living organisms, and has substrate specificity to monophenol and diphenol (N. Lee et al., 2015; McLarin & Leung, 2020; Sendovski, Kanteev, Shuster Ben-Yosef, Adir, & Fishman, 2010; Son et al., 2018). When the phenolic substrate undergoes two consecutive hydroxylation reactions by tyrosinase, quinone is formed. The semi-quinone radical formed from quinone can be intramolecular crosslinking with other quinones or with amine, thiol by Michael addition, and Schiff base reaction, which are reactive functional groups of amino acids (Fujieda et al., 2020; Liebscher, 2019). Therefore, using a substrate-specific crosslinking reaction mediated by tyrosinase, a covalent bonded network is constructed by reacting with a biomaterial substituted with a monophenol group. Several studies have also been reported using hyaluronic acid with phenolic moieties to fabricate biomedical hydrogels mediated by the tyrosinase reaction (N. Kim, Lee, Han, Kim, & Choi, 2021; S.-H. Kim et al., 2020; S.-H. Kim et al., 2018). Tyrosinase-mediated covalent crosslink network suggests that enzyme coating is possible in a moderate reaction condition where enzyme is

stabilized.

In this study, we performed enzyme stabilization using a polysaccharide-tyramine conjugate using *Streptomyces avermitilis* tyrosinase (SaTy), which is specialized for the crosslinking reaction of polymeric materials with large molecular sizes (N. Lee et al., 2015). The charge state of the protein surface changes according to the ionic state that exists in the buffer environment due to the functional residue of amino acids (S. Kim et al., 2020). Polysaccharides also have a charge depending on the monomer, forming a polyelectrolyte complex through electrostatic interaction with proteins (MARGOLIN, SHERSTYUK, IZUMRUDOV, ZEZIN, & KABANOV, 1985; Pasche, Vörös, Griesser, Spencer, & Textor, 2005). However, only electrostatic interaction is easy to dissociate by the surrounding environment (e.g. high salt concentration, competing protein-protein interaction), so it is necessary to capture and stabilize the protein-electrolyte complex. A rigid enzyme-polysaccharide coating (EPC) was prepared by introducing covalent crosslinking through a tyrosinase reaction into a complex formed by weak interaction between protein-polysaccharide. As a model enzyme, trypsin (TR, Protein database (PDB) ID: 1S0Q (Chamorro Gavilanes, Cuesta-Seijo, & Garcia-Granda)), which is widely used in industry and has a positively charged surface, was selected. An EPC was prepared using alginate-tyramine polymer (Alg), which was conjugated with tyramine to alginate, a negatively charged biocompatible polysaccharide (Alg-TR). By measuring the enzyme kinetics of Alg-TR and free-TR as control, the characteristics of the enzyme

before and after enzyme coating were characterized, and improvements in thermal stability and storage stability were investigated.

3.3 Materials and methods

3.3.1 Materials

Luria-Bertani(LB) broth, LB agar were purchased from BD Difco (Sparks, USA). Ni-NTA agarose was purchased from Qiagen (Hilden, Germany). Alginate sodium salt, 1-Ethyl-3-(3-dimethylaminopropyl) carbodiimide hydrochloride (EDC hydrochloride) and 3-(*p*-hydroxyphenyl) propionic acid were purchased from Thermo Fisher Scientific Korea (Seoul, Korea), trypsin from bovine pancreas, chitosan, dextran, and all the other chemicals were purchased from Sigma-Aldrich Korea (Seoul, Republic of Korea).

3.3.2 Expression and purification of *Streptomyces avermitilis* tyrosinase (*SaTy*)

NcoI In order to express recombinant *SaTy*, the expression plasmid prepared by referring to the method of the previous study (N. Lee et al., 2015) was transformed into *E.coli* BL21 (DE3). The transformed strain was selected on LB agar plate with antibiotic selection marker ampicillin (50 µg/ml). A single colony was inoculated into a test tube with 3 ml of the same LB broth with ampicillin, and the cell was cultured in a shaking incubator at 37 °C, 200 rpm overnight. 500 µl of cultured cells were transformed into 50 ml of fresh LB medium with antibiotic markers, and then cells were grown to approximately 0.6 at OD600. Furthermore, the protein expression was

induced by adding 0.1 mM of IPTG and 1.0 mM of CuSO₄. After 20 h at 37 °C culture, cells were harvested by centrifugation at 4000 rpm for 20 min. Cell pellets were resuspended in 50 mM Tris buffer, pH 8.0, and disrupted by ultrasonication. After ultracentrifugation at 16,000 rpm for 30 min, the supernatant was collected. The supernatant was applied to the Ni-NTA agarose column for enzyme purification. After pre-equilibrium with 50 mM Tris buffer, pH 8.0 with 5.0 mM imidazole, 300 mM NaCl buffer, cell lysate was subsequently applied onto the Ni-NTA column. Bounded proteins were washed with 50 mM Tris buffer pH 8.0 with 30 mM imidazole, 300 mM NaCl buffer. The tyrosinase was eluted by 50 mM Tris buffer pH 8.0 with 250 mM imidazole. The concentration of purified enzyme was measured by Bradford assay.

3.3.3 Synthesis of phenol-moiety conjugated polysaccharides

The phenol-moiety conjugated alginate and chitosan were synthesized using the previously reported method with slight modification (Sakai, Yamada, Zenke, & Kawakami, 2009). In order to covalently conjugate a phenolic moiety to alginate, the carboxylic group of alginate and the primary amine group of tyramine were coupled by EDC-NHS coupling. First, 500 mg (1 w/v%) of alginate was added to 50 ml of 50 mM MES buffer and mixed, then titrated to pH 6.0 with 3N NaOH, and then mixed with vigorous stirring

at room temperature for 30 minutes. Then, 484 mg (2.525 mmol) of EDC hydrochloride and 291 mg (2.529 mmol) of NHS were added to the reaction mixture and stirred for 45 minutes. Finally, 217 mg (1.25 mmol) of tyramine hydrochloride was added, and the phenol moiety conjugation reaction was started while stirring at room temperature for 24 hours. For phenol-moiety conjugated chitosan, 250 mg (1.505 mmol) of 3-(*p*-hydroxyphenyl) propionic acid was added instead of tyramine hydrochloride. After the reaction, the phenol-moiety conjugated polysaccharide was precipitated with 90 v/v% ethanol and recovered by centrifugation at 4000 rpm for 10 minutes. Precipitate was resuspended in 90 v/v% ethanol and centrifuged again to remove residual EDC, NHS, and free phenol moiety. This process was repeated until the 280 nm UV-vis spectrum peak of the free phenol moiety did not remain in the supernatant. Finally, the recovered sample was vacuum dried.

For the synthesis of dextran conjugate, tyramine conjugation was performed by referring to other methods.(Han et al., 2020) 500 mg of dextran was added to 12.5 ml of anhydrous DMSO and mixed. 578 mg (2.985 mmol) of 1,1'-carbonyldiimidazole was dissolved in 5ml of DMSO, transferred to a dextran solution, and stirred at room temperature for 30 minutes. Then, 401 mg (2.309 mg) of tyramine hydrochloride was dissolved in 2.5 ml of DMSO, mixed with dextran solution, and the conjugation reaction was carried out for 12 hours while stirring at room temperature. After completion of the reaction, the conjugated polysaccharide was recovered by same precipitation protocol

using 90 v/v% ethanol.

Before the enzyme polymer complex reaction, tyramine conjugated alginate (ALT) and tyramine conjugated dextran (DeT) were dissolved in DW at 2.5 w/v%, and 3-(p-hydroxyphenyl) propionic acid conjugated chitosan (ChT) was prepared by dissolving 0.3 w/v% in 0.5 v/v% acetic acid.

3.3.4 Fabrication of trypsin-polysaccharide coating with tyrosinase reaction using phenol-moiety conjugated polysaccharides

In a glass vial, add trypsin 0.3 mg/ml, *SaTy* 500 nM (0.018 mg/ml), 10 mM or 50 mM Tris buffer, pH 8.0 in order, and mixed with gentle stirring. Then, the phenol-moiety conjugate polysaccharide was added to the reaction mixture to a final concentration of 0.1 v/v%, and the enzyme-polysaccharide complex (EPC) reaction was started. The reaction volume of the final reaction mixture was 2 ml, and the reaction was performed at 37 °C, 200 rpm in a shaking incubator.

3.3.5 Fabrication of immobilized trypsin on glass bead and polysaccharide complex with tyrosinase reaction using phenol-moiety conjugated polysaccharides

Tyrosinase immobilization on glass beads (80-100 μm diameter) was fabricated with some modifications to the previously reported research (Yuan,

Mullett, & Pawliszyn, 2001). First, 500 mg of glass beads were placed in 5 ml of 5 v/v% HNO₃ and incubated for 1 h in an 80 °C water bath for activation. Then, the beads were separated by centrifugation at 4000 rpm for 10 min and washed with 50 ml of DW. Repeat the washing process one more time in the same way. Add 4.5 ml of DW and 0.5 ml of 3-aminopropyltriethoxysilane (APTES) per 250 mg of glass bead, and adjust the pH to 3 with 6 N HCl. Bead silanization is performed by incubating the prepared APTES solution in a 75 °C water bath for 2 h. And wash twice with DW in the washing method mentioned above. Add 150 mg of amino silanized beads to 3.75 ml of a solution containing 2.5 v/v% glutaraldehyde in 50 mM sodium phosphate buffer, pH 7.0, and incubate at room temperature for 1 h to cross-link glutaraldehyde on the bead surface. After that, it is washed twice with DW in the same way. Treat 40 ml of a 5 mg/ml trypsin solution dissolved in 50 mM sodium phosphate buffer, pH 7.0 per 1 g of glass beads, and incubate overnight with agitation at 4 °C. Trypsin immobilized beads are recovered by centrifugation at 4000 rpm for 10 min, washed twice with 50 mM sodium phosphate buffer, pH 7.0, and refrigerated.

3.3.6 Measurement of trypsin activities and enzyme kinetics

For the proteolytic activity assay of native trypsin (free-TR) and Alg coated trypsin (Alg-TR) for small molecules, the formation of UV absorbance

$\lambda = 410$ nm peak of 4-nitroaniline ($\epsilon = 8800 \text{ M}^{-1}\text{cm}^{-1}$ at 410 nm) according to the degradation of nitroanilide derivative substrate was measured. The enzyme-containing solution was diluted in 100 mM Tris buffer, pH 8.0 so that the final trypsin concentration was 0.1 mg/ml. Before the activity assay, the enzyme solution was incubated at 37 °C for 10 minutes. For each reaction, 1 mM of *N*_α-Benzoyl-L-arginine 4-nitroanilide (BAPNA) or succinyl-L-Ala-L-Ala-L-Pro-L-Phe-*p*-nitroanilide (Suc-AAPF-NA) was added to the solution to start the proteolytic assay. To measure TR activity in water organic solvent, tetrahydrofuran (THF), dimethylsulfoxide (DMSO), acetonitrile (ACN), methanol (MeOH), ethanol (EtOH), and isopropanol (IpOH) were mixed in the reaction mixture at 40 v/v%. After incubation at 37 °C for 10 minutes, activity assay for BAPNA was performed. The initial activity of trypsin was measured by measuring the UV absorbance at 410 nm a total of 20 times at 60 second intervals. To measure enzyme kinetic parameters, enzyme assay was performed with a substrate of 0.1-3 mM, and the obtained data was fitted by Michaelis-Menten equation and nonlinear regression analysis was performed. To study the effect of heating on TR activity, Free-TR and Alg-TR (0.1 mg/ml for TR) were incubated at 50 °C in 10mM Tris buffer, pH 8.0, and then cooled down on ice before activity assay. The relative activity of TR was determined by the following equation:

Relative activity of TR (%)

$$= \frac{\text{Initial activity of each experiment}}{\text{Initial activity of Free - TR at } t = 0} \times 100 \text{ (\%)}$$

3.3.7 Measurement of thermal stability of enzyme and EPC

The protein thermal stability (melting temperature, T_M) was measured by the excitation-emission wavelength profile of SYPRO Orange (Sigma Aldrich; 5000 \times) generated while the temperature was increased while heating (Huynh & Partch, 2015; P. G. Lee et al., 2019). In brief, a reaction mixture was prepared with 10 mM Tris buffer, pH 8.0 and 50 mM NaCl at 0.1 mg/ml of TR and 2 \times SYPRO Orange dye to final concentrations. Each experiment was repeated three times.

3.3.8 Estimation of storage stability of trypsin by accelerated stability test

The storage stability of Free-TR and Alg-TR was estimated according to the previously reported degradation model (Magari, 2002) by measuring the proteolytic activity of TR at accelerated temperature, plotting the relative activity data, and performing non-linear regression.

Assuming that the degradation of TR is a first-order reaction, the degradation pattern (D) is as follows.

$$D = \alpha \exp(-\delta t)$$

α is intercept, lot performanc at time zero ($t = 0$), δ is degradation rate, and t is time ($t > 0$). The results from the actual experiment through the real

degradation pattern (Y) are as follows.

$$Y = D + \varepsilon = \alpha \exp(-\delta t) + \varepsilon$$

ε is a random experimental error, and although there are self-cleavage and experimental errors appearing by protease, it is assumed that these are first order kinetics that are ignored in this study. Then, the relationship between degradation rate and temperature can be explained by the Arrhenius equation.

$$\delta = A \exp\left(\frac{-E_a}{RT}\right)$$

A is Arrhenius factor, E_a is the degradation activation energy (kcal mol⁻¹), R is gas constant (0.00199 kcal mol⁻¹ K⁻¹), and T is temperature (K = °C + 273.15). To compare degradation patterns between two different enzyme storage temperatures, the acceleration factor (λ) is as follows,

$$\lambda = \frac{\delta_e}{\delta_s} = \frac{A \exp\left(\frac{-E_a}{RT_e}\right)}{A \exp\left(\frac{-E_a}{RT_s}\right)}$$

$$\lambda = \exp\left[\frac{E_a}{0.00199} \left(\frac{1}{T_s} - \frac{1}{T_e}\right)\right]$$

where T_e is accelerated temperature and T_s is actual storage temperature. Therefore, if we know the activation energy, we can predict the storage time (t_s) from the accelerated factor obtained by the accelerated degradation time (t_e).

$$t_s = \lambda t_e = \exp\left[\frac{E_a}{0.00199} \left(\frac{1}{T_s} - \frac{1}{T_e}\right)\right] t_e$$

We incubated free-TR and Alg-TR at accelerated temperatures of 50, 60,

and 70 °C and measured the relative proteolytic activity on the BAPNA. Arrhenius plots were plotted on the obtained data through nonlinear regression, and an accelerated storage model was constructed.

3.3.9 Instrumental analysis

NMR spectroscopy was applied for structural elucidation of phenolic moiety-modified polysaccharides. Samples of lyophilized phenolic moiety conjugated polysaccharides were dissolved in D₂O (7 to 10 mg/mL) and analyzed by scanning 32 times at 25 °C. ¹H NMR spectra were recorded using AvanceIII-500 (Bruker, German) installed at the National Center for Inter-University Research Facilities (NCIRF) at Seoul National University, and integration and deconvolution were conducted using TopSpin 4.0.9 software. UV-vis spectrum was measured by SPECTROstar Nano UV-vis spectrophotometer (BMG LABTECH, Germany) from 220 nm to 1000 nm. The average hydrodynamic diameter and zeta potential of the TRs were measured by dynamic light scattering (DLS) using a Zetasizer Nano-ZS system (Malvern Instruments, Inc., UK). The particle size measurement of TRs were performed using field emission scanning electron microscopy (FE-SEM). AIT-TR was freeze-dried and platinum-coated in sputter before the FE-SEM analysis. The morphology and size analyzed by FE-SEM 7800 Prime (JEOL Ltd., Japan) installed at the National Center for Inter-University Research Facilities (NCIRF) at Seoul National University with an

accelerating voltage of 5.0 kV.

3.3.10 Prediction of surface potential of trypsin

To predict the surface potential of Trypsin, a webserver (<https://server.poissonboltzmann.org/>) was used for PDB2PQR and APBS analysis (Unni et al., 2011). Based on the structure of bovine trypsin (Protein database (PDB) ID: 1S0Q (Chamorro Gavilanes et al.)), the electrostatic potential at pH 8.0 was calculated using the PROKA option. Electrostatic potential results were visualized in UCSF Chimera 1.11.2 software.(Pettersen et al., 2004)

3.4 Result and discussion

3.4.1 Fabrication of enzyme-polysaccharide coating (EPC) and identification of physical properties

Alkaline protease is an enzyme of high industrial value widely used in detergents, leather processing, food, medicine, and proteomics (Jablaoui et al., 2018). The optimum activity pH of most alkaline proteases is between 8 and 11, and the isoelectric point is close to the optimum activity range. Therefore, since many positively charged amino acids are distributed, alkaline proteases are positively charged. We selected one of the alkaline protease, trypsin (TR) with an isoelectric point of 10.5 (Walsh, 1970) as a model protein for tyrosinase-mediated enzyme coating. As a strategy to improve the stability of TR, i) maintain the charge balance on the protein surface, ii) cover the periphery of the enzyme with polysaccharides to stabilize the tertiary structure, and iii) prepare an enzyme-polymer complex by covalent crosslinking. Therefore, a polysaccharide with phenolic moiety is synthesized. A monophenol moiety was introduced into alginate, a negatively charged polysaccharide, chitosan, a positively charged polysaccharide, and dextran, a neutral charged polysaccharide by EDC-NHS coupling. (**Figure 3.1a**) After modification of the phenolic moiety of polysaccharides by EDC-NHS coupling, structural analysis was performed by $^1\text{H-NMR}$. After the synthesis of alginate-tyramine (Alg), chitosan-3-hydroxyphenyl propionic acid (Chi), and dextran-tyramine (Dex) from each polysaccharide, the phenolic group of

tyramine or 3-(*p*-hydroxyphenyl) propionic acid aromatic proton (6.8 - 7.2 ppm) was present. (**Figure 3.2**) After the quinone is made by tyrosinase reaction, and the spontaneous crosslinking reaction makes trypsin coating. (**Figure 3.1b**) **Figure 3.1c** shows quinone located on the trypsin surface, lysine with a primary amine group that can be a Michael addition / Schiff base reaction, and tyrosine with a phenyl group.

An EPC was synthesized at pH 8.0, the optimum pH of *Sa_Ty*, by mixing trypsin 0.3 mg/ml and polysaccharide-phenol moiety conjugate 0.1%. Natural polysaccharide derivatives have a vast molecular size range than synthetic polymers, whose degree of polymerization can be easily controlled. Therefore, it is difficult to determine how many are attached to the protein surface by covalent bonds. Instead, we tried to prove that the quinone from a small molecule produced by tyrosinase can bind to the target protein's surface. It is expected that 3-(4-hydroxyphenyl) propionic acid (HPA) will be converted to quinone by successive hydroxylation reactions and crosslinking with trypsin surface tyrosine residue or lysine residue. The existence of 28 possible binding sites could be indirectly identified by analyzing the intact protein mass. (**Figure 3.3**) Since HPA is a single chemical, it can ideally predict the binding of 28, but a smaller number of phenol-conjugated polysaccharide of several tens of kDa will covalently binding with trypsin.

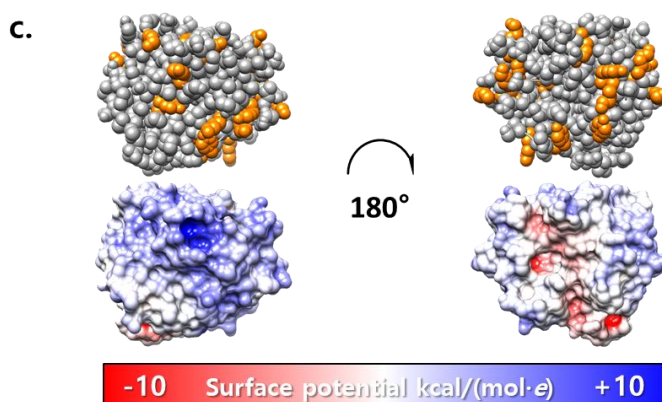
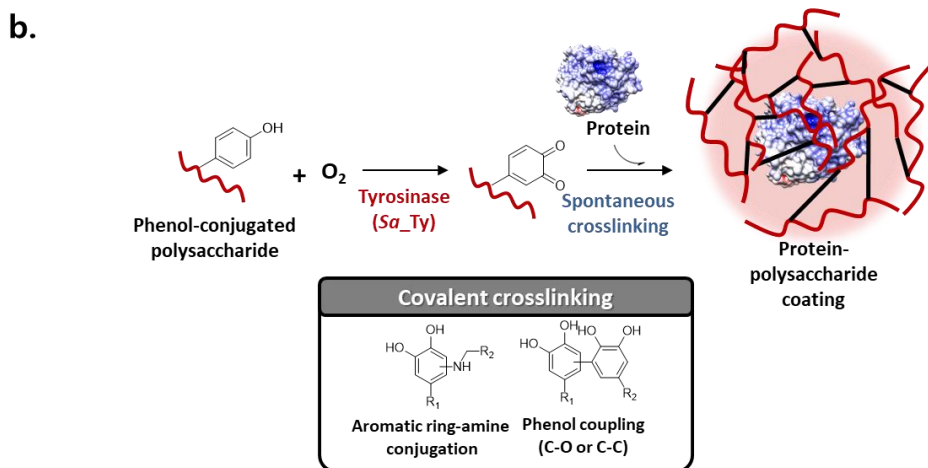
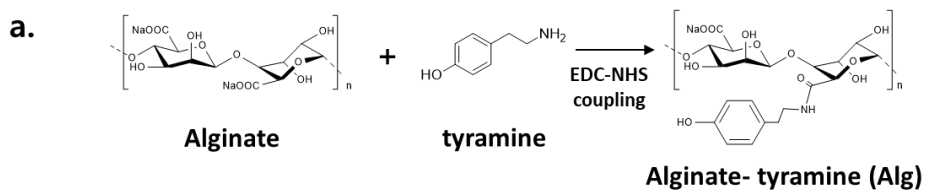


Figure 3.1 Schematic diagram of the synthesis of the entire EPC and the surface properties of the target protein trypsin.

(a) Chemical structure of alginate-tyramine (Alg) by tyramine conjugation to alginate, a polysaccharide, by EDC-NHS coupling. (b) Scheme for preparing protein-polysaccharide complex by tyrosinase-mediated AIT

hydroxylation. (c) Lysine and tyrosine residues are located on the trypsin (TR) surface, and the TR surface charge is predicted at pH 8.0 (net charge = 6.0). Lysine and tyrosine residues are indicated in orange in the TR drawn with a ball and stick structure, and other residues are indicated in gray. The blue ~ red gradient color indicates the surface potential of TR. The surface potential is in the range of -10 to $+10$ kcal mol⁻¹ e⁻¹.

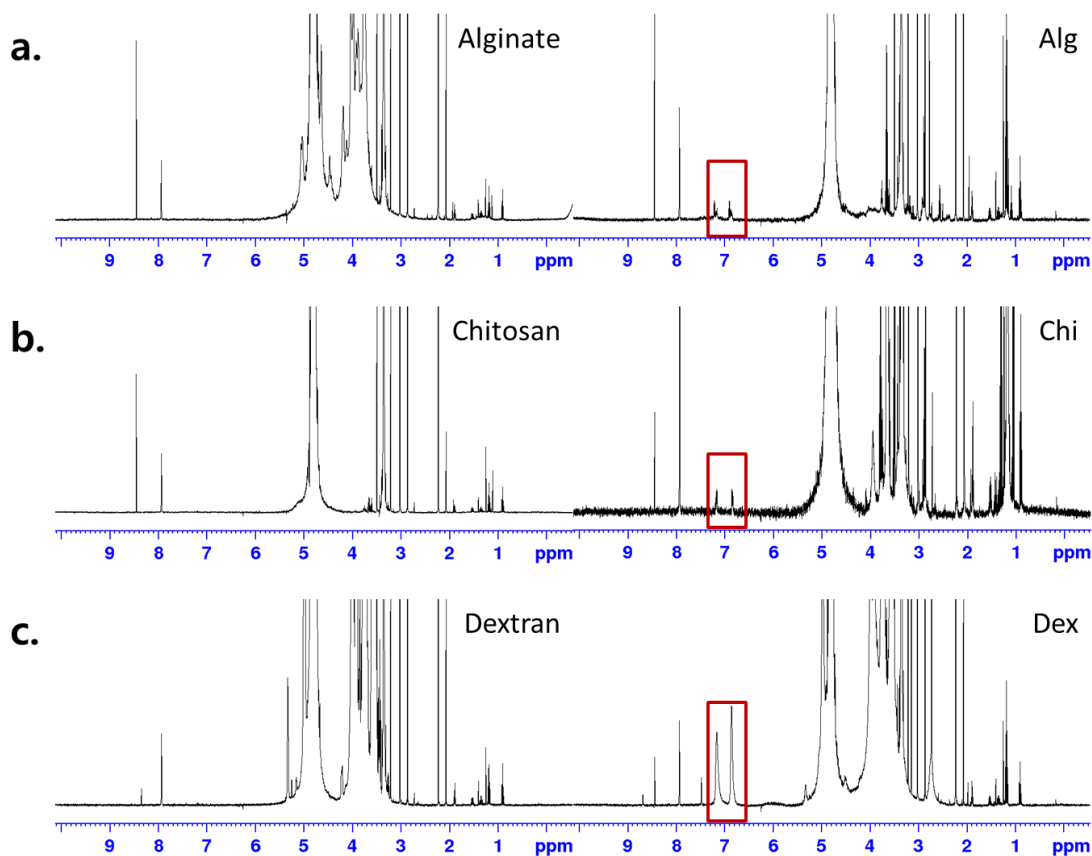


Figure 3.2 $^1\text{H-NMR}$ spectrum of polysaccharide-phenol moiety conjugated synthesized by EDC-NHS coupling chemistry.

Alginate and Dextran were conjugated with tyramine and Chitosan with 3-(p-hydroxyphenyl) propionic acid to form Alg, Dex, and Chi, respectively. The aromatic protons (6.8 - 7.2 ppm) of each phenolic substrate appeared in the NMR spectrum (right side) after conjugation, and are indicated by a red box. All samples were lyophilized and then dissolved in D_2O at a concentration of 7.5 to 10 mg/ml, and analyzed by ^1H NMR, 500 MHz.

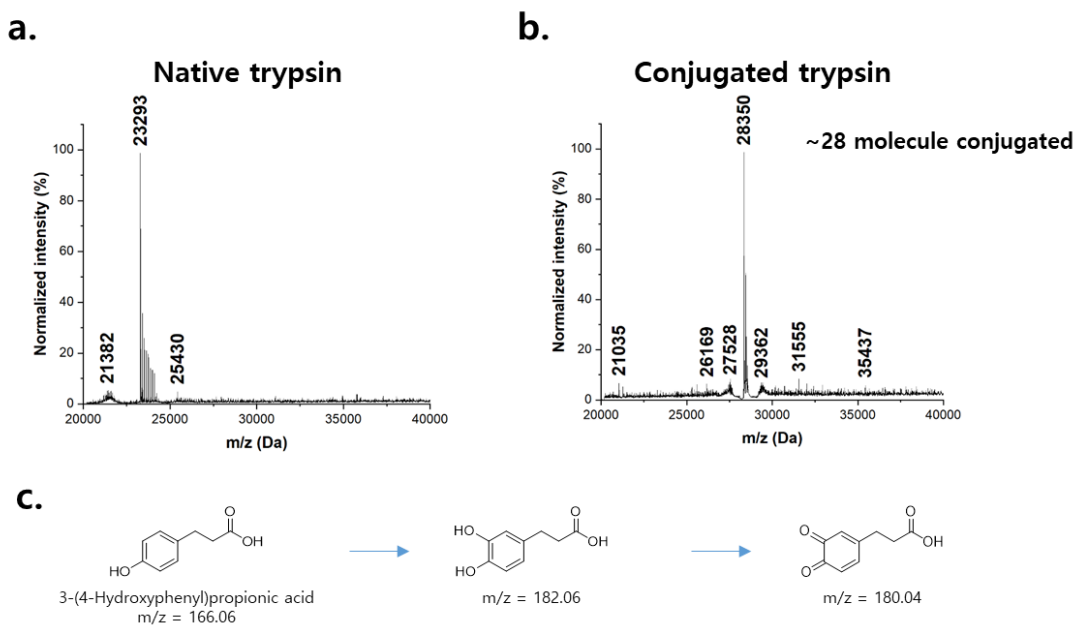


Figure 3.3 Intact mass spectrometer (MS) spectrum of trypsin before and after 3-(4-hydroxyphenyl) propionic acid conjugation by *Sa*Ty

Comparing (a) the intact MS spectrum of bovine TR with (b) the intact MS spectrum of TR conjugated with the quinolic moiety generated by the tyrosinase reaction, it is estimated that TR conjugated 28 small molecules. The chemical structure of 3-(4-hydroxyphenyl) propionic acid modified by tyrosinase is shown in (c). TR is covalently bound with quinolic chemical at m/z 180.04 by Michael addition or Schiff base reaction.

The monophenol derivatives of alginate, dextran, and chitosan were formed EPC under optimized reaction conditions. Chitosan forms a haze solution because it is insoluble above neutral pH (i.e., pH 6.0). The synthesized Alg-TR has a red-brown color and forms a clear solution that does not show the Tyndall scattering effect even when irradiating laser light. **(Figure 3.4a)**. Alg-TR shows a cluster shape of tiny particles of about 20-50 nm in the SEM image. **(Figure 3.4b)** After incubation of Alg-TR, Dex-TR, and Chi-TR at 50 °C for 1 hour, TR activity for *N*_α-Benzoyl-L-arginine 4-nitroanilide (BAPNA) was measured, and TR of each EPC stability was compared. The stability of all Alg, Dex, and Chi-TR complexes was improved compared to the uncoated Free-TR, but in particular, only Alg-TR was able to maintain 91.79% of its initial activity after high-temperature incubation. **(Figure 3.5a)** Therefore, we selected Alg, a negatively charged polysaccharide, for the coating of positively charged trypsin.

Alginate obtained from natural sources is a bulky material small molecule with a wide distribution. The TR activity of Alg-TR to the small molecular substrate increased compared to that of Free-TR but somewhat increased. Conversely, Alg-TR was assayed for protease activity in skim milk, a large molecule composed of protein. **(Figure 3.5b)** Unlike the BAPNA degradation, the initial activity of Alg-TR was significantly decreased in skim milk. Even considering that the main protein constituting skim milk is casein with a negative surface charge such as alginate, the initial activity of Alg-TR was reduced to 28.84% compared to Free-TR. However, there was no effect

on thermal stability, and after enzyme incubation at 50 °C for 120 minutes, the activity decreased in Alg-TR compared to Free-TR, as in the small molecule assay. The hydrogel-like network formed by intermolecular crosslinking between Alg and TR by tyrosinase and intramolecular crosslinking between Alg affected the diffusion of large molecules. However, since there was no problem with the effect on thermal stability, actual long-term storage or industrial applications will be possible.

The stability improvement of Alg-TR will be compounded by the effect of covalent binding of Alg on the TR surface and the effect of Alg forming a network like a hydrogel, contributing to stabilization. We decided to bind Alg to immobilized TR (imTR) with a tyrosinase reaction to speculate which of the two possibilities might contribute to enzyme stabilization. TR was immobilized on a glass bead with a diameter of 80-100 µm using 3-aminopropyltriethoxysilane (APTES) and glutaraldehyde chemistry (Yuan et al., 2001). The immobilization yield of 5 mg/ml Free-TR was 5.68%. And Alg was bound using *Sa*_Ty, and BAPNA activity was measured between Free-imTR and Alg-imTR that did not undergo tyrosinase reaction. As a result, Alg-imTR generated by the tyrosinase reaction still stably maintained enzyme activity compared to Free-imTR even when thermal stress was applied to the enzyme. After incubation at 50 °C for 1 hour, Free-TR maintained 15.66% of the initial activity, but Alg-imTR maintained 106.75% of activity. Enzyme stability improvement was possible only by binding to the TR surface of Alg by tyrosinase, excluding the formation of a crosslinked alginate complex by

immobilization on the bead. This result suggests that the formation of the covalent binding complex of the enzyme surface polysaccharide significantly contributed to the improvement of enzyme stability.

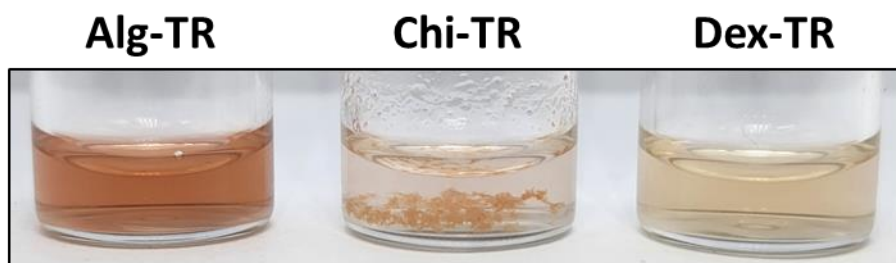


Figure 3.4 (a) Digital picture of Alg-TR, Chi-TR, Dex-TR reaction mixture

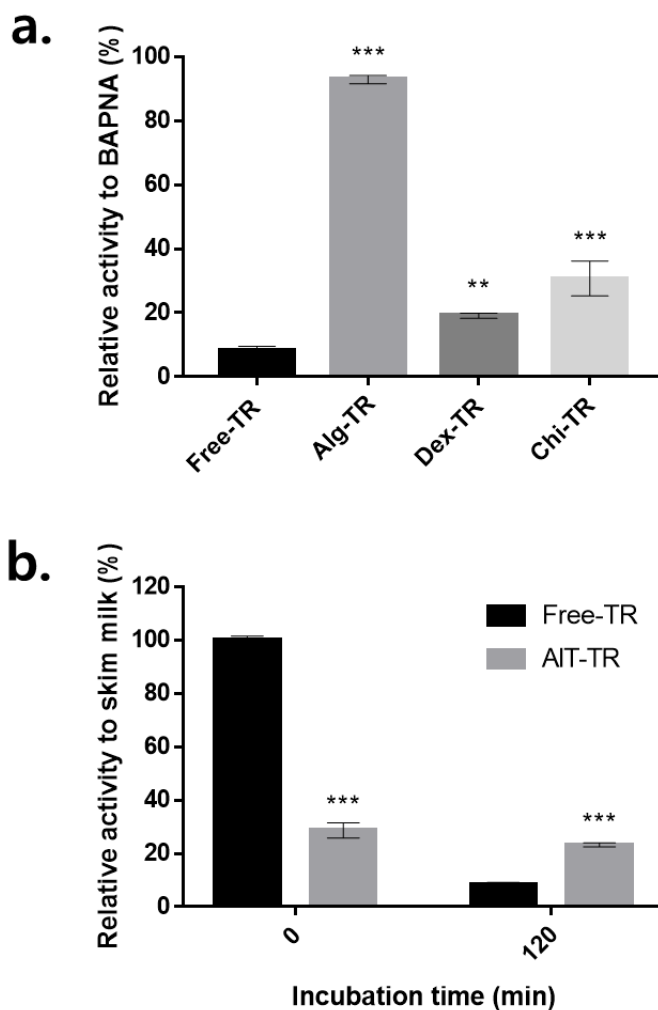


Figure 3.5 Changes in the activity properties of Alg-TR for small molecule (BAPNA) and large molecule (skim milk) compared to Free-TR

(a) TR assay for BAPNA after 50 °C incubation for 120 min measuring the improved enzyme stability and optimal pH changed by the EPC synthesized by *SaTy* reaction. The final concentration of TR was 0.1 mg/ml in the TR assay mixture. (b) Comparison of Free-TR and Alg-TR activity

against large molecules (skim milk). Activity assay for BAPNA after incubation of EPC and native TR at 50 °C for 120 min according to polysaccharide charge. Free-TR is native trypsin as a control, alginate-tyramine and conjugate are Alg-TR, chitosan-3-(p-hydroxyphenyl) propionic acid and conjugate are Chi-TR, and conjugate with dextran-tyramine is Dex-TR, respectively. The relative activity was calculated by setting the initial activity of Free-TR at 0 min to 100%. The final concentration of TR was 0.1 mg/ml in the TR assay mixture.

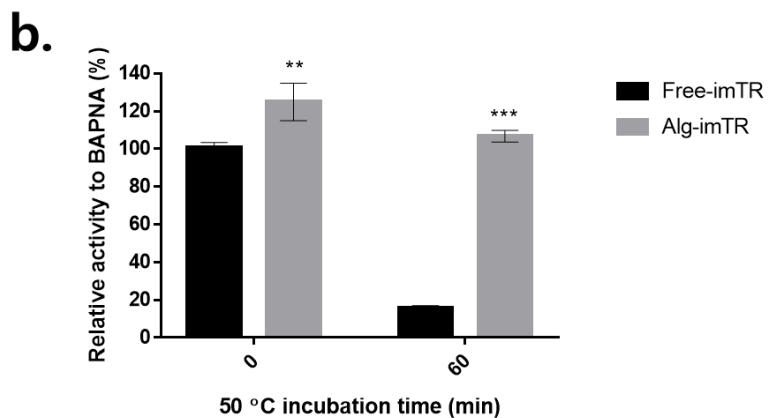
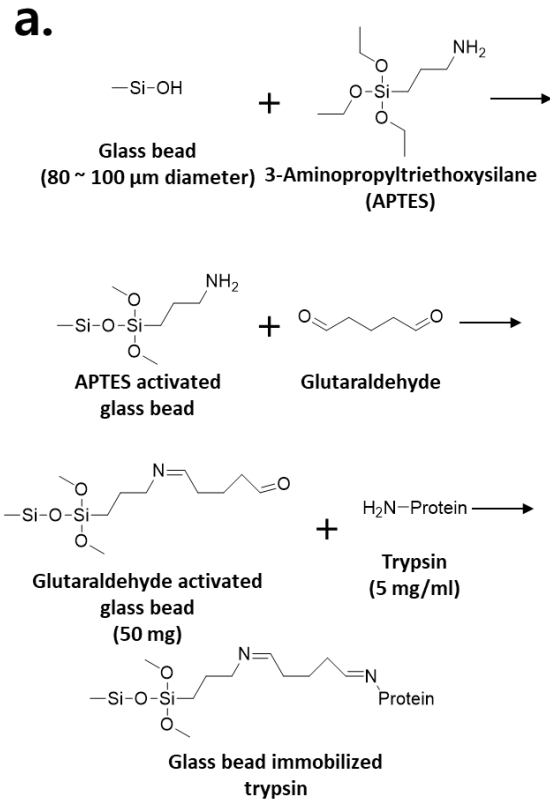


Figure 3.6 Enzyme stabilization measurement by Alg complex formation of TR immobilized on glass beads

(a) TR immobilization reaction scheme using APTES and glutaraldehyde on a glass bead. (b) Comparison of enzyme activity for

BAPNA after thermal stress between Free-imTR and Alg-imTR. Free-imTR is TR immobilized on a glass bead, and Alg-imTR was synthesized by reacting Alg for 30 minutes by tyrosinase reaction. Each enzyme activity before and after incubation at 50 °C for 60 minutes was measured against 1 mM BAPNA substrate at 37 °C for 30 minutes. Free-imTR and Alg-imTR used for BAPNA analysis were used at a concentration of 2.5 mg/ml for glass beads.

3.4.2 Alg-TR synthesis reaction optimization

After Alg is added to the reaction mixture containing *Sa_Ty* and TR, the hydroxylation reaction by tyrosinase starts immediately. UV absorption of the monophenol moiety at 280 nm of Alg decreases within 15 minutes from the start of the reaction, and the absorption spectrum of aminochrome structure, a ring cyclization derivative of quinone-amine, which appears widely at 490 nm along with quinone at 290–300 nm (Pezzella, Panzella, et al., 2009). The production of melanin-like derivatives produced by tyrosinase is completed within 30 to 45 minutes after the reaction, and the change in the absorption spectrum of the reaction mixture was no longer observed. Therefore, enzyme crosslinking reaction mediated by tyrosinase suggests that coating can be formed quickly within 30 minutes. (**Figure 3.7**)

We selected the optimal coating combination by controlling the respective concentrations of Alg and TR. First, EPC was prepared by fixing the concentration of TR to 0.3 mg/ml and adjusting the concentration of Alg. As the concentration of Alg increased, the viscosity of the reaction solution increased, and accordingly, the TR activity against BAPNA decreased after 120 minutes of Alg-TR thermal incubation at 50 °C. As the reaction solution's viscosity increases, the substrate's diffusion and enzyme activity decrease. Therefore, we selected 0.1% of Alg having the highest activity after 120 minutes of thermal stress as the most optimal concentration (**Figure 3.8a**). Next, the concentration of Alg was fixed at 0.1 w/v%, and the concentration

of TR was changed. As the concentration of TR contained in the reaction solution increased, the turbidity of the solution increased after Alg was added. After the coating reaction with *Sa_Ty*, insoluble particles continued to remain (**Figure 3.8b**). This phenomenon is caused by forming a polyelectrolyte complex according to the electrostatic interaction between charged polymers (Lv et al., 2014). The charge balance becomes zero between materials with opposite charges, forming a hydrophobic part (Quiñones, Peniche, & Peniche, 2018). It also represents that coating starts with a charged interaction between Alg and TR. Alg-TR formed as the concentration of TR increased and maintained higher activity than that of Free-TR even under thermal stress, but the relative activity decreased as the TR concentration increased and the formation of insoluble particles increased. Therefore, we selected TR 0.3 mg/ml, which has the best activity, as the optimized coating reaction condition (**Figure 3.8c**).

The high ionic strength of the buffer can interfere with the electrostatic interaction between the charged materials (Antipov, Sukhorukov, & Möhwald, 2003; Y. Wang et al., 2020). Therefore, we hypothesized that if the ionic strength of the reaction buffer were adjusted, the polysaccharide-protein electrostatic interaction would be improved, and the mutual binding strength would be increased. The Tris buffer used for the synthesis of EPC was 10 and 50 mM, and the ionic strength is 3 mM and 18 mM, respectively. (**Figure 3.9**) The stability of Free-TR was reduced in the 10 mM buffer than 50 mM buffer. However, after Alg coating, it was confirmed that the enzyme stability was

elevated more in 10mM buffer. As a result, enzyme coating was performed using a moderate strength buffer as a reaction buffer.

Since alginate is a polysaccharide capable of trapping water, the hydrodynamic diameter measured by DLS of Alg-TR synthesized by reaction optimization was 78.71 nm (**Table 3.1**), which is larger than that observed in SEM. The pI of TR is 10.5, which has a positively charged surface, and the zeta potential is also 10.6 mV, which has a positive charge. After conjugation of negatively charged polysaccharide, the size was increased, and the zeta potential was also negatively charged particles to -23.6 mV. (**Table 3.1**)

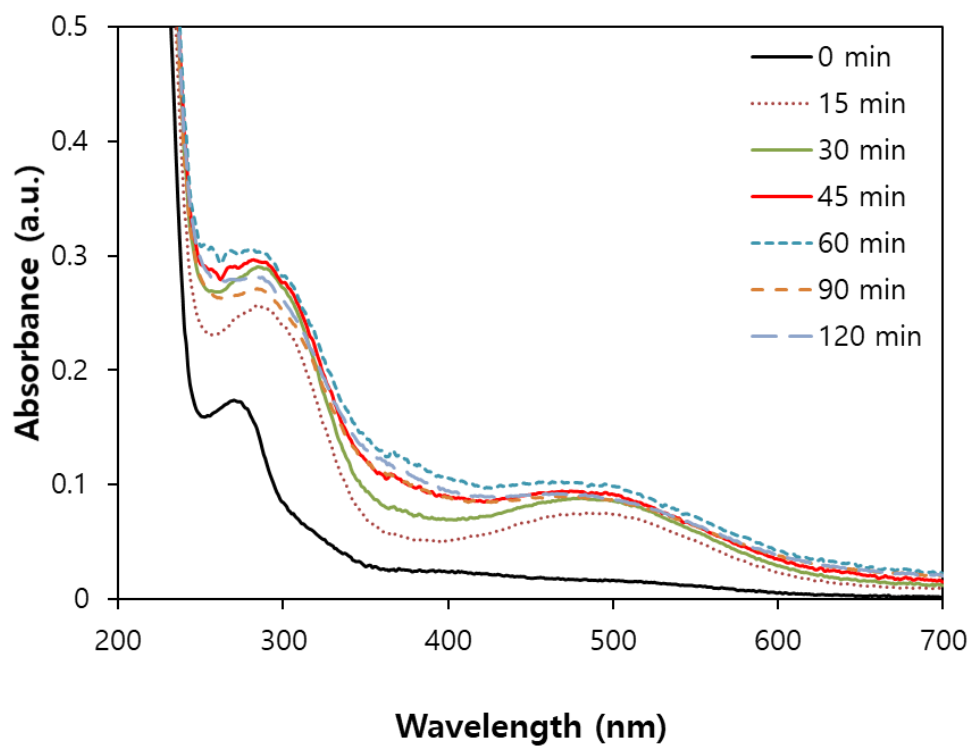


Figure 3.7 UV spectrum change profile of reaction mixture according to Alg-TR synthesis time

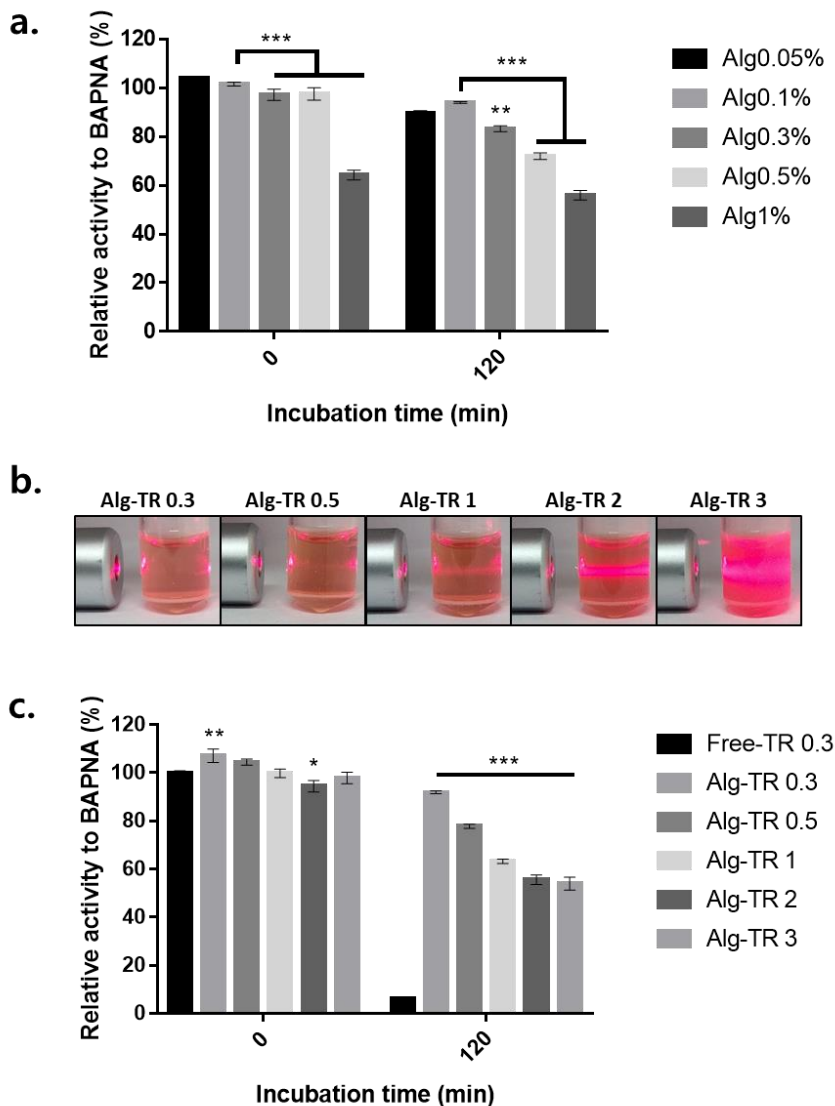


Figure 3.8 Alg-TR optimal reaction condition screening according to Alg and TR concentration gradient

(a) Comparison of relative activity of BAPNA before and after 50 °C incubation of Alg-TR according to Alg concentration variation (0.05, 0.1, 0.3, 0.5, 0.1 w/v%). The concentration of TR was fixed to 0.3 mg/ml. (b) Tyndall scattering effect for 600 nm laser light of the reaction mixture

according to the change in TR concentration (0.3, 0.5, 1, 2, 3 mg/ml), and (c) BAPNA before and after 50°C incubation of Alg-TR. A comparison of relative activity for Alg concentration was fixed to 0.1 w/v%. All assays were diluted so that the final TR concentration of the assay mixture was 0.1 mg/ml. And the degradation activity of Free-TR to 1 mM BAPNA at 37 °C for 20 minutes was set as 100% relative activity.

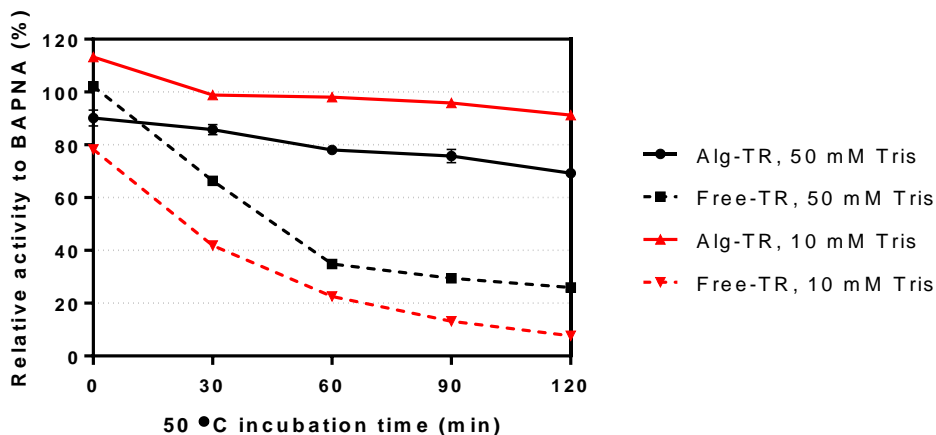


Figure 3.9 TR stability assay that changes according to the ionic strength of the Alg-TR synthesis buffer.

After incubation at 50 °C, the activity of BAPNA was measured to measure the activity of TR in 10 mM or 50 mM pH 8.0 buffer. The relative activity was calculated by setting the initial activity of Free-TR at time 0 to 100%. The final concentration of TR was 0.1 mg/ml in the TR assay mixture. The activity assay result of Free-TR before the tyrosinase reaction is indicated by a dotted line, and a solid line indicates Alg-TR.

Table 3.1 Hydrodynamic diameter and surface potential of Free-TR and Alg-TR measured by DLS

	Average diameter (d.nm)	Zeta potential (mV)
Free-TR	4.27 ± 0.81	10.6 ± 4.3
Alg-TR	78.71 ± 48.3	-23.6 ± 17.8

3.4.3 Enzyme kinetics of EPC according to the charge of small molecule substrates

Since Alg-TR is an environment in which the charged material is covalently bonded around the TR by the charged polymer, the enzyme kinetics will change depending on the charge of substrates (J. Thiele et al., 2018). A pH shift occurred in the TR complex with a polymer of opposite charge as in the previously reported polyelectrolyte complex study. Free-TR has an optimum pH of 8, whereas Alg-TR has a pH optimum of 10 or higher. **(Figure 3.10)** It suggests that the formation of a polyelectrolyte complex between positively charged protein and negatively charged polysaccharide was involved in improving TR stability and pH optimum.

Therefore, BAPNA, a positively charged substrate including an arginine residue, and succinyl-L-Ala-L-Ala-L-Pro-L-Phe-*p*-nitroanilide (Suc-AAPF-NA) with a negative charge including a succinyl moiety were selected to measure TR enzyme kinetics (k_{cat} , K_M , k_{cat}/K_M). **(Table 3.2)** Since the covalently bonded polymer environment reduced TR flexibility, the k_{cat} of Alg-TR was reduced compared to that of Free-TR, regardless of the substrate charge. In particular, since repulsion occurs for Suc-AAPF-NA, which has the same charge as alginate surrounding the enzyme surface, the k_{cat} reduction of Alg-TR is significant. However, the changing profile of K_M is quite different from k_{cat} according to the charge of the substrate. The K_M value

decreased only in BAPNA, a positively charged substrate, indicating that the affinity with the substrate increased. This can be interpreted because the substrate of the charge opposite the negatively charged polymer has a better electrical affinity, making it easier to access the enzyme. The change in K_M according to the charge of the substrate suggests that the enzyme surface-immobilized polymer significantly affects the enzyme kinetics. As a result, an increase or decrease in enzyme efficiency (k_{cat}/K_M) occurred depending on the substrate charge due to the polymeric environment around the enzyme.

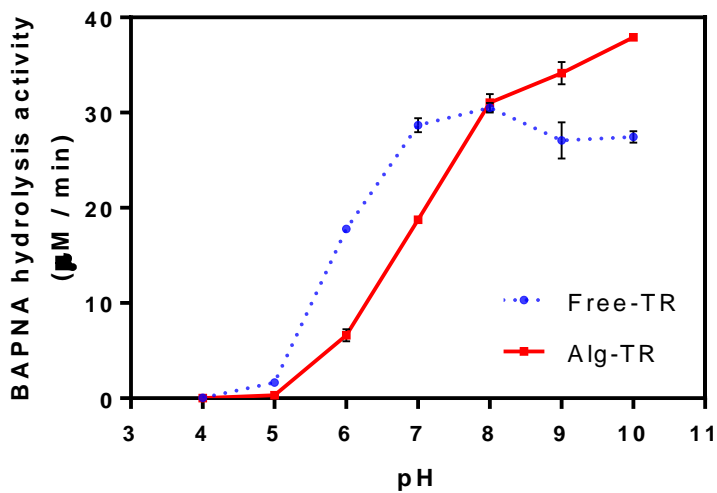


Figure 3.10 Changes in the optimum pH properties of AIT-TR

A graph measuring the activity of Free-TR and AIT-TR on BAPNA in 50 mM buffer corresponding to each pH. The relative activity was calculated by setting the initial activity of Free-TR at 0 min to 100%. The final concentration of TR was 0.1 mg/ml in the TR assay mixture.

Table 3.2 Comparison of enzyme kinetics of Free-TR and Alg-TR according to the charge of small molecule substrates

BAPNA as a positively charged substrate and Suc-AAPF-NA as a negatively charged substrate were used, respectively.

Substrate	Enzyme complex	k_{cat} (10^{-4} s^{-1})	K_{M} (10^{-4} M)	$k_{\text{cat}} / K_{\text{M}}$
BAPNA	Free-TR	1.79 ± 0.36	10.49 ± 3.24	0.17
	Alg-TR	1.66 ± 0.2	8.86 ± 1.45	0.19
Suc-AAPF-NA	Free-TR	1.18 ± 0.05	1.17 ± 0.02	0.99
	Alg-TR	0.92 ± 0.004	1.16 ± 0.01	0.79

3.4.4 Measurement of EPC stability increase for thermal and water-miscible organic solvents

Next, we compared the effect of complex formation by covalent crosslinking on improving TR thermal stability. (**Figure 3.11a**) When only Alg and TR were mixed (Alg + TR), and the tyrosinase crosslinking reaction was not carried out, it did not significantly improve stability compared to Free-TR. Instead, the decrease in activity within the first 30 minutes of 50°C incubation was more significant in Alg + TR than in Free-TR. This supposed to be the increase in enzyme activity and the increase in the self-degradation activity of the trypsin due to the polymer electrolyte combination that exists freely in the solution. When the two materials were mixed without tyrosinase crosslinking, the T_m value of Alg + TR increased to 46.18°C. Compared to Free-TR, significant change in thermal stability of Alg-TR was not observed. As a result of inducing crosslinking between materials with *Sa_Ty*, the stability of Alg-TR after incubation at 50 °C for 2 h was significantly improved compared to Free-TR. The melting temperature (T_m) of the protein was measured to identify the thermal stability of TR. Alg-TR has a T_m value of 58.11 °C, whereas Free-TR is 45.14 °C. (**Table 3.3**) The same increasing tendency in the melting temperature as the BAPNA assay result.

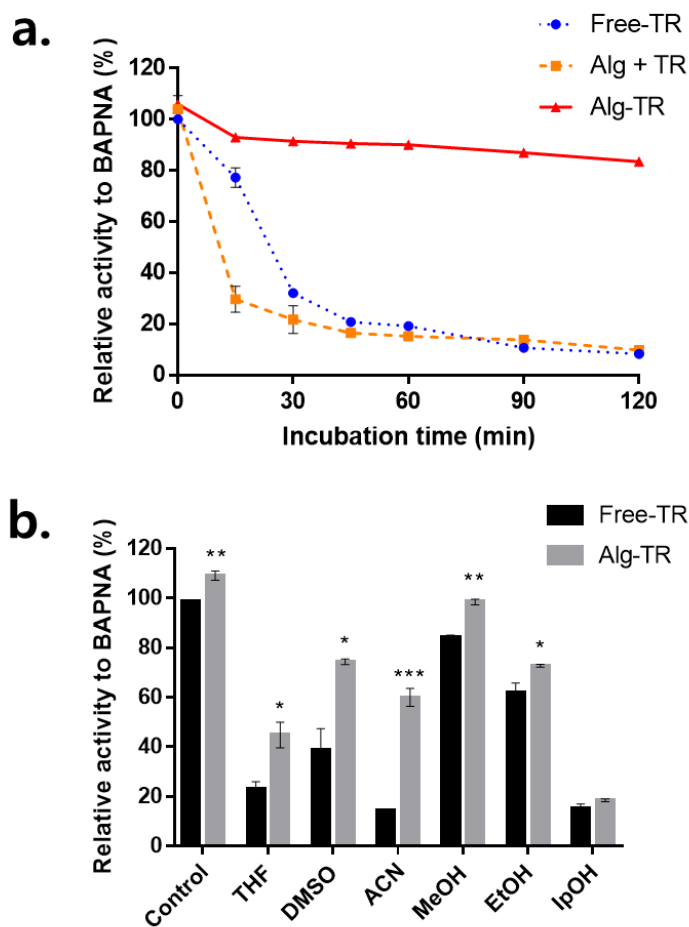


Figure 3.11 BAPNA activity assay for improvement of thermal stability and organic solvent stability of AIT-TR

(a) Native TR (Free-TR) and Alginate-tyramine and TR were mixed without SaTy reaction (Alg + TR), and enzyme-polysaccharide complex (Alg-TR) synthesized by SaTy reaction was incubated at 50 °C, respectively. BAPNA assay was performed for 30 min, and activity at each time period was plotted. (b) BAPNA assay in pH 8.0 Tris buffer reaction mixture containing 40 v/v% of water miscible organic solvents. As a control, pH 8.0 Tris buffer

without organic solvent was used. The relative activity was calculated by setting the initial activity of Free-TR at 0 min to 100%. The final concentration of TR was 0.1 mg/ml in the TR assay mixture.

Table 3.3 Protein melting temperature (T_m , °C) measurement to estimate the thermal resistance of TR

	T_m (°C)
Free-TR	45.14 ± 0.17
Alg + TR	46.18 ± 0.63
Alg-TR	58.11 ± 0.72

Although water is an ideal liquid for biological reactions, it is somewhat lacking in industrially used synthetic reactions. Therefore, industrially used enzymes are required to act as catalysts in a reaction system containing an organic solvent to dissolve the hydrophobic substrate and eliminate the side effect caused by water (Stepankova et al., 2013). However, most natural enzymes do not have low catalytic efficiency due to structural changes in organic solvents. The structure of Alg-TR can be stabilized by interaction with protein surface residues instead of water molecules by the hydrophilic polysaccharide shell surrounding the TR. Therefore, Alg-TR's ability to capture water for surrounding enzyme structure will be better compared to Free-TR. Even when the reaction mixture contains water-miscible organic solvent, it can be expected that stability will be improved by maintaining the water environment around the enzyme. To test the stability of Alg-TR in organic solvents, we used water-miscible organic solvents such as tetrahydrofuran (THF), dimethyl sulfoxide (DMSO), acetonitrile (ACN), methanol (MeOH), ethanol (EtOH), and isopropanol (IpOH), respectively. TR activity assay for BAPNA was performed in a mixture containing 40 v/v% of organic solvent. (**Figure 3.11b**) As a result, it was shown that Alg-TR was more stable than Free-TR in the reaction environment containing all water-miscible organic solvents. Depending on the type of organic solvent, the activity was 1.06 to 3.87 times higher than Free-TR.

3.4.5 Increased storage stability of TR by EPC formation

The accelerated storage stability test was measured at 50, 60, and 70 °C to determine the storage stability of Alg-TR. (**Figure 3.12**) After 30 minutes of incubation at 50 °C for Free-TR, the relative hydrolysis activity for BAPNA was reduced by less than half to 31.76%. After 120 minutes of incubation, the activity was 8.31%. After incubation at 60 °C, the relative activity decreased by less than half within 15 minutes. However, Alg-TR maintained 77.4% of its initial activity even after incubation at 50 °C for 300 minutes. Assuming that protein degradation is first-order reaction kinetics without considering TR self-degradation, storage stability according to temperature was predicted (Magari, 2002).

Half of the initial activity was maintained until incubation at 60 °C for 90 minutes, and it took 120 minutes to decrease to less than 10% of the initial activity at 70 °C. The storage stability of Free-TR and Alg-TR was modeled based on the previous studies. (**Figure 3.12 and 3.13**) The estimated TR's storage stability time (t_s) was based on the point in time when 50% of the initial Free-TR activity remained, assuming that the TR was stored in pH 8.0, 10 mM Tris buffer. As a result, t_s at ambient temperature (25 °C) was 0.05 days for Free-TR but 68.15 days for Alg-TR. (**Table 3.4**) The thermal stability and storage stability of Alg-TR was significantly improved compared to the control by charged interaction and covalent crosslinking. The binding between the charged carbohydrate and protein in the tyrosinase reaction

suggests the advantage of protecting and stabilizing the enzyme under high temperature and harsh storage conditions.

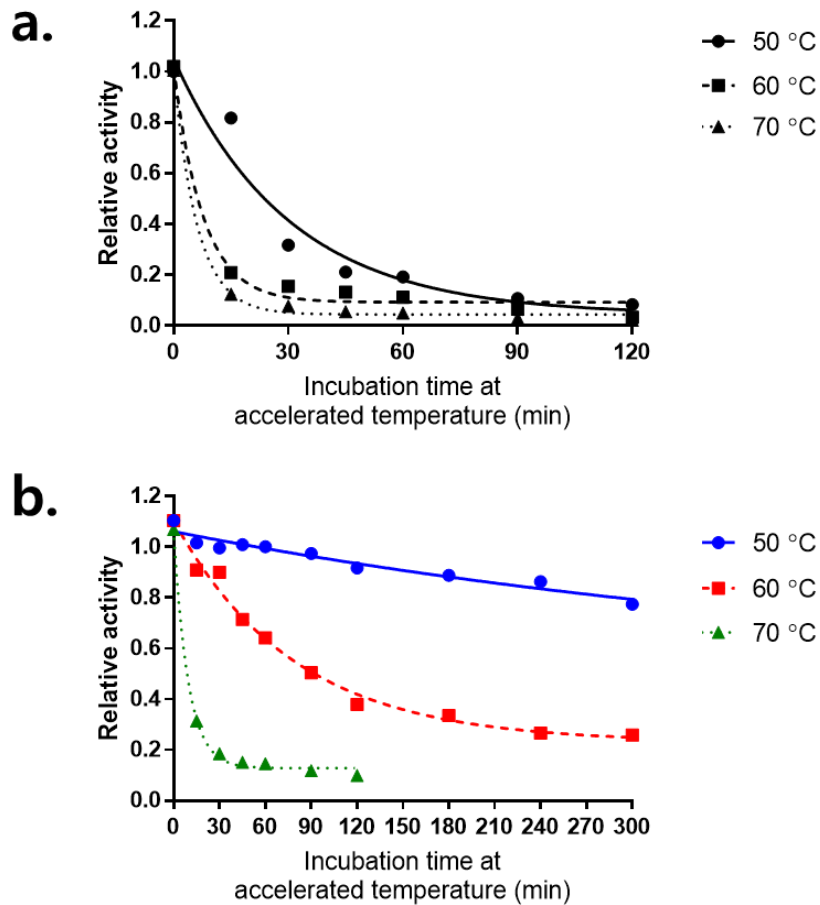


Figure 3.12 Decrease in enzymatic activity of TR according to accelerated temperature activity test

BAPNA assay was performed at 50, 60, and 70 °C for the accelerated temperature activity test. (a) is Free-TR, and (b) is accelerated stability data for Alg-TR. Based on the obtained data, non-linear regression was performed, and an arrhenius plot was drawn to obtain the degradation activation energy based on the obtained slope (k). The relative activity was calculated by setting the initial activity of Free-TR at 0 min to 100%. The final concentration of

TR was 0.1 mg/ml in the TR assay mixture.

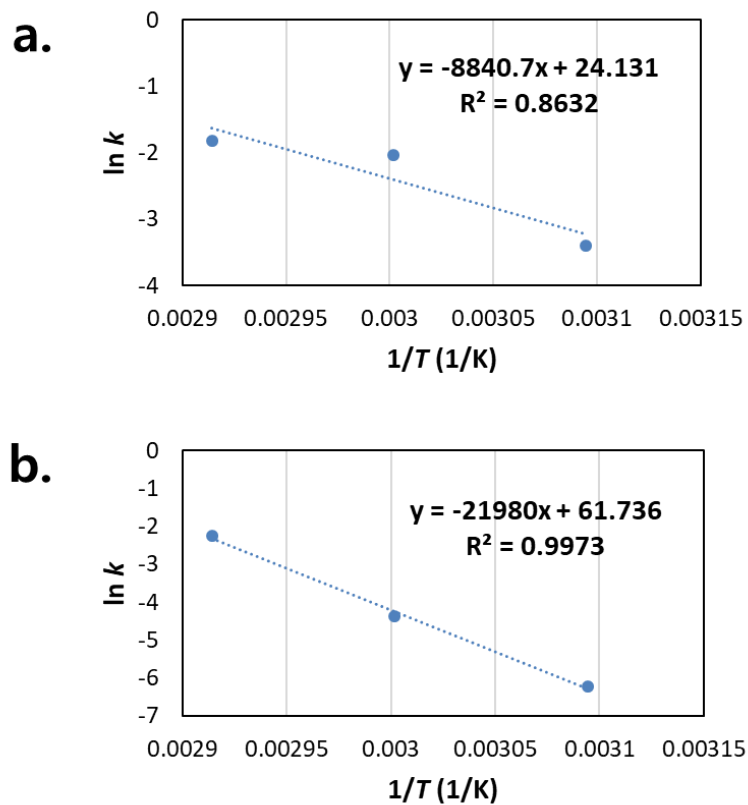


Figure 3.13 Arrhenius plot on the degradation of (a) Free-TR and (b) Alg-TR

Table 3.4 Estimated storage stability time of (a) Free-TR and (b) Alg-TR

a. Free-TR		
Temperature (°C)	Temperature (K)	Estimated storage time (t_s)
		day
4	277.15	0.48
10	283.15	0.25
15	288.15	0.14
20	293.15	0.09
25	298.15	0.05
30	303.15	0.03
35	308.15	0.02
40	313.15	0.01

b. Alg-TR

Temperature (°C)	Temperature (K)	Estimated storage time (t_s)
		day
4	277.15	18173.59
10	283.15	3385.27
15	288.15	880.25
20	293.15	239.65
25	298.15	68.15
30	303.15	20.20
35	308.15	6.23
40	313.15	1.99

3.4.6 Enzyme-protein coating for the application to various enzymes

In order to find out whether enzyme stabilization using Alg and *SaTy* is applied to other enzymes other than trypsin, additional candidate enzymes were selected. Elastase (ES) from porcine pancreas (PDB ID: 1QNJ (Würtele, Hahn, Hilpert, & Höhne, 2000)), Protease (subtilisin, ST) from *Bacillus licheniformis* (PDB ID: 1C3L), chymotrypsin (CT) from bovine pancreas (PDB ID: 5J4Q (Tornøe, Johansson, & Wahlund, 2017)) belonging to the serine protease group with trypsin were selected. **(Figure 3.14a, b and c)** The isoelectric points of ES, ST, and CT are positively charged surface potentials with 8.44, 6.57, and 8.52, respectively, and it was expected that there would be an enzyme stabilization effect by the charged interaction with AIT. Moreover, α -glucosidase (GC) from baker's yeast (PDBI ID: 4J5T (Barker & Rose, 2013)), have an isoelectric point of 5.4 and expected to negatively charged surface potential, was selected. **(Figure 3.14c)** In the case of GC, because our enzyme stabilization method was based on a charged interaction, it was used as an example that may not apply to all enzymes.

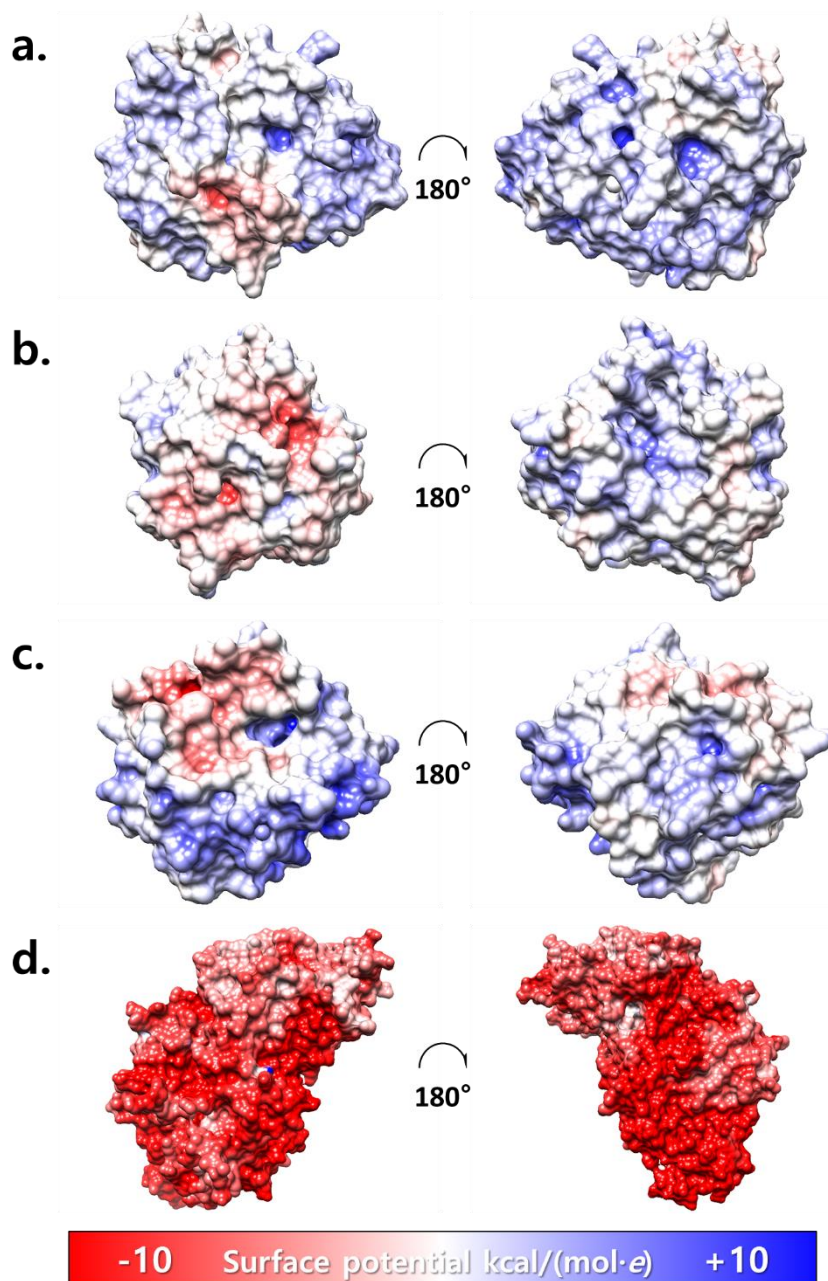


Figure 3.14 Surface charge of various proteins at pH 8.0

Predicted surface potential of (a) elastase (ES), (b) subtilisin (ST), (c) chymotrypsin (CT), and (d) a-glucosidase (GC) at pH 8.0

For ES, ST, CT, and GC, free-form and Alg-complex forms were incubated at 50 °C to perform a trypsin assay. For each enzyme, Suc-AAPF-NA was used as a substrate for ES, CT, and ST, and p-nitrophenyl α -glucose was used as a substrate for GC. As a result of comparing the relative activities of the free-form and the Alg-form, there was a clear difference in the change in enzyme stability between the positive, neutral charged protein and the negatively charged protein (**Figure 3.15**). First, in the case of positive and neutral charged ES (net charge = 6.00), CT (net charge = 6.00), and ST (net charge = 5.66×10^{-15}), the activity was slightly lower in the initial 0 min in the Alg-form than in the free-form. This is expected because the charge of the substrate, Suc-AAPF, is the same as that of Alg. After thermal incubation, it was confirmed that the enzyme activity was better maintained in the Alg complex than in the free form. After incubation at 50 °C for 120 minutes, ES, ST, and CT showed 1.07, 2.85, and 116.09 times higher Alg complex activity than free form, respectively.

On the other hand, negatively charged GC (net charge = -4.30×10^1) had a significant difference between the free-form and Alg complex in the 0 min sample, but both types lost their activity after incubation 120min. In particular, even though the covalent network was formed, Alg did not help improve thermal stability. As we mentioned, it can be suggested that both charged and covalent interactions are involved in enzyme stabilization. In other words, for enzyme stabilization through crosslinking network formation using

tyrosinase and polysaccharide suggests that additional research is needed on the stabilization tendency according to the surface charge of various proteins.

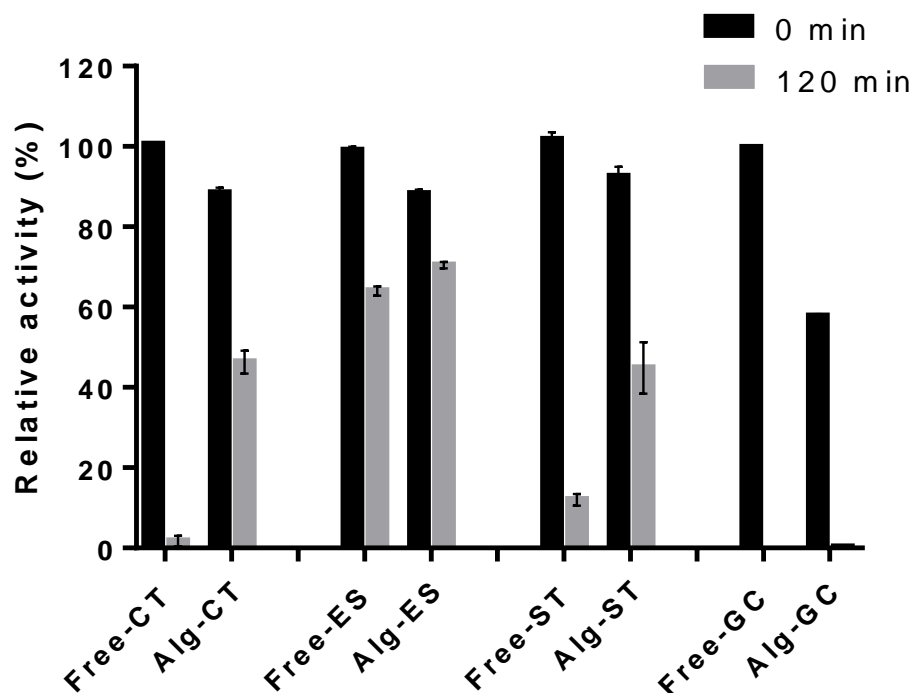


Figure 3.15 Comparison of relative activity after 50 °C incubation for ES, ST, CT, and GC

ES, ST, and CT activities were measured for Suc-AAPF-NA, and GC for *p*-nitrophenyl α -glucose, respectively. The relative activities of free-form and AIT-form were compared before and after incubation at 50 °C for 120 minutes. The final concentration of the enzyme used in each reaction was 0.1 mg/ml for ES, ST, and GC, and 0.0001 mg/ml for ST.

3.5 Conclusion

From the effort to discover stable enzymes to the production of single enzyme nanoparticles wrapped around a single enzyme, research on ways to increase the stability of enzymes has been ongoing for a long time. While increasing the stability of the enzyme, it is not easy to take care of substrate specificity, enzyme activity, pH stability, thermal stability, storage storability, and organic solvent stability at the same time (Chapman & Stenzel, 2019). If enzyme activity is lost in the process of compartmentalization to stabilize the enzyme, it will ultimately not be an ideal stabilization method. Therefore, it is necessary to develop a method for stabilizing the enzyme within a short time in an environment where the enzyme is as stable as possible.

This study showed a method for stabilizing an enzyme (TR) using an enzyme (*SaTy*). By wrapping the enzyme surface with polysaccharides, it was intended to replace the water-protein non-covalent interaction around the enzyme. The interaction between charged polysaccharides and proteins was also selected to stabilize the enzyme structure. In addition, the structure was completed by forming an EPC by covalent bonding between the enzyme and polysaccharide through a crosslinking reaction mediated by the reaction of tyrosinase with substrate specificity to monophenol and diphenol substrates. TR, which we used as a model enzyme, is a positively charged protein, and an enzyme- polysaccharide complex was implemented using alginate of the

opposite charge. Alg-TR synthesized under moderate conditions using only enzymes, and tyramine-conjugated polysaccharides showed remarkable improvements in thermal stability, organic solvent stability, enzyme kinetics, and storage stability compared to Free-TR, as we expected. Therefore, with our enzyme stabilization method, it is possible to use a biocompatible, inexpensive, and readily available polysaccharide to preserve the enzyme activity as much as possible while ensuring stabilization. In addition to the negatively charged polysaccharide-positively charged protein combination used in this study, polysaccharides such as dextran, cellulose, and chitosan exist, so a platform can be used to stabilize various industrial proteins can be created. Furthermore, there is a possibility to synthesize an enzyme drug (D. H. Kim et al., 2020) using a charged polysaccharide found in the human body, such as hyaluronic acid.

Chapter 4.

Overall Conclusion and Further Suggestions

4.1 Overall conclusion

In the field of bioactive nanoparticle synthesis, many researchers are conducting research aimed at medical applications as well as industrial applications. Therefore, interest in an enzymatic synthesis method that is biocompatible, minimizes the use of toxic chemicals, and can preserve the properties of fragile biomacromolecules is constantly increasing (Sanket & Das, 2021). Here, we studied a reaction method to control the crosslinking reaction produced through the phenolic substrate-specific hydroxylation of tyrosinase. As a result, *Burkholderia cepacia* tyrosinase and *Streptomyces avermilitis* tyrosinase with two different properties were used to create melanin and an enzyme-polymer network.

We showed that *BcTy* could be used to synthesize homogeneous eMNPs under optimal reaction conditions of pH 3-5. The enzymatic method was able to synthesize various substrates and soluble eMNPs with a size of 5-20 nm by controlling the reaction at pH 5.0 or lower and pH 3.0 or higher. It was found that the leading cause of soluble melanin synthesis revealed through physicochemical analysis of eMNP was possible by preventing random crosslinking at acidic pH. Because eMNP preserves the catechol structure containing many hydroxyl groups, it showed antioxidant activity comparable to that of ascorbic acid, a natural antioxidant. Moreover, similar to the surface adhesion ability of mussel foot protein, eMNP was included in the gelatin

hydrogel, contributing to the increase in the stickiness of the hydrogel. We synthesized a melanin structure with a linear structure longer than 8 mer by using a method to control crosslinking reaction by oxidation in acid using *BcTy*.

Next, we constructed an enzyme-polysaccharide complex that enhances the stability of the enzyme by using the crosslinked network itself induced by *SaTy*. A robust enzyme-polysaccharide complex was synthesized by packing the protein structure with non-covalent bonding and forming a complex between polysaccharide and enzyme, which is well known for contributing to stability improvement and forming a covalent bonding network through tyrosinase crosslinking. For TR, a model enzyme with a positive surface charge only negatively charged AIT conjugated with tyramine affected increasing enzyme stability, and thermal stability, organic solvent stability, and storage stability were increased by tyrosinase crosslinking. The melting temperature (T_m) of the synthesized AIT-TR after optimizing the reaction conditions was increased by about 13°C compared to the Free-TR. Stability to water-miscible organic solvents THF, DMSO, ACN, MeOH, EtOH, and IpOH was increased by 1.06 to 3.87 times. Furthermore, the accelerated degradation test and degradation model prediction predicted that AIT-TR has a shelf life of about 8 months at room temperature.

4.2 Further suggestions

4.2.1 Immobilization of tyrosinase enzyme to limit excessive hydroxylation product formation reaction

Although the enzymatic synthesis method is greener than the chemical synthesis method, in the end, the effect of the enzyme catalyst remaining on the final product cannot be ignored. Since the tyrosinase we used to be recombinant, a complicated approval process will be required to use the final product containing tyrosinase as a practical application product. In addition, until the tyrosinase activity is wholly lost, the crosslinking reaction through the hydroxylation reaction may be continuously catalyzed to form an aggregate finally.

Methods have been reported to solve the problem, such as inhibiting the tyrosinase reaction by adding an inhibitor or limiting further crosslinking by reducing the tyrosinase reaction product. However, if additional chemicals are added to the biomedical material used in the human body, this inevitably leads to uncomplicated results (Fernandes & Kerkar, 2017; S. H. Lee et al., 2016).

Therefore, we propose a method for immobilizing tyrosinase through physical beads or column immobilization and producing hydroxylation products in a continuous flow reactor (**Figure 4.1**) (Saini et al., 2015; Wee et al., 2019; Wu et al., 2017). Both the melanin synthesis and the enzyme-

polymer complex we studied require only the product of the tyrosinase reaction. By immobilizing tyrosinase with the solid support immobilization method, it is expected that not only tyrosinase can be reused, but also the additional reaction by highly active hydroxylation enzyme in the reaction final product will not be continued.

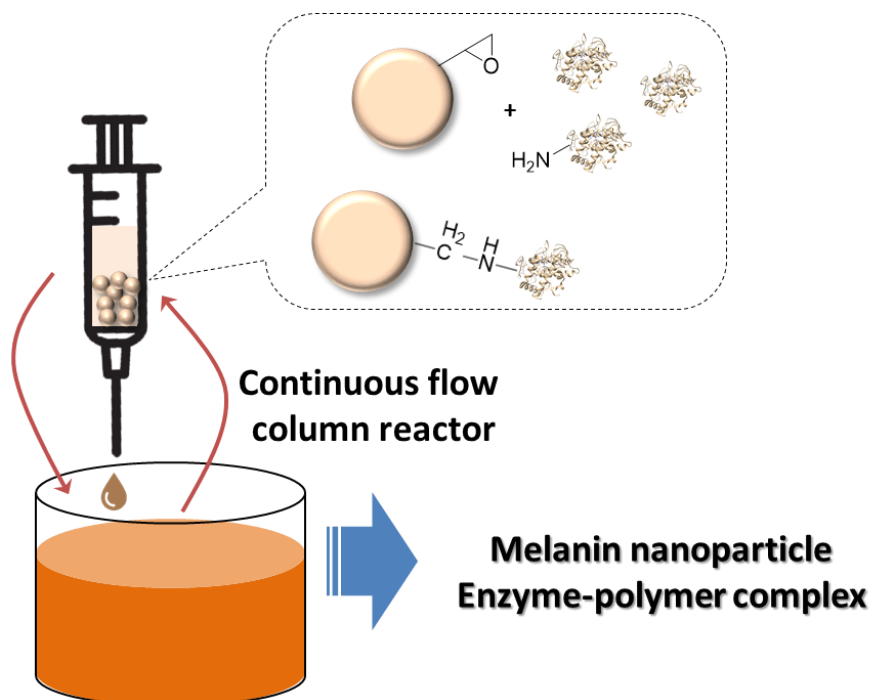


Figure 4.1 Schematic diagram for crosslink product production through tyrosinase immobilization and continuous flow column reactor production

4.2.2 Melanin dyeing at pH 5 or lower to maintain the stability of animal fibers.

Since animal fibers such as silk and wool are made of protein, they are vulnerable to degradation, high temperature, and oxidizing agents in alkaline conditions. Therefore, traditionally in the textile industry, dyes were dyed with acid dyes to preserve the properties of animal fibers consisting of proteins. However, there is a risk of staining and discoloration. There is a drawback that environmental regulations restrict the use of the dye itself (Q. Zhou, Wu, & Xing, 2022). A dyeing method using laccase in acidic conditions has been reported as a method that preserves the fastness and color depth of animal fabrics and can additionally impart antibacterial and antioxidant abilities. The pigment produced by polymerization of the phenolic substrate is adsorbed as an aggregate on the silk surface, enabling strong dyeing through non-covalent bonds such as hydrogen bonding and π - π interaction, and Michael addition (Zhang et al., 2017). Therefore, the eMNP using tyrosinase proposed in this study can also be used for dyeing animal fabrics. Based on the broad substrate specificity and fast reaction rate of tyrosinase, we propose a method for staining animal fibers using polyphenol substrates of various colors derived from plants. **(Figure 4.2)**

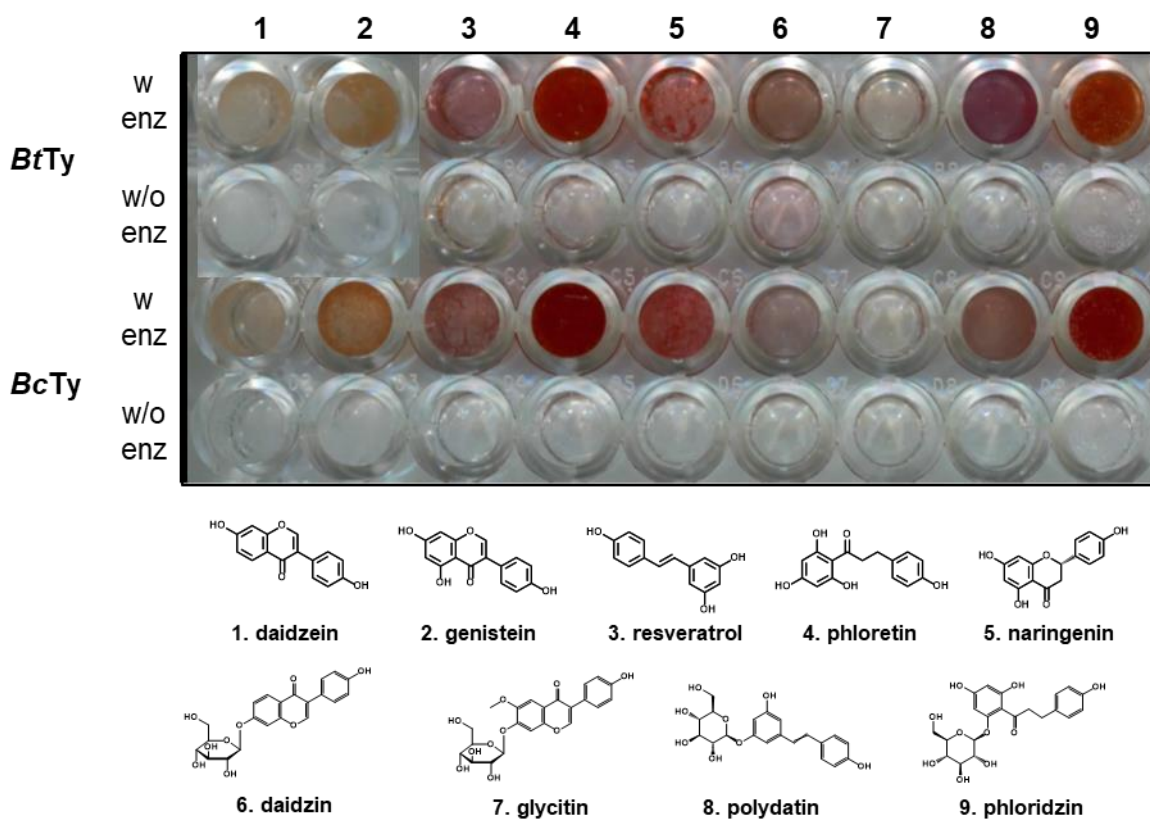


Figure 4.2 Production of natural pigments by bioconversion of plant-derived polyphenols into *Burkholderia thailandensis* tyrosinase (*BtTy*) and *Burkholderia cepaica* tyrosinase (*BcTy*) with high activity under acidic reaction conditions below pH 5

4.2.3 Establishment of polymer design strategy for universal application and biomedical use of enzyme-polymer complex with improved stability

The enzyme-polysaccharide complex synthesized in this study has a pI value higher than the synthesis condition (ca. pH 8.0), has a neutral net surface potential, and was effective against a protein of 0 or higher. However, there are proteins with an innumerable variety of amino acids in the vast nature. At least, stabilizing proteins with most charged surfaces suggests that a method for forming a polysaccharide complex with a charge other than negatively charged alginate is required. However, the solubility of chitosan, the only positively charged polysaccharide, is pH-dependent, so its use is limited. Therefore, alternative materials with improved solubility, such as chitosan glycol, can be used. In addition, it is necessary to study enzyme-complex formation and characterization using polycationic biopolymers (e.g., polyethylene imine, poly (L-lysine), polyamidoamine) not limited to polysaccharides.

References

- Aguilera, F., McDougall, C., & Degnan, B. M. (2013). Origin, evolution and classification of type-3 copper proteins: lineage-specific gene expansions and losses across the Metazoa. *BMC evolutionary biology*, *13*(1), 1-12.
- Agunbiade, M., & Roes-Hill, L. (2022). Application of bacterial tyrosinases in organic synthesis. *World Journal of Microbiology and Biotechnology*, *38*(1), 1-19.
- Ajito, S., Iwase, H., Takata, S.-i., & Hirai, M. (2018). Sugar-mediated stabilization of protein against chemical or thermal denaturation. *The Journal of Physical Chemistry B*, *122*(37), 8685-8697.
- Alfieri, M. L., Micillo, R., Panzella, L., Crescenzi, O., Oscurato, S. L., Maddalena, P., . . . d'Ischia, M. (2017). Structural basis of polydopamine film formation: Probing 5, 6-dihydroxyindole-based eumelanin type units and the porphyrin issue. *ACS applied materials & interfaces*, *10*(9), 7670-7680.
- Antipov, A. A., Sukhorukov, G. B., & Möhwald, H. (2003). Influence of the ionic strength on the polyelectrolyte multilayers' permeability. *Langmuir*, *19*(6), 2444-2448.
- Ba, S., & Vinoth Kumar, V. (2017). Recent developments in the use of tyrosinase and laccase in environmental applications. *Critical reviews in biotechnology*, *37*(7), 819-832.
- Barker, M. K., & Rose, D. R. (2013). Specificity of processing α -glucosidase I is guided by the substrate conformation: crystallographic and in

- silico studies. *Journal of Biological Chemistry*, 288(19), 13563-13574.
- Beloqui, A., Kobitski, A. Y., Nienhaus, G. U., & Delaittre, G. (2018). A simple route to highly active single-enzyme nanogels. *Chemical science*, 9(4), 1006-1013.
- Bergtold, C., Hauser, D., Chaumont, A., El Yakhlifi, S., Mateescu, M., Meyer, F., . . . Ihiawakrim, D. (2018). Mimicking the chemistry of natural eumelanin synthesis: The KE sequence in polypeptides and in proteins allows for a specific control of nanosized functional polydopamine formation. *Biomacromolecules*, 19(9), 3693-3704.
- Burzio, L. A., & Waite, J. H. (2000). Cross-linking in adhesive quinoproteins: studies with model decapeptides. *Biochemistry*, 39(36), 11147-11153.
- Cabrera-Valladares, N., Martínez, A., Pinero, S., Lagunas-Munoz, V. H., Tinoco, R., De Anda, R., . . . Gosset, G. (2006). Expression of the melA gene from *Rhizobium etli* CFN42 in *Escherichia coli* and characterization of the encoded tyrosinase. *Enzyme and microbial technology*, 38(6), 772-779.
- Chamorro Gavilanes, J., Cuesta-Seijo, J., & Garcia-Granda, S. Pancreatic bovine Trypsin native and inhibited with Benzamidine from synchotron data. *Protein Data Bank*, 10.
- Chapman, R., & Stenzel, M. H. (2019). All wrapped up: stabilization of enzymes within single enzyme nanoparticles. *Journal of the American Chemical Society*, 141(7), 2754-2769.
- Chen, C.-T., Chuang, C., Cao, J., Ball, V., Ruch, D., & Buehler, M. J. (2014).

- Excitonic effects from geometric order and disorder explain broadband optical absorption in eumelanin. *Nature communications*, 5, 3859.
- Chen, T.-P., Liu, T., Su, T.-L., & Liang, J. (2017). Self-polymerization of dopamine in acidic environments without oxygen. *Langmuir*, 33(23), 5863-5871.
- Choi, S., Ahn, H., & Kim, S. H. (2022). Tyrosinase-mediated hydrogel crosslinking for tissue engineering. *Journal of Applied Polymer Science*, 139(14), 51887.
- Danner, E. W., Kan, Y., Hammer, M. U., Israelachvili, J. N., & Waite, J. H. (2012). Adhesion of mussel foot protein Mefp-5 to mica: an underwater superglue. *Biochemistry*, 51(33), 6511-6518.
- Deri, B., Kanteev, M., Goldfeder, M., Lecina, D., Guallar, V., Adir, N., & Fishman, A. (2016). The unravelling of the complex pattern of tyrosinase inhibition. *Scientific Reports*, 6, 34993. doi:10.1038/srep34993
- Dolashki, A., Voelter, W., Gushterova, A., Van Beeumen, J., Devreese, B., & Tchobanov, B. (2012). Isolation and characterization of novel tyrosinase from *Laceyella sacchari*. *Protein and Peptide Letters*, 19(5), 538-543.
- Dreyer, D. R., Miller, D. J., Freeman, B. D., Paul, D. R., & Bielawski, C. W. (2012). Elucidating the structure of poly (dopamine). *Langmuir*, 28(15), 6428-6435.

- Ehrbar, M., Rizzi, S. C., Schoenmakers, R. G., San Miguel, B., Hubbell, J. A., Weber, F. E., & Lutolf, M. P. (2007). Biomolecular hydrogels formed and degraded via site-specific enzymatic reactions. *Biomacromolecules*, 8(10), 3000-3007.
- Espín, J. C., Soler-Rivas, C., Cantos, E., Tomás-Barberán, F. A., & Wichers, H. J. (2001). Synthesis of the antioxidant hydroxytyrosol using tyrosinase as biocatalyst. *Journal of agricultural and food chemistry*, 49(3), 1187-1193.
- Faccio, G., Kruus, K., Saloheimo, M., & Thöny-Meyer, L. (2012). Bacterial tyrosinases and their applications. *Process Biochemistry*, 47(12), 1749-1760.
- Fairhead, M., & Thöny-Meyer, L. (2012). Bacterial tyrosinases: old enzymes with new relevance to biotechnology. *New biotechnology*, 29(2), 183-191.
- Falatach, R., Li, S., Sloane, S., McGlone, C., Berberich, J. A., Page, R. C., . . . Konkolewicz, D. (2015). Why synthesize protein–polymer conjugates? The stability and activity of chymotrypsin-polymer bioconjugates synthesized by RAFT. *Polymer*, 72, 382-386.
- Fenoll, L. G., Rodríguez-López, J. N., García-Sevilla, F., García-Ruiz, P. A., Varón, R., García-Cánovas, F., & Tudela, J. (2001). Analysis and interpretation of the action mechanism of mushroom tyrosinase on monophenols and diphenols generating highly unstable o-quinones. *Biochimica et Biophysica Acta (BBA) - Protein Structure and*

Molecular Enzymology, 1548(1), 1-22.

doi:[http://dx.doi.org/10.1016/S0167-4838\(01\)00207-2](http://dx.doi.org/10.1016/S0167-4838(01)00207-2)

Fernandes, M. S., & Kerkar, S. (2017). Microorganisms as a source of tyrosinase inhibitors: a review. *Annals of Microbiology*, 67(4), 343-358.

Fujieda, N., Umakoshi, K., Ochi, Y., Nishikawa, Y., Yanagisawa, S., Kubo, M., . . . Itoh, S. (2020). Copper-oxygen Dynamics in Tyrosinase Mechanism. *Angewandte Chemie*.

Gibson, T. D., Higgins, I. J., & Woodward, J. R. (1992). Stabilization of analytical enzymes using a novel polymer-carbohydrate system and the production of a stabilized, single reagent for alcohol analysis. *Analyst*, 117(8), 1293-1297.

Guo, J., Rao, Z., Yang, T., Man, Z., Xu, M., Zhang, X., & Yang, S.-T. (2015). Cloning and identification of a novel tyrosinase and its overexpression in *Streptomyces kathirae* SC-1 for enhancing melanin production. *FEMS Microbiology Letters*, 362(8), fmv041.

Haemers, S., Koper, G. J., & Frens, G. (2003). Effect of oxidation rate on cross-linking of mussel adhesive proteins. *Biomacromolecules*, 4(3), 632-640.

Han, J., Cui, Y., Han, X., Liang, C., Liu, W., Luo, D., & Yang, D. (2020). Super-Soft DNA/Dopamine-Grafted-Dextran Hydrogel as Dynamic Wire for Electric Circuits Switched by a Microbial Metabolism Process. *Advanced Science*, 7(13), 2000684.

- Heck, T., Faccio, G., Richter, M., & Thöny-Meyer, L. (2013). Enzyme-catalyzed protein crosslinking. *Applied microbiology and biotechnology*, 97(2), 461-475.
- Hong, S., Na, Y. S., Choi, S., Song, I. T., Kim, W. Y., & Lee, H. (2012). Non-covalent self-assembly and covalent polymerization co-contribute to polydopamine formation. *Advanced Functional Materials*, 22(22), 4711-4717.
- Hong, S., Wang, Y., Park, S. Y., & Lee, H. (2018). Progressive fuzzy cation- π assembly of biological catecholamines. *Science advances*, 4(9), eaat7457.
- Hu, J., Yang, L., Yang, P., Jiang, S., Liu, X., & Li, Y. (2020). Polydopamine free radical scavengers. *Biomaterials science*, 8(18), 4940-4950.
- Huang, L., Liu, M., Huang, H., Wen, Y., Zhang, X., & Wei, Y. (2018). Recent advances and progress on melanin-like materials and their biomedical applications. *Biomacromolecules*, 19(6), 1858-1868.
- Huynh, K., & Partch, C. L. (2015). Analysis of protein stability and ligand interactions by thermal shift assay. *Current protocols in protein science*, 79(1), 28.29. 21-28.29. 14.
- J. Thiele, M., Davari, M. D., König, M., Hofmann, I., Junker, N. O., Mirzaei Garakani, T., . . . Schwaneberg, U. (2018). Enzyme–polyelectrolyte complexes boost the catalytic performance of enzymes. *ACS Catalysis*, 8(11), 10876-10887.
- Jablaoui, A., Kriaa, A., Akermi, N., Mkaouar, H., Gargouri, A., Maguin, E.,

- & Rhimi, M. (2018). Biotechnological applications of serine proteases: a patent review. *Recent patents on biotechnology*, 12(4), 280-287.
- Jesionowski, T., Zdarta, J., & Krajewska, B. (2014). Enzyme immobilization by adsorption: A review. *Adsorption*, 20(5), 801-821.
- Ju, K.-Y., Degan, S., Fischer, M. C., Zhou, K. C., Jia, X., Yu, J., & Warren, W. S. (2019). Unraveling the molecular nature of melanin changes in metastatic cancer. *Journal of biomedical optics*, 24(5), 051414.
- Ju, K.-Y., Fischer, M. C., & Warren, W. S. (2018). Understanding the Role of Aggregation in the Broad Absorption Bands of Eumelanin. *ACS nano*, 12(12), 12050-12061.
- Ju, K.-Y., Kang, J., Pyo, J., Lim, J., Chang, J. H., & Lee, J.-K. (2016). pH-Induced aggregated melanin nanoparticles for photoacoustic signal amplification. *Nanoscale*, 8(30), 14448-14456.
- Ju, K.-Y., Lee, J. W., Im, G. H., Lee, S., Pyo, J., Park, S. B., . . . Lee, J.-K. (2013). Bio-inspired, melanin-like nanoparticles as a highly efficient contrast agent for T₁-weighted magnetic resonance imaging. *Biomacromolecules*, 14(10), 3491-3497.
- Ju, K.-Y., Lee, Y., Lee, S., Park, S. B., & Lee, J.-K. (2011). Bioinspired polymerization of dopamine to generate melanin-like nanoparticles having an excellent free-radical-scavenging property. *Biomacromolecules*, 12(3), 625-632.
- Kampatsikas, I., & Rompel, A. (2021). Similar but Still Different: Which Amino Acid Residues Are Responsible for Varying Activities in Type-

III Copper Enzymes? *ChemBioChem*, 22(7), 1161-1175.

Kariduraganavar, M. Y., Kittur, A. A., & Kamble, R. R. (2014). Polymer synthesis and processing. In *Natural and synthetic biomedical polymers* (pp. 1-31): Elsevier.

Kashima, C., Tomotake, A., & Omote, Y. (1987). Photolysis of the ozonide derived from 1, 4-benzodioxins. Synthesis of labile o-benzoquinones. *The Journal of organic chemistry*, 52(25), 5616-5621.

Kim, D. H., Lee, H. S., Kwon, T.-W., Han, Y.-M., Kang, N.-W., Lee, M. Y., . . . Lee, J.-Y. (2020). Single enzyme nanoparticle, an effective tool for enzyme replacement therapy. *Archives of Pharmacal Research*, 43(1), 1-21.

Kim, H., Kim, H., & Choi, Y. S. (2014). Recent advances in tyrosinase research as an industrial enzyme. *KSBB Journal*, 29(1), 1-8.

Kim, H., Yeon, Y. J., Choi, Y. R., Song, W., Pack, S. P., & Choi, Y. S. (2016). A cold-adapted tyrosinase with an abnormally high monophenolase/diphenolase activity ratio originating from the marine archaeon *Candidatus Nitrosopumilus koreensis*. *Biotechnology letters*, 38(9), 1535-1542.

Kim, H., Yi, J.-Y., Kim, B.-G., Song, J. E., Jeong, H.-J., & Kim, H. R. (2020). Development of cellulose-based conductive fabrics with electrical conductivity and flexibility. *PLoS One*, 15(6), e0233952.

Kim, N., Lee, H., Han, S. Y., Kim, B. J., & Choi, I. S. (2021). Enzyme-mediated film formation of melanin-like species from ortho-diphenols:

Application to single-cell nanoencapsulation. *Applied Surface Science Advances*, 5, 100098.

Kim, S.-H., Kim, K., Kim, B. S., An, Y.-H., Lee, U.-J., Lee, S.-H., . . . Hwang, N. S. (2020). Fabrication of polyphenol-incorporated anti-inflammatory hydrogel via high-affinity enzymatic crosslinking for wet tissue adhesion. *Biomaterials*, 242, 119905.

Kim, S.-H., Lee, S.-H., Lee, J.-E., Park, S. J., Kim, K., Kim, I. S., . . . Kim, B.-G. (2018). Tissue adhesive, rapid forming, and sprayable ECM hydrogel via recombinant tyrosinase crosslinking. *Biomaterials*, 178, 401-412.

Kim, S., Sureka, H. V., Kayitmazer, A. B., Wang, G., Swan, J. W., & Olsen, B. D. (2020). Effect of protein surface charge distribution on protein-polyelectrolyte complexation. *Biomacromolecules*, 21(8), 3026-3037.

Kong, J.-N., Lee, H.-J., Jo, D.-H., & Kong, K.-H. (2010). Characterization of human tyrosinase ectodomain expressed in *Escherichia coli*. *Protein and Peptide Letters*, 17(8), 1026-1030.

Krogsgaard, M., Nue, V., & Birkedal, H. (2016). Mussel-inspired materials: self-healing through coordination chemistry. *Chemistry—A European Journal*, 22(3), 844-857.

Kutyrev, A. A., & Moskva, V. V. (1991). Nucleophilic reactions of quinones. *Russian Chemical Reviews*, 60(1), 72.

Lee, H., Scherer, N. F., & Messersmith, P. B. (2006). Single-molecule mechanics of mussel adhesion. *Proceedings of the National Academy*

of Sciences, 103(35), 12999-13003.

- Lee, K., Park, M., Malollari, K. G., Shin, J., Winkler, S. M., Zheng, Y., . . . Messersmith, P. B. (2020). Laser-induced graphitization of polydopamine leads to enhanced mechanical performance while preserving multifunctionality. *Nature communications*, 11(1), 1-8.
- Lee, N., Lee, S.-H., Baek, K., & Kim, B.-G. (2015). Heterologous expression of tyrosinase (MelC2) from *Streptomyces avermitilis* MA4680 in *E. coli* and its application for ortho-hydroxylation of resveratrol to produce piceatannol. *Applied microbiology and biotechnology*, 99(19), 7915-7924.
- Lee, P. G., Lee, S. H., Hong, E. Y., Lutz, S., & Kim, B. G. (2019). Circular permutation of a bacterial tyrosinase enables efficient polyphenol-specific oxidation and quantitative preparation of orobol. *Biotechnology and bioengineering*, 116(1), 19-27.
- Lee, S. H., Baek, K., Lee, J. E., & Kim, B. G. (2016). Using tyrosinase as a monophenol monooxygenase: A combined strategy for effective inhibition of melanin formation. *Biotechnology and bioengineering*, 113(4), 735-743.
- Lemaster, J. E., Jeevarathinam, A. S., Kumar, A., Chandrasekar, B., Chen, F., & Jokerst, J. V. (2019). Synthesis of Ultrasmall Synthetic Melanin Nanoparticles by UV Irradiation in Acidic and Neutral Conditions. *ACS Applied Bio Materials*, 2(10), 4667-4674.
- Li, F., Yu, Y., Wang, Q., Yuan, J., Wang, P., & Fan, X. (2018). Polymerization

- of dopamine catalyzed by laccase: Comparison of enzymatic and conventional methods. *Enzyme and microbial technology*, 119, 58-64.
- Li, T., Zhang, N., Yan, S., Jiang, S., & Yin, H. (2021). A Novel Tyrosinase from *Armillaria ostoyae* with Comparable Monophenolase and Diphenolase Activities Suffers Substrate Inhibition. *Applied and Environmental Microbiology*, 87(12), e00275-00221.
- Liebscher, J. (2019). Chemistry of Polydopamine—Scope, Variation, and Limitation. *European Journal of Organic Chemistry*, 2019(31-32), 4976-4994.
- Lin, Q., Gourdon, D., Sun, C., Holten-Andersen, N., Anderson, T. H., Waite, J. H., & Israelachvili, J. N. (2007). Adhesion mechanisms of the mussel foot proteins mfp-1 and mfp-3. *Proceedings of the National Academy of Sciences*, 104(10), 3782-3786.
- Liu, Y., Ai, K., & Lu, L. (2014). Polydopamine and its derivative materials: synthesis and promising applications in energy, environmental, and biomedical fields. *Chemical reviews*, 114(9), 5057-5115.
- López-serrano, D., Sánchez-Amat, A., & Solano, F. (2002). Cloning and molecular characterization of a SDS-activated tyrosinase from *Marinomonas mediterranea*. *Pigment cell research*, 15(2), 104-111.
- Lozano, P., Combes, D., & Iborra, J. (1994). Effect of polyols on α -chymotrypsin thermostability: a mechanistic analysis of the enzyme stabilization. *Journal of biotechnology*, 35(1), 9-18.
- Lu, Q., Danner, E., Waite, J. H., Israelachvili, J. N., Zeng, H., & Hwang, D.

- S. (2013). Adhesion of mussel foot proteins to different substrate surfaces. *Journal of The Royal Society Interface*, *10*(79), 20120759.
- Luo, H., Gu, C., Zheng, W., Dai, F., Wang, X., & Zheng, Z. (2015). Facile synthesis of novel size-controlled antibacterial hybrid spheres using silver nanoparticles loaded with poly-dopamine spheres. *RSC Advances*, *5*(18), 13470-13477.
- LV, Y., Zhang, J., Song, Y., Wang, B., Wang, S., Zhao, S., . . . Ma, X. (2014). Natural anionic polymer acts as highly efficient trypsin inhibitor based on an electrostatic interaction mechanism. *Macromolecular rapid communications*, *35*(18), 1606-1610.
- Lyu, Q., Hsueh, N., & Chai, C. L. (2019). Unravelling the polydopamine mystery: is the end in sight? *Polymer Chemistry*, *10*(42), 5771-5777.
- Lyu, Q., Hsueh, N., & Chai, C. L. L. (2019). Direct Evidence for the Critical Role of 5,6-Dihydroxyindole in Polydopamine Deposition and Aggregation. *Langmuir*, *35*(15), 5191-5201.
doi:10.1021/acs.langmuir.9b00392
- Ma, H., Fan, Q., Fan, B., Zhang, Y., Fan, D., Wu, D., & Wei, Q. (2018). Formation of Homogeneous Epinephrine-Melanin Solutions to Fabricate Electrodes for Enhanced Photoelectrochemical Biosensing. *Langmuir*, *34*(26), 7744-7750.
- Magari, R. T. (2002). Estimating degradation in real time and accelerated stability tests with random lot-to-lot variation: a simulation study. *Journal of pharmaceutical sciences*, *91*(3), 893-899.

- MARGOLIN, A. L., SHERSTYUK, S. F., IZUMRUDOV, V. A., ZEZIN, A. B., & KABANOV, V. A. (1985). Enzymes in polyelectrolyte complexes: The effect of phase transition on thermal stability. *European journal of biochemistry*, 146(3), 625-632.
- Marshall, J. J., & Rabinowitz, M. (1975). Enzyme stabilization by covalent attachment of carbohydrate. *Archives of Biochemistry and Biophysics*, 167(2), 777-779.
- Martínez, L. M., Martínez, A., & Gosset, G. (2019). Production of melanins with recombinant microorganisms. *Frontiers in bioengineering and biotechnology*, 7, 285.
- McLarin, M.-A., & Leung, I. K. (2020). Substrate specificity of polyphenol oxidase. *Critical Reviews in Biochemistry and Molecular Biology*, 1-35.
- Mensink, M. A., Frijlink, H. W., van der Voort Maarschalk, K., & Hinrichs, W. L. (2017). How sugars protect proteins in the solid state and during drying (review): Mechanisms of stabilization in relation to stress conditions. *European Journal of Pharmaceutics and Biopharmaceutics*, 114, 288-295.
- Micillo, R., Panzella, L., Iacomino, M., Prampolini, G., Cacelli, I., Ferretti, A., . . . d'Ischia, M. (2017). Eumelanin broadband absorption develops from aggregation-modulated chromophore interactions under structural and redox control. *Scientific reports*, 7, 41532.
- Micillo, R., Panzella, L., Koike, K., Monfrecola, G., Napolitano, A., &

- d'Ischia, M. (2016). "Fifty shades" of black and red or how carboxyl groups fine tune eumelanin and pheomelanin properties. *International journal of molecular sciences*, 17(5), 746.
- Mishra, K., Ojha, H., & Chaudhury, N. K. (2012). Estimation of antiradical properties of antioxidants using DPPH assay: A critical review and results. *Food chemistry*, 130(4), 1036-1043.
- Molloy, S., Nikodinovic-Runic, J., Martin, L. B., Hartmann, H., Solano, F., Decker, H., & O'Connor, K. E. (2013). Engineering of a bacterial tyrosinase for improved catalytic efficiency towards D-tyrosine using random and site directed mutagenesis approaches. *Biotechnology and bioengineering*, 110(7), 1849-1857.
- Nadal-Jimenez, P., Koch, G., Reis, C. R., Muntendam, R., Raj, H., Jeronimus-Stratingh, C. M., . . . Quax, W. J. (2014). PvdP is a tyrosinase that drives maturation of the pyoverdine chromophore in *Pseudomonas aeruginosa*. *Journal of bacteriology*, 196(14), 2681-2690.
- Nguyen, H. H., & Kim, M. (2017). An overview of techniques in enzyme immobilization. *Applied Science and Convergence Technology*, 26(6), 157-163.
- Pandey, N., Soto-Garcia, L. F., Liao, J., Zimmern, P., Nguyen, K. T., & Hong, Y. (2020). Mussel-inspired bioadhesives in healthcare: design parameters, current trends, and future perspectives. *Biomaterials science*, 8(5), 1240-1255.
- Panis, F., Krachler, R. F., Krachler, R., & Rompel, A. (2021). Expression,

- Purification, and Characterization of a Well-Adapted Tyrosinase from Peatlands Identified by Partial Community Analysis. *Environmental Science & Technology*, 55(16), 11445-11454.
- Park, J., Moon, H., & Hong, S. (2019). Recent advances in melanin-like nanomaterials in biomedical applications: a mini review. *Biomaterials Research*, 23(1), 1-10.
- Pasche, S., Vörös, J., Griesser, H. J., Spencer, N. D., & Textor, M. (2005). Effects of ionic strength and surface charge on protein adsorption at PEGylated surfaces. *The Journal of Physical Chemistry B*, 109(37), 17545-17552.
- Pelegri-O'Day, E. M., & Maynard, H. D. (2016). Controlled radical polymerization as an enabling approach for the next generation of protein-polymer conjugates. *Accounts of chemical research*, 49(9), 1777-1785.
- Perrin, D. D. (1972). *Dissociation constants of organic bases in aqueous solution: supplement 1972* (Vol. 1): Franklin Book Company.
- Pettersen, E. F., Goddard, T. D., Huang, C. C., Couch, G. S., Greenblatt, D. M., Meng, E. C., & Ferrin, T. E. (2004). UCSF Chimera—a visualization system for exploratory research and analysis. *Journal of computational chemistry*, 25(13), 1605-1612.
- Pezzella, A., Iadonisi, A., Valerio, S., Panzella, L., Napolitano, A., Adinolfi, M., & d'Ischia, M. (2009). Disentangling eumelanin “black chromophore”: Visible absorption changes as signatures of oxidation

state-and aggregation-dependent dynamic interactions in a model water-soluble 5, 6-dihydroxyindole polymer. *Journal of the American Chemical Society*, 131(42), 15270-15275.

Pezzella, A., Panzella, L., Crescenzi, O., Napolitano, A., Navaratnam, S., Edge, R., . . . d'Ischia, M. (2009). Lack of visible chromophore development in the pulse radiolysis oxidation of 5, 6-dihydroxyindole-2-carboxylic acid oligomers: DFT investigation and implications for eumelanin absorption properties. *The Journal of organic chemistry*, 74(10), 3727-3734.

Ponzio, F., Barthès, J., Bour, J., Michel, M., Bertani, P., Hemmerlé, J., . . . Ball, V. (2016). Oxidant control of polydopamine surface chemistry in acids: A mechanism-based entry to superhydrophilic-superoleophobic coatings. *Chemistry of Materials*, 28(13), 4697-4705.

Quan, J., & Tian, J. (2011). Circular polymerase extension cloning for high-throughput cloning of complex and combinatorial DNA libraries. *Nature protocols*, 6(2), 242-251.

Quiñones, J. P., Peniche, H., & Peniche, C. (2018). Chitosan based self-assembled nanoparticles in drug delivery. *Polymers*, 10(3), 235.

Repenko, T., Fokong, S., De Laporte, L., Go, D., Kiessling, F., Lammers, T., & Kuehne, A. J. (2015). Water-soluble dopamine-based polymers for photoacoustic imaging. *Chemical communications*, 51(28), 6084-6087.

Rios, M., Habecker, B., Sasaoka, T., Eisenhofer, G., Tian, H., Landis, S., . . .

- Roffler-Tarlov, S. (1999). Catecholamine synthesis is mediated by tyrosinase in the absence of tyrosine hydroxylase. *Journal of Neuroscience*, *19*(9), 3519-3526.
- Rodriguez-Abetxuko, A., Sánchez-deAlcázar, D., Muñumer, P., & Beloqui, A. (2020). Tunable polymeric scaffolds for enzyme immobilization. *Frontiers in bioengineering and biotechnology*, *8*, 830.
- Ryu, J. H., Messersmith, P. B., & Lee, H. (2018). Polydopamine surface chemistry: a decade of discovery. *ACS applied materials & interfaces*, *10*(9), 7523-7540.
- Şahutoğlu, A. S., & Akgül, C. (2020). One-phase synthesis of single enzyme nanoparticles (SENs) of *Trametes versicolor* laccase by in situ acrylamide polymerisation. *Biocatalysis and Biotransformation*, *38*(1), 64-74.
- Saini, A. S., Tripathi, A., & Melo, J. S. (2015). On-column enzymatic synthesis of melanin nanoparticles using cryogenic poly (AAM-co-AGE) monolith and its free radical scavenging and electro-catalytic properties. *RSC Advances*, *5*(106), 87206-87215.
- Sakai, S., Yamada, Y., Zenke, T., & Kawakami, K. (2009). Novel chitosan derivative soluble at neutral pH and in-situ gellable via peroxidase-catalyzed enzymatic reaction. *Journal of Materials Chemistry*, *19*(2), 230-235.
- Salomaki, M., Marttila, L., Kivela, H., Ouvinen, T., & Lukkari, J. (2018). Effects of pH and oxidants on the first steps of polydopamine

formation: A thermodynamic approach. *The Journal of Physical Chemistry B*, 122(24), 6314-6327.

Sanket, S., & Das, S. K. (2021). Role of Enzymes in Synthesis of Nanoparticles. In H. Thatoi, S. Mohapatra, & S. K. Das (Eds.), *Bioprospecting of Enzymes in Industry, Healthcare and Sustainable Environment* (pp. 139-153). Singapore: Springer Singapore.

Sendovski, M., Kanteev, M., Shuster Ben-Yosef, V., Adir, N., & Fishman, A. (2010). Crystallization and preliminary X-ray crystallographic analysis of a bacterial tyrosinase from *Bacillus megaterium*. *Acta Crystallographica Section F: Structural Biology and Crystallization Communications*, 66(9), 1101-1103.

Sharma, O. P., & Bhat, T. K. (2009). DPPH antioxidant assay revisited. *Food chemistry*, 113(4), 1202-1205.

Silva, C., Martins, M., Jing, S., Fu, J., & Cavaco-Paulo, A. (2018). Practical insights on enzyme stabilization. *Critical reviews in biotechnology*, 38(3), 335-350.

Solomon, E. I., Baldwin, M. J., & Lowery, M. D. (1992). Electronic structures of active sites in copper proteins: contributions to reactivity. *Chemical reviews*, 92(4), 521-542.

Solomon, E. I., Sundaram, U. M., & Machonkin, T. E. (1996). Multicopper oxidases and oxygenases. *Chemical reviews*, 96(7), 2563-2606.

Son, H. F., Lee, S.-H., Lee, S. H., Kim, H., Hong, H., Lee, U.-J., . . . Kim, K.-J. (2018). Structural basis for highly efficient production of catechol

- derivatives at acidic pH by tyrosinase from *Burkholderia thailandensis*. *ACS Catalysis*, 8(11), 10375-10382.
- Stepankova, V., Bidmanova, S., Koudelakova, T., Prokop, Z., Chaloupkova, R., & Damborsky, J. (2013). Strategies for stabilization of enzymes in organic solvents. *ACS Catalysis*, 3(12), 2823-2836.
- Stevens, C. A., Kaur, K., & Klok, H.-A. (2021). Self-assembly of protein-polymer conjugates for drug delivery. *Advanced Drug Delivery Reviews*, 174, 447-460.
- Sugumaran, M., & Berek, H. (2016). Critical analysis of the melanogenic pathway in insects and higher animals. *International journal of molecular sciences*, 17(10), 1753.
- Sun, G., Zu, F., Koch, N., Rappich, J., & Hinrichs, K. (2019). In situ infrared spectroscopic monitoring and characterization of the growth of polydopamine (PDA) films. *physica status solidi (b)*, 256(2), 1800308.
- Thalmann, C., & Lötzbeyer, T. (2002). Enzymatic cross-linking of proteins with tyrosinase. *European Food Research and Technology*, 214(4), 276-281.
- Thompson, A., Land, E. J., Chedekel, M. R., Subbarao, K. V., & Truscott, T. G. (1985). A pulse radiolysis investigation of the oxidation of the melanin precursors 3, 4-dihydroxyphenylalanine (dopa) and the cysteinyl dopas. *Biochimica et Biophysica Acta (BBA)-General Subjects*, 843(1-2), 49-57.
- Tishchenko, K., Beloglazkina, E., Mazhuga, A., & Zyk, N. (2016). Copper-

containing enzymes: Site types and low-molecular-weight model compounds. *Review Journal of Chemistry*, 6(1), 49-82.

Tornøe, C. W., Johansson, E., & Wahlund, P.-O. (2017). Divergent protein synthesis of Bowman–Birk protease inhibitors, their hydrodynamic behavior and co-crystallization with α -chymotrypsin. *Synlett*, 28(15), 1901-1906.

Unni, S., Huang, Y., Hanson, R. M., Tobias, M., Krishnan, S., Li, W. W., . . . Baker, N. A. (2011). Web servers and services for electrostatics calculations with APBS and PDB2PQR. *Journal of computational chemistry*, 32(7), 1488-1491.

Upadhyay, R., Kim, J. Y., Hong, E. Y., Lee, S. G., Seo, J. H., & Kim, B. G. (2019). RiSLnet: Rapid identification of smart mutant libraries using protein structure network. Application to thermal stability enhancement. *Biotechnology and bioengineering*, 116(2), 250-259.

Walsh, K. (1970). [4] Trypsinogens and trypsins of various species. In *Methods in enzymology* (Vol. 19, pp. 41-63): Elsevier.

Waltmann, C., Mills, C. E., Wang, J., Qiao, B., Torkelson, J. M., Tullman-Ercek, D., & Olvera de la Cruz, M. (2022). Functional enzyme–polymer complexes. *Proceedings of the National Academy of Sciences*, 119(13), e2119509119.

Wan, X., Chai, B., Liao, Y., Su, Y., Ye, T., Shen, P., & Chen, X. (2009). Molecular and biochemical characterization of a distinct tyrosinase involved in melanin production from *Aeromonas media*. *Applied*

microbiology and biotechnology, 82(2), 261-269.

Wang, F., Xu, Z., Wang, C., Guo, Z., Yuan, Z., Kang, H., . . . Liu, Y. (2021).

Biochemical characterization of a tyrosinase from *Bacillus aryabhatai* and its application. *International journal of biological macromolecules*, 176, 37-46.

Wang, X. H., Chen, Z., Yang, P., Hu, J. F., Wang, Z., & Li, Y. W. (2019). Size

control synthesis of melanin-like polydopamine nanoparticles by tuning radicals. *Polymer Chemistry*, 10(30), 4194-4200.
doi:10.1039/c9py00517j

Wang, Y., Cheng, Y. T., Cao, C., Oliver, J. D., Stenzel, M. H., & Chapman, R.

(2020). Polyion Complex-Templated Synthesis of Cross-Linked Single-Enzyme Nanoparticles. *Macromolecules*, 53(13), 5487-5496.

Wang, Y., Milewska, M., Foster, H., Chapman, R., & Stenzel, M. H. (2021).

The Core–Shell Structure, Not Sugar, Drives the Thermal Stabilization of Single-Enzyme Nanoparticles. *Biomacromolecules*, 22(11), 4569-4581.

Wee, Y., Park, S., Kwon, Y. H., Ju, Y., Yeon, K.-M., & Kim, J. (2019).

Tyrosinase-immobilized CNT based biosensor for highly-sensitive detection of phenolic compounds. *Biosensors and Bioelectronics*, 132, 279-285.

Würtele, M., Hahn, M., Hilpert, K., & Höhne, W. (2000). Atomic resolution

structure of native porcine pancreatic elastase at 1.1 Å. *Acta Crystallographica Section D: Biological Crystallography*, 56(4), 520-

523.

- Wu, Q., Xu, Z., Duan, Y., Zhu, Y., Ou, M., & Xu, X. (2017). Immobilization of tyrosinase on polyacrylonitrile beads: biodegradation of phenol from aqueous solution and the relevant cytotoxicity assessment. *RSC Advances*, 7(45), 28114-28123.
- Xiang, S., Yang, P., Guo, H., Zhang, S., Zhang, X., Zhu, F., & Li, Y. (2017). Green tea makes polyphenol nanoparticles with radical-scavenging activities. *Macromolecular rapid communications*, 38(23), 1700446.
- Xiao, L., Chen, X., Yang, X., Sun, J., & Geng, J. (2020). Recent Advances in Polymer-Based Photothermal Materials for Biological Applications. *ACS Applied Polymer Materials*, 2(10), 4273-4288.
- Xie, W., Pakdel, E., Liang, Y., Kim, Y. J., Liu, D., Sun, L., & Wang, X. (2019). Natural eumelanin and its derivatives as multifunctional materials for bio-inspired applications: a review. *Biomacromolecules*, 20(12), 4312-4331.
- Yan, M., Ge, J., Liu, Z., & Ouyang, P. (2006). Encapsulation of single enzyme in nanogel with enhanced biocatalytic activity and stability. *Journal of the American Chemical Society*, 128(34), 11008-11009.
- Yang, J., Stuart, M. A. C., & Kamperman, M. (2014). Jack of all trades: versatile catechol crosslinking mechanisms. *Chemical Society Reviews*, 43(24), 8271-8298.
- Yang, S. J., Zou, L. Y., Liu, C., Zhong, Q., Ma, Z. Y., Yang, J., . . . Xu, Z. K. (2020). Codeposition of Levodopa and Polyethyleneimine: Reaction

Mechanism and Coating Construction. *ACS Appl Mater Interfaces*, 12(48), 54094-54103. doi:10.1021/acsami.0c16142

Yang, Y., Qi, P., Ding, Y., Maitz, M. F., Yang, Z., Tu, Q., . . . Huang, N. (2015).

A biocompatible and functional adhesive amine-rich coating based on dopamine polymerization. *Journal of materials chemistry B*, 3(1), 72-81.

Yu, X., Fan, H., Liu, Y., Shi, Z., & Jin, Z. (2014). Characterization of carbonized polydopamine nanoparticles suggests ordered supramolecular structure of polydopamine. *Langmuir*, 30(19), 5497-5505.

Yuan, H., Mullett, W. M., & Pawliszyn, J. (2001). Biological sample analysis with immunoaffinity solid-phase microextraction. *Analyst*, 126(8), 1456-1461.

Zaidi, K. U., Ali, A. S., Ali, S. A., & Naaz, I. (2014). Microbial tyrosinases: promising enzymes for pharmaceutical, food bioprocessing, and environmental industry. *Biochemistry research international*, 2014.

Zhang, T., Bai, R., Wang, Q., Fan, X., Wang, P., Yuan, J., & Yu, Y. (2017). A novel strategy to improve the dyeing properties in laccase-mediated coloration of wool fabric. *Coloration Technology*, 133(1), 65-72.

Zheng, W., Fan, H., Wang, L., & Jin, Z. (2015). Oxidative self-polymerization of dopamine in an acidic environment. *Langmuir*, 31(42), 11671-11677.

Zhou, Q., Wu, W., & Xing, T. (2022). Study on the mechanism of laccase-

catalyzed polydopamine rapid dyeing and modification of silk. *RSC Advances*, 12(6), 3763-3773.

Zhou, X., McCallum, N. C., Hu, Z., Cao, W., Gnanasekaran, K., Feng, Y., . . .

Gianneschi, N. C. (2019). Artificial Allomelanin Nanoparticles. *ACS nano*.

Zou, Y., Chen, X., Yang, P., Liang, G., Yang, Y., Gu, Z., & Li, Y. (2020).

Regulating the absorption spectrum of polydopamine. *Science advances*, 6(36), eabb4696.

Appendix

A.1 Introduction

Isoflavonoids, which are physiologically active substances, are well known as phytoestrogens because most of them exhibit biological effects through estrogen receptors. Among them, isoflavonoids present in soybeans can be used as cosmetic, functional materials such as wrinkle suppression, whitening, and moisturizing and are active substances that also function as pharmaceuticals for regulating immune function antioxidant and anti-obesity effects(Miadoková, 2009).

In particular, Orobol, a hydroxylation derivative of genistein, which accounts for many soy isoflavones, has a lipid accumulation inhibitory effect compared to other isoflavones(Yang et al., 2019). We conducted a study to produce ortho-hydroxylation derivatives through biotransformation in a 4L lab-scale reactor using *Bacillus megaterium* tyrosinase(Lee, Baek, Lee, & Kim, 2016). Furthermore, we conducted a scale-up study for the industrialization of functional isoflavonoids. We established the upstream process of cell culture and Orobol bioconversion reaction and the downstream process corresponding to the separation and purification of the final product and were able to develop the final 400L scale mass production process. All processes of cell mass production, recombinant protein expression, orobol mass production, separation and purification were carried out at the Chuncheon Bioindustry Foundation (Chuncheon, Republic of Korea).

Polyphenol, a secondary metabolite of plants, exists mainly in the form of

glycosides in which sugar molecules are covalently bound in nature. The form to which no sugar is attached is called aglycone, and the form to which sugar is attached is called glycone. Aglycone is insoluble, so it is challenging to deliver a high content to the human body, and it is vulnerable to oxidation, so it is easily decomposed or browned in an aqueous solution. However, glycones in which one or more sugar moieties are conjugated with O- or C-bonds significantly increase water solubility (Nazir, Sulisty, Hashmi, Ho, & Khan, 2018; Pham & Shah, 2009; Szeja, Gryniewicz, & Rusin, 2017). Therefore, intestinal absorption is easier compared to aglycone. Also, because the reactive hydroxyl group is shielded, glycoside can exist in a stable form compared to aglycone. Therefore, functional polyphenol derivatives can be produced using stable glycosides present in large amounts in plants, which can bring the advantage of increasing the absorption rate of the human body as well as the storage stability of the product.

In a previous study, we attempted to produce a catechol-type functional polyphenol by bioconversion of aglycone by tyrosinase ortho-hydroxylation. In order to prevent oxidation of the catechol-type product, either chelation and protection of dihydroxyl moiety using boric acid or reduction of quinone produced by additional hydroxylation reaction with ascorbic acid, a reducing agent, to catechol to prevent melanin production. However, due to a large amount of hydroxyl moiety in glycone, it is challenging to shield the functional catechol group of polyphenol by boric acid chelation. If a large amount of ascorbic acid, a reducing

agent, is used to cover this shortcoming, the pH of the reaction buffer is reduced, and tyrosinase activity is inevitably lost. Therefore, to solve the shortcomings, we produced functional polyphenol glycoside derivatives by ortho-hydroxylation reaction of *Burkholderia thailandensis* tyrosinase, which has high activity even under acidic conditions below pH 5.

A.2 Orobol mass production protocol

A.2.1 Materials

Luria-Bertani(LB) broth, LB agar were purchased from BD Difco (Sparks, USA). Chemicals used for 40L scale auto-induction media (Tryptone, yeast extract, Na₂HPO₄, KH₂PO₄, NH₄Cl, Na₂SO₄, MgSO₄, glycerol, glucose, lactose, CuSO₄·7H₂O), and orobol mass production and purification (NaOH, boric acid, DMSO, ascorbic acid, concentrated HCl) were purchased from Duksan science (Seoul, Republic of Korea). And all the other chemicals were purchased from Sigma-Aldrich Korea (Seoul, Republic of Korea). A 70 L incubator, a 500 L incubator, and a tubular centrifuge were used by borrowing equipment from the Chuncheon Bioindustry Foundation (Chuncheon, Republic of Korea).

A.2.2 Recombinant *Bacillus megaterium* tyrosinase (*BmTy*) subculture for 40L scale large-capacity cell culture

Recombinant BmTy is cloned into pET28a vector and expressed in *E. coli* BL21(DE3) as in previously reported studies(Lee et al., 2016). Incubate *E. coli* cloned with BmTy overnight in 3 ml LB medium containing 50 mg/L kanamycin antibiotics. All cell culture times should not exceed 20 hours to prevent cell death.

And the next day, scale up with 50 ml LB culture. Similarly, inoculate 3 ml of initial culture in an amount of 1 v/v% in 50 ml of LB medium containing 50 mg/L of kanamycin antibiotics, and culture overnight. And finally, 50ml LB medium in an amount of 1 v/v% is inoculated into 400 ml LB medium containing 50 mg/L of kanamycin antibiotics.

A.2.3 Recombinant *Bacillus megaterium* tyrosinase (*BmTy*) subculture for 40L scale large-capacity cell culture

Isopropyl β -D-1-thiogalactopyranoside (IPTG) is used as a potent recombinant protein expression inducer of pET28a vector in lab scale, but it is not affordable in industrial scale. Therefore, we use lactose, an inducer of natural lac operon, to mass-produce 40L scale cells in lactose-auto induction medium. Dissolve auto-induction media ingredient (**Table A.2.1**) in 40L of tap water in a 70L scale reactor and proceed with auto-clave for 2 H at 121 °C. However, for divalent ions that can be aggregated with phosphate contained in tap water or auto-induction media ingredients such as MgSO₄ and CuSO₄, sterilize with 0.2 μ m filter, and then mix with auto-induction media that has been autoclaved. Next, adjust the temperature of 40L of auto-claved auto-induction medium to 37 °C. Then, inoculate 400 ml of *BmTy* subculture prepared. Cell culture is performed for 12 hours at 37 °C with 200rpm agitation and 1 vvm (40 L/min) of air injected.

Table A.2.5 40L *BmTy* auto induction media composition

Ingredient	Requirement	Requirement(g)
Tryptone	1 w/v% (10 g/L)	400
Yeast Extract	0.5 w/v% (5 g/L)	200
Na₂HPO₄ (m.w. 141.96)	25 mM	141.2
KH₂PO₄ (m.w. 136.09)	25 mM	136.1
NH₄Cl (m.w. 53.49)	50 mM	107
Na₂SO₄ (m.w. 142.04)	5 mM	28.4
MgSO₄ (m.w. 120.37)	2 mM	9.6
Glycerol	0.5 w/v%	200
Glucose	0.05 w/v%	20
Lactose	0.2 w/v%	80
CuSO₄ 7H₂O (m.w. 285.72)	1 mM	11.43

A.2.4 Cell recovery and preparation of orobol bioconversion reaction mixture

Incubate in auto-induction medium so that the O.D.600 of *E. coli* including *BmTy* becomes 7-8 or higher within 16 hours. After cell down in a tubular centrifuge, dissolve the cells by hand in 10 to 20 L of tap water and wash (**Figure A.2.1**). And after going through the cell down process again, dissolve the cells in tap water for cell lysis. At this time, determine the volume of the cell lysis solution by making the final O.D. of the cell 0.7 in 400L reaction buffer.

During the cell lysis process, prepare a reaction mixture in a 500L incubator (**Table A.2.2**). Add NaOH and boric acid to 350 L of 37 °C tap water in order, and adjust the pH to be between 8 and 9. Then, add ascorbic acid and cell lysate in order, add tap water to adjust the reaction mixture to 400L, and wait for the temperature to reach 37 °C. Since ascorbic acid is oxidized by natural auto-oxidation at the pH of the reaction buffer between 8 and 9, unnecessary time should not be required for all preparation processes.

Table A.2.6 400L orobol production reaction solution composition

Ingredient	Requirement(g)
NaOH	3400
Boric acid	12400
Genistein	1200
DMSO	4L
Ascorbic acid	2000

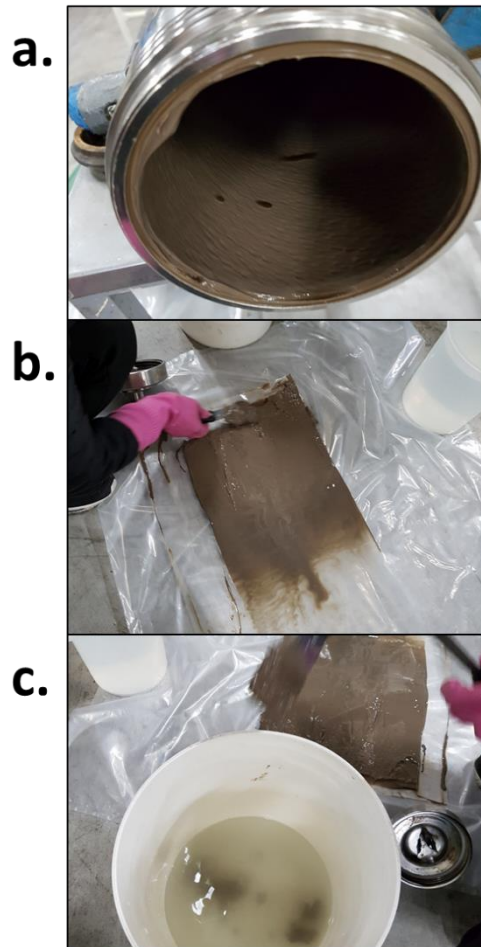


Figure A.2.3 Preparation of cell lysis solution after 40L cell culture

A.2.5 Production of orobol in 400 L scale reaction

While the temperature of the reaction mixture is raised to 37 °C, dissolve 1.2 kg of genistein powder in 4 L of DMSO. When the reaction mixture temperature reaches 37 °C, immediately put the DMSO solution in which the substrate is dissolved into the reactor. The reaction is performed with the agitation of 150 rpm at 37 °C, and 0.25 vvm of air is injected to maintain the dissolved oxygen level between 23-25 ppm. When the substrate is added to the reaction solution, insoluble granules between white and yellow are formed immediately (**Figure A.2.2a**). Furthermore, the liquid flow becomes silky. If the size of the granules increases, it is also proof that the reaction does not start. Therefore, 1 mM of Cu²⁺ ion, a cofactor of tyrosinase, should be added in the form of CuSO₄ solution, or the air rate is increased to 0.5 vvm. When the air rate is excessively high, the insoluble substrate can form more aggregate by hydrophobic interaction, so it is necessary to set an appropriate value while continuously monitoring the reaction. As the reaction progresses, bubbles are generated on the top surface of the reaction mixture, so while monitoring the reaction periodically, add about 1 ml of an antifoaming agent to prevent the bubbles from overflowing. As the orobol bioconversion reaction proceeds, if granules are no longer formed in the reaction solution and the reaction solution turns orange, the reaction is complete. The reaction is usually completed within 2-3 hours. If the reaction proceeds excessively, the solution becomes

brownish with melanin production (Figure A.2.2b and c).

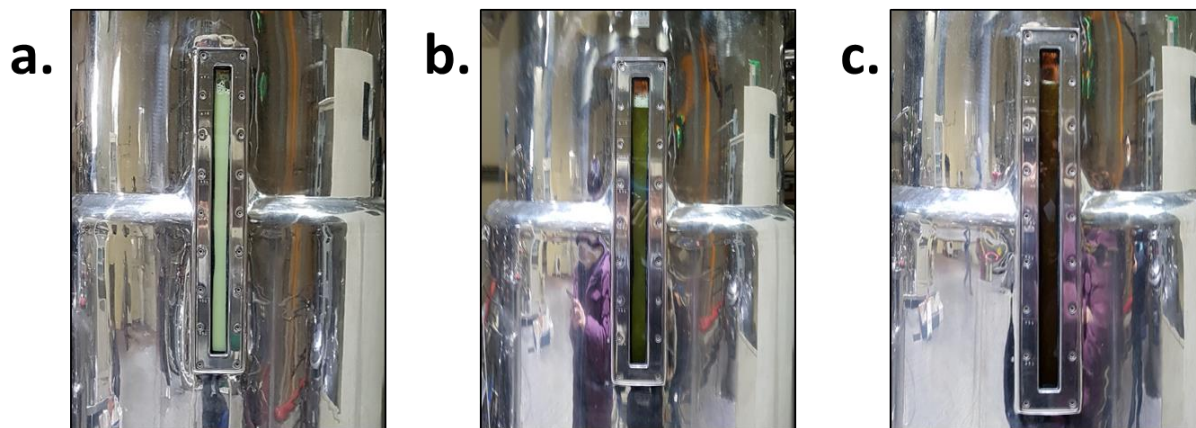


Figure A.2.4 Color change of orobol production solution over reaction time

A.2.6 Purification of orobol

In order to terminate the orobol bioconversion reaction, the reaction solution is transferred from the reactor to a separately prepared vessel. Transfer the solution to a plastic container while filtering cell debris and impurities through a sieve. Natural oxidation and oxidation by tyrosinase proceed rapidly so that the final product is easy to be melanized, so it should proceed as quickly as possible. The reaction is terminated by adding 2 L of 35% hydrochloric acid per 80 L of the transferred reaction solution to lower the pH of the solution to 3 or less. Immediately after HCl is added, a beige or yellow precipitate begins to form (**Figure A.2.3a**). After mixing well to lower the pH of the entire solution, insoluble granules are precipitated overnight at 4 °C to prevent oxidation at high temperatures. After removing the clear supernatant of the precipitated solution as much as possible, use a tubular centrifuge to separate the precipitate (**Figure A.2.3b**). Furthermore, wash the collected cakes in 30-40 L DW. Repeat this process 3-5 times until the pH of the supernatant of the solution becomes neutral. Finally, freeze-drying the collected orobol cake and store it at -20 °C.



Figure A.2.5 Separation and purification of the final produced orobol

A.3 glycoside hydroxylation

A.3.1 Materials

NcoI and HindII restriction enzymes were purchased from Thermo Scientific. Luria-Bertani(LB) broth, LB agar were purchased from BD Difco (Sparks, USA). Ni-NTA agarose was purchased from Qiagen (Hilden, Germany). And all the other chemicals were purchased from Sigma-Aldrich Korea (Seoul, Republic of Korea).

A.3.2 Expression and purification of *BtTy*

For the expression of *Bt* Tyrosinase (*BtTy*), the expression vector was transformed into *E. coli* BL21 (DE3) by heat shock treatment (Son et al., 2018), and the transformed strain was selected on LB agar plate with antibiotic selection marker kanamycin (50 µg/ml). A single colony was inoculated into a test tube with 3 ml of the same LB broth with kanamycin, and the cell was cultured in a shaking incubator at 37 °C, 200 rpm overnight. 500 µl of cultured cells were transformed into 50 ml of fresh LB medium with antibiotic markers, and then cells were grown to approximately 0.6 at OD600. Furthermore, the protein expression was induced by adding 0.1 mM of IPTG and 1.0 mM of CuSO₄. After 20 h at 37 °C culture, cells were harvested by centrifugation at 4000 rpm for 20 min. Cell pellets were resuspended in 50 mM Tris buffer, pH 8.0, and disrupted by ultrasonication. After

ultracentrifugation at 16,000 rpm for 30 min, the supernatant was collected. The supernatant was applied to the Ni-NTA agarose column for enzyme purification. Cell lysate was subsequently applied onto the Ni-NTA column after pre-equilibrium with 50 mM Tris buffer, pH 8.0 with 5.0 mM imidazole, and 300 mM NaCl buffer. Bounded proteins were washed with 50 mM Tris buffer pH 8.0 with 30 mM imidazole, 300 mM NaCl buffer. The tyrosinase was eluted by 50 mM Tris buffer pH 8.0 with 250 mM imidazole. The concentration of purified enzyme was measured by Bradford assay.

A.3.3 Synthesis and analysis of ortho-hydroxylated polyphenol glycosides using *BtTy*

To produce *ortho*-hydroxylated polyphenol glycoside, the reaction mixture was prepared as follows. 100 nM of *BtTy* and 10 μ M of CuSO₄ as a tyrosinase cofactor were added to pH 5.0, 50 mM sodium citrate buffer. Then, polyphenol glycoside prepared at 100 mM in ascorbic acid and DMSO was added to the reaction solution to have final concentrations of 10 and 1 mM, respectively. The prepared reaction solution was transferred to a 37 °C water bath and reaction was performed. 100 μ l of the reaction solution was sampled for each time point, and 100 μ l of ethanol was added to terminate the reaction. Then, after performing a 3 k

filter at 16,000 rpm for 15 minutes, HPLC analysis was performed.

A.3.4 Synthesis of ortho-hydroxylated derivatives from O- and C-glycosylated polyphenols

Previously, the production of ortho-hydroxylated polyphenol used two special strategies to prevent excessive oxidation of the product. First, protection of the product using boric acid was used (**Figure A.3.1a and b**) (Lee et al., 2016). However, since polyphenol glycoside already contains a diol moiety in the glyco part, chelation to boric acid even before hydroxylation was a problem (**Figure A.3.1c**). Therefore, we tried to solve this by adjusting the pH of the existing reaction conditions. In the past, polyphenol derivatives were synthesized at pH 8 or higher using *BmTy*, and a boric acid protection system was essential as it was vulnerable to natural oxidation reactions. Accordingly, we were able to synthesize polyphenol derivatives through hydroxylation of polyphenol glycosides using *BtTy*.

ortho-hydroxylation of polyphenol converted to a functional derivative of catechol is converted into a quinone-type substance by further enzymatic or natural oxidation. It is subsequently melanized in a spontaneous reaction. Therefore, to prevent this, the product was preserved by returning the quinone-type material to catechol by adding a reducing agent. Ascorbic acid was used as a reducing agent, but when it was added in excess, the pH of the buffer decreased, and the enzyme

efficiency of *BmTy* decreased (**Figure A.3.1a**). However, *BtTy*, which has a very high activity at acidic pH, is free even when pH is reduced, allowing the use of ascorbic acid with a high concentration of 10 mM or more.

BtTy was confirmed to have substrate specificity by forming melanin pigments for daidzein, genistein, resveratrol, phloretin and each *O*-glycoside (**Figure A.3.2**). It was confirmed that hydroxylation of monophenol group to catechol was possible regardless of structures such as flavone, isoflavone, chalcone, and stilbene. As a result of the reaction progress for 60 minutes, 100% of all *O*-glycosylated and *C*-glycosylated polyphenol 1 mM substrates were able to be hydroxylated, showing a yield of 70% or more (**Figure A.3.3**). Although *BtTy* is blocked by the C-terminal CAP domain (Son et al., 2018), further studies are needed to determine whether it can show good activity on glycosylated substrates that have increased in size.

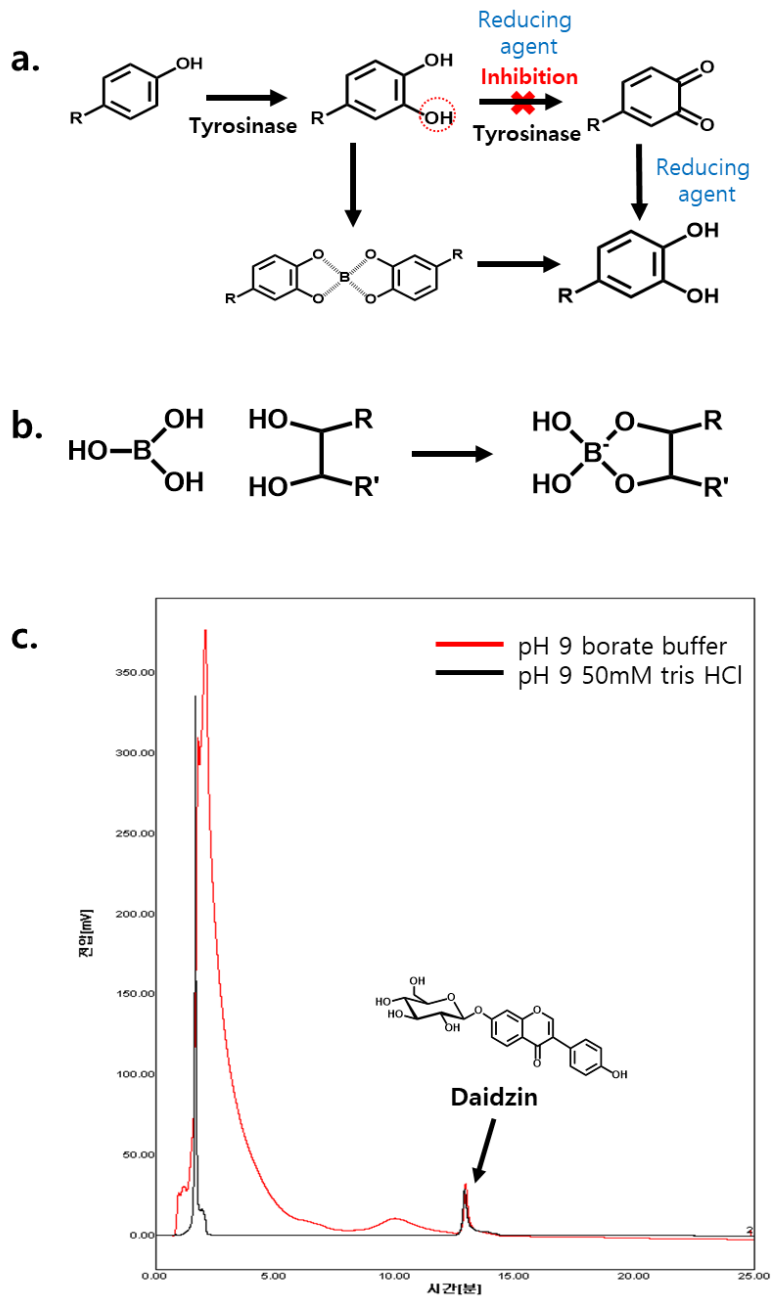


Figure A.3.1 Propensity for boric acid chelation of polyphenol aglycone and glycone

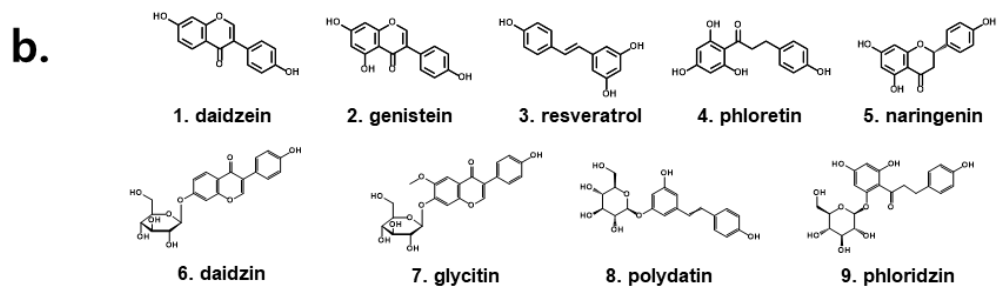
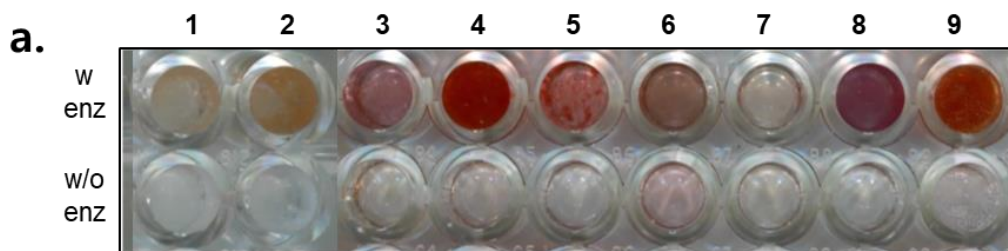


Figure A.3.2 Confirmation of enzymatic reactivity through melanogenesis reaction for polyphenol aglycone and glycone of *BfTy*

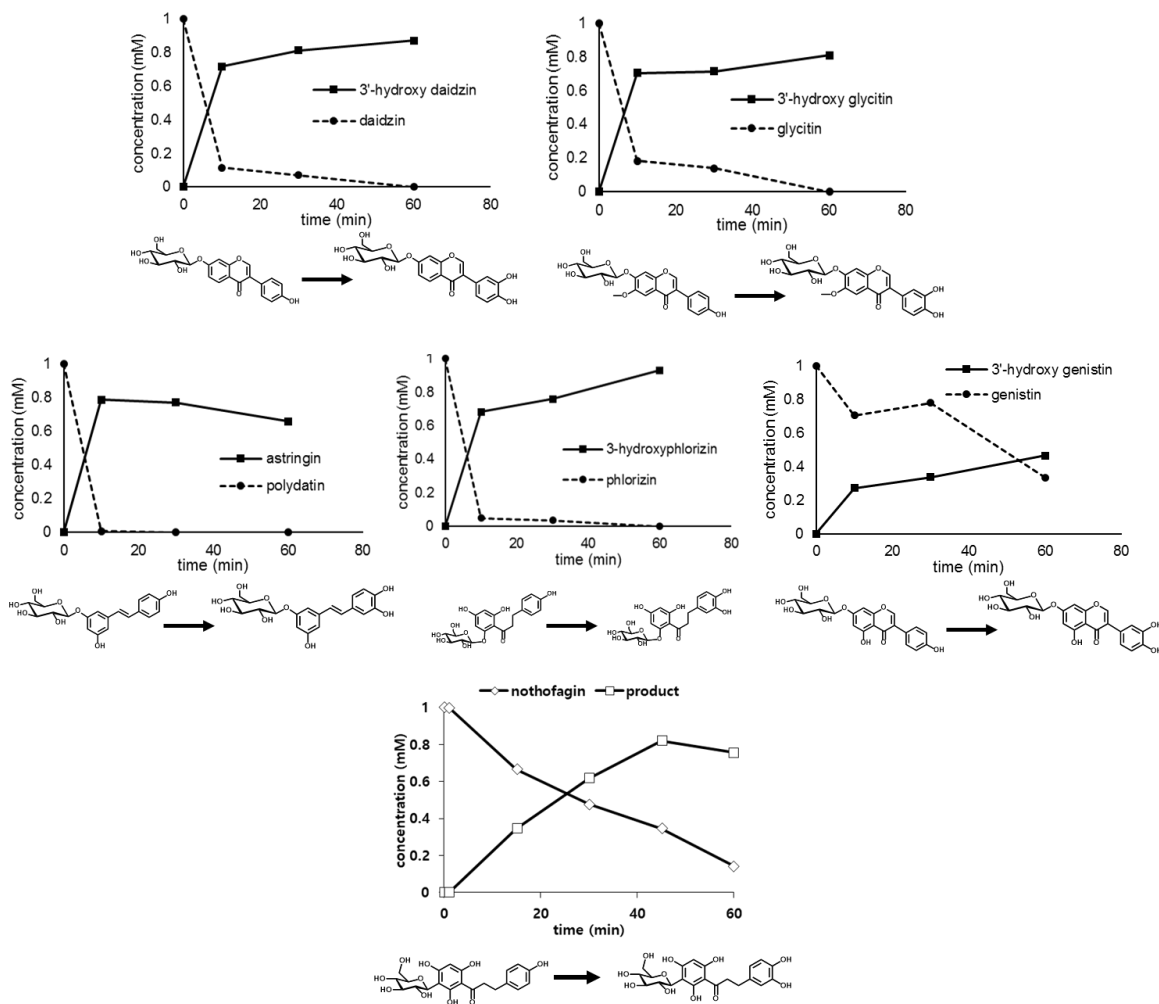


Figure A.3.3 Bioconversion profile of *BfTy* to polyphenol glycosides with various backbone structures

References

- Lee, S. H., Baek, K., Lee, J. E., & Kim, B. G. (2016). Using tyrosinase as a monophenol monooxygenase: A combined strategy for effective inhibition of melanin formation. *Biotechnology and bioengineering*, 113(4), 735-743.
- Miadoková, E. (2009). Isoflavonoids—an overview of their biological activities and potential health benefits. *Interdisciplinary toxicology*, 2(4), 211.
- Nazir, S., Sulistyó, J., Hashmi, M. I., Ho, A. L., & Khan, M. S. (2018). Enzymatic synthesis of polyphenol glycosides catalyzed by transglycosylation reaction of cyclodextrin glucanotransferase derived from *Trichoderma viride*. *Journal of food science and technology*, 55(8), 3026-3034.
- Pham, T. T., & Shah, N. P. (2009). Hydrolysis of isoflavone glycosides in soy milk by β -galactosidase and β -glucosidase. *Journal of food biochemistry*, 33(1), 38-60.
- Son, H. F., Lee, S.-H., Lee, S. H., Kim, H., Hong, H., Lee, U.-J., . . . Kim, K.-J. (2018). Structural basis for highly efficient production of catechol derivatives at acidic pH by tyrosinase from *Burkholderia thailandensis*. *ACS Catalysis*, 8(11), 10375-10382.
- Szeja, W., Gryniewicz, G., & Rusin, A. (2017). Isoflavones, their glycosides and glycoconjugates. Synthesis and biological activity. *Current Organic Chemistry*, 21(3), 218-235.
- Yang, H., Lee, S. H., Ji, H., Kim, J.-E., Yoo, R., Kim, J. H., . . . Heo, Y.-S.

(2019). Orobol, an enzyme-convertible product of genistein, exerts anti-obesity effects by targeting casein kinase 1 epsilon. *Scientific reports*, 9(1), 1-11.

국문 초록

생활성이 있는 나노 물질의 합성은 점점 가속화된 관심을 받고있는 분야이다. 나노 물질 합성은 물리, 화학, 생물적 합성법이 알려져있다. 나노물질은 일반적으로 크기, 물리화학적 성질의 조절에 따라 응용 방식이 결정된다. 효소적 합성 방식은 앞선 2 가지 방식에 비해서 균질하지 못한 입자의 생산 방식으로 알려져 있어, 반응에 대한 심층적인 분석이 어려웠다. 하지만 효소 촉매는 화학 촉매에 비해 친환경적이고, 생체 분자에 온화한 반응에서의 반응을 촉매한다. 따라서 생체 분자에 가혹한 반응 조건 (온도, pH, 유기용매)에서 손상되기 쉬운 생활성 물질의 제작에 적합하다. 따라서 생활성 나노물질의 효소적 합성은 효과적인 대안을 제공할 수 있다.

우리는, 모노페놀에 기질 특이성을 가진 티로시나아제를 활용하여 정교한 조절이 가능한 생활성 나노물질을 합성하고자 하였다. 티로시나아제는 단백질 도메인 구조에 따라 최적 반응 pH 가 변하며, 다양한 기질에 대한 기질특이성이 있는 효소이다. 티로시나아제의 연속적인 수산화 반응에 의해 만들어지는 카테콜과 퀴논을 활용해, 효소적인 방법으로 가교결합 물질을 합성하고, 물리화학적 성질에 대한 자세한 분석을 하였다.

Chapter 1 에서, pH 5 이하 산성에서 강한 활성이 있는 *Burkholderia cepacia* 유래 티로시나아제를 활용해 20 nm 이하의 균질한 멜라닌 나노파티클을 합성하였다. 중성 이상 반응 환경에서 무작위적인 산화 반응에 의해 합성되는 멜라닌은 단백질과 무작위적인 가교결합 집합체를 형성했다. 하지만 산성 조건에서 카테콜의 양성자화를 유도함으로써, 무작위적인

가교결합을 조절하였고, 그 결과 효소적인 방법으로 균질한 멜라닌 나노 입자를 합성할 수 있었다.

Chapter 2 에서는, 효소 안정화를 도모하기 위해, 페놀 잔기가 도입된 다당류를 티로시나아제 반응으로 효소 표면에 가교 결합하여 효소-다당류 복합체를 이루었다. 효소 표면으로부터 활성 부위까지의 거리가 짧아 고분자 기질에 반응성이 높은 *Streptomyces avermitilis* 티로시나아제로 효소 표면 티로신, 리신 잔기와 페놀 잔기가 부착된 다당류 표면 모노페놀간의 가교결합을 생성하였다. 티로시나아제 가교반응으로 pH 8 의 생체 분자 친화적인 환경에서 30 분 내에 모델 효소인 트립신과 알긴산-티라민 결합체로 이루어진 복합체를 합성할 수 있었다. 그 결과, 트립신의 열 안정성, 유기 용매 안정성 및 저장 안정성이 증대되었다.

주요어: 티로시나아제, 산성 조건, 수용성 멜라닌 나노파티클, 가교 결합, 효소-다당류 복합체

학번: 2016-22788